https://ntrs.nasa.gov/search.jsp?R=19790007850 2020-03-22T01:30:02+00:00Z

General Disclaimer

One or more of the Following Statements may affect this Document

- This document has been reproduced from the best copy furnished by the organizational source. It is being released in the interest of making available as much information as possible.

- This document may contain data, which exceeds the sheet parameters. It was furnished in this condition by the organizational source and is the best copy available.

- This document may contain tone-on-tone or color graphs, charts and/or pictures, which have been reproduced in black and white.

- This document is paginated as submitted by the original source.

- Portions of this document are not fully legible due to the historical nature of some of the material. However, it is the best reproduction available from the original submission.

Produced by the NASA Center for Aerospace Information (CASI)

NASA CR-156791

FINAL REPORT

GEOS-2 REFRACTION PROGRAM

SUMMARY DOCUMENT

(NASA-CR-156791) GEOS-2 REFRACTION PROGRAM SUMMARY DOCUMENT Final Report (Communications Research Labs.) 168 p HC A08/MF A01 CSCL 22B G3/12 N79-16021 Unclas 27064

AUG 1978
RECEIVED
NASA STI FACILITY

ABSTRACT

The Wallops Island Collocation Experiment consisted of an intensive 3-month period (April - June, 1968) of tracking and data collection from collocated tracking instrumentation at Wallops Island, using the GEOS-2 satellite as target vehicle.

The experiment resulted in a wealth of data regarding the ionospheric and tropospheric propagation errors, the theoretical and data analysis of which has been documented in some 30 separate reports over the last 6 years.

This report presents a self-sufficient unifying overview of the entire project results with references to the underlying reports for details.

TABLE OF CONTENTS

TABLE OF CONTENTS, Cont'd.

LIST OF FIGURES

LIST OF FIGURES, Cont'd.

LIST OF FIGURES, Cont'd.

LIST OF TABLES

LIST OF SYMBOLS

	Defined in Sec.
a = radius of earth, 6378 km	5.2
B (Subscript) = pertaining to bent path	3.2
c = velocity of light, 2.99795×10^{8} m/sec	2.4.1
d (Subscript) = day	4.1
e = electron charge, 1.60207×10^{-19} Coulombs	3.3
E = elevation angle of geometric line-of-sight	3.2
E = partial pressure of water vapor, mb	4.1
E_o = elevation measured at ground level	
f = frequency, Hz	3.2
f_H = magneto-gyro frequency = $\frac{eB}{2\pi m}$	6.3
f_c = ionospheric plasma frequency = $\left(80.614 N_e\right)^{1/2}$	3.3
G_m = geometrical coefficient of m^{th} moment $= \frac{1}{m!} \frac{d^m}{dh^m} \sec(\phi(h)) \Big\vert_{h=h_c}$	5.2
$G'_m = \frac{\partial G_m}{\partial E}$	5.2
h = height	
h_c = expansion center height for moment expansion	5.2
h_m = height of ionospheric layer maximum	7
h_s = satellite height	
h_t = tropospheric scale ht.	4.1
H = relative humidity, %	4.1
H_s = scale height	
i (Subscript) = ionosphere	
m = electron mass, 9.1085×10^{-31} Kg	3.3
M_m = m^{th} refractivity moment = $\int_0^{h_s} (h - h_c)^m N(h)\, dh$	5.2
$n = n_p$ = refractive index (phase)	3.1

LIST OF SYMBOLS, Cont'd.

	Defined in Sec.
n_g = group refractive index = $\frac{d}{df}(fn_p(f))$	3.3
$N \triangleq$ "refractivity $\triangleq n-1$	5.2
N_e electron density, e/m^3	3.3
$N_s = N_o$ = surface refractivity	2.4.1
P = ray path	3.3
P = pressure, millibars	4.1
r = a+h = geocentric radius	
R = true range	3.1
s = geometric path length	3.1
S (Subscript) = pertaining to straight path	3.2
t (Subscript) = troposphere	
t_{pca} = time of point-of-closest-approach	6.5
T = temperature, ^oK	4.1
w (Subscript) = wet	4.1
Y = transfer function	
z = normalized ionospheric height = $\frac{h-h_m}{H_s}$	
α = bending angle defined on Figure 3.2-1	3.2
β = bending angle defined on Figure 3.2-1	3.2
δ = elevation angle of a ray relative to the initial horizontal direction	3.1
$\Delta r_x = \epsilon_x$ = range error = $\rho_x - R$	3.3
ΔR = range error = $\rho - R = \epsilon_\rho$	3.1
ϵ_B = bending error	3.1
ϵ_o = dielectric constant of free space, $\approx \frac{10^{-9}}{36\pi}$ farad/m	3.3
ϵ_R = retardation error	3.1
θ = earth central angle	3.1
ρ = Alouette-GEOS coincidence parameter	2.8

LIST OF SYMBOLS, Cont'd

	Defined in Sec.
ρ_x = apparent radio range	3.3
where x = g (Subscript) group	
p (Subscript) phase	
τ = ionospheric slab thickness	3.2
τ_g = group time delay	3.3
τ_p = phase time delay	3.3
φ = local elevation angle of ray	3.1
Φ = zenith angle	3.2

1. DESCRIPTION OF EXPERIMENT

1.1 Background

The Wallops Island Collocation Experiment (WICE) (also known as the GEOS-II Collocation Experiment) was performed during April, May, and June 1968 as a part of the Observation Systems Intercomparison Investigation (OSII), a subtask of the National Geodetic Satellite Program (NGSP). The general objective of the OSII program is to improve the accuracy and the estimates of accuracy of the geodetic tracking systems through systematic intercomparisons of the data afforded by the several tracking systems involved. The WICE Experiment in particular was designed to perform certain significant comparisons among an extensive array of collocated instrumentation at the Wallops Island Test Facility thus effectively avoiding a number of external error sources in the comparison due to survey errors, gravitational perturbations, orbital perturbations and timing errors.

The wide frequency range covered by the assembled instrumentation along with the availability of various refraction measuring instruments also afforded a unique opportunity for separation and analysis of refraction errors, and a considerable effort was devoted to the analysis, development, and testing through these means of various proposed algorithms for improved, higher-accuracy refraction corrections.

As the program developed the continuing quest for improved refraction correction accuracy led to reanalyses of a number of finer points of the usual assumptions of refraction analysis which are believed to be of some interest for their own sake.

References 5-13 and 16-21 summarize much of the work done on individual tasks under the WICE analysis program. This document is intended to serve as an overall guide to the program by explaining the interrelationships, the principal assumptions, approach and results of the various tasks, referring generally to the task reports where possible for details.

1.2 Objectives

The principal objectives of the WICE were:

- Determination by theoretical and experimental intercomparisons of the practical achievable accuracy limitations of various tropospheric and ionospheric correction techniques.
- Careful examination of the theoretical bases and derivation of improved refraction correction techniques as appropriate.
- Estimation of internal systematic and random error levels of the various tracking systems.

1.3 Organization

The WICE experiment and its subsequent analyses were performed under the overall direction of Mr. John Berbert of NASA, GSFC, Experiment Chairman and NASA Principal Investigator for the OSII. Other personnel instrumental in the final results include

Experiment

H.R.Stanley - NASA Wallops - Wallops Project Coordinator and C-Band Radar Project Manager

Dr. H. Plotkin and T. Johnson - NASA Goddard - Laser Representatives

D.Harris - NASA Goddard - PTH 100 Camera Representative

P.Kuldell - Naval Air Systems Command - Tranet Doppler Representative

R.Vitek, F.Varnum, Dr. F.Rhode, M.Warden - Army Map Service - Secor Representatives

G.Godwin - NASA Wallops - Wallops Project Engineer

C.Leitar - NASA Wallops - C-Band Radar and BC-4 Camera Data Engineer

T.Savage - NASA Wallops - Timing Engineer

J.Spurling - NASA Wallops - Meteorological Engineer

C.Nichols and C.Myers - NASA Goddard - Survey Engineers

Data Reduction and Analysis

H. Parker - RCA - Project Engineer and Technical Information Coordinator

Dr. A. J. Mallinckrodt - Communications Research Laboratories - Refraction Analysis

Dr. A. Tucker - University of Texas Applied Research Laboratory - Tranet Data Analysis

Reference 5 contains details of the WICE experiment organization and operations.

2. DATA DESCRIPTION

2.1 General

The vehicle for these studies was the GEOS-II satellite whose principal relevant characteristics are compiled in Table 2.1.

The principal data sources utilized in the WICE analysis include

- NASA Laser Tracker
- BC-4 and PTh 100 Cameras
- C-Band Radars - FPQ-6 and FPS-16
- SECOR Ranging System
- TRANET System (Including the 3-frequency TRANET)
- Ground Meteorological Instrumentation
- Balloon Sondes
- Bottomside Ionospheric Soundings
  (Wallops, Grand Bahama and Ottowa)
- Topside Ionospheric Soundings
  (Allouette)

TABLE 2.1

GEOS II CHARACTERISTICS

Orbit:	Altitude	≈	1334 km
	Eccentricity	≈	.03
	Inclination	≈	105^{o}
	R.A. Asc Node	≈	275^{o}
	Avg. Perigee		260.3^{o}
	Mean Anomaly		83.6^{o}
	As of Epoch		[illegible]/25/1968

Satellite Instrumentation

- C-Band Transponders (2)
- C-Band Passive Reflector (Retrodirective Array)
- U.S. Navy Doppler Beacon
- Corner-Cube Optical Reflectors
- Optical Beacon
- NASA Minitrack Beacon
- NASA Range and Range-Rate Beacon
- U.S. Army SECOR Beacon

2.2 Laser

The laser tracking system, which was moved to Wallops Island for the duration of this test, was built and operated by the Optical Systems Branch (OSB) of Goddard. This system uses an intense, highly collimated, short-duration beam of light for illuminating the spacecraft being tracked. At the spacecraft, the beam is reflected back towards the ground station by an array of cube corner reflectors. The returning light is detected photoelectrically, and its transit time is measured to yield the range data. The actual laser transmitter is mounted on a radar pedestal along with a Cassegranian telescope used for receiving the reflected laser beam. When the laser system is tracking, the transmitter is flashed at 1 pulse/sec. Each transmitter pulse starts a time-interval-measuring unit necessary for range measurement. During the pass, the mount, equipped with digital encoders, is directed toward the expected position of the spacecraft by a programmer fed with punched paper tape. By using a telescope, the operator can see the spacecraft and make corrections to keep it within the illuminating beam, which is only about 1.2 milliradians wide. Along with a range measurement, both the azimuth and elevation of the spacecraft are recorded from the position mount. At the time of these tests, in 1968, the laser tracking system was probably unbiased to 0.15 meter in range, with a random noise component of about 1.2 meters, and could produce range rates through an orbital fit to the range data which were good to about 1 cm/sec. Now, in 1975, the laser bias and random noise have both been reduced by an order of magnitude. These estimates include all known error sources except the scaling error of 1 part in 10^6 due to the uncertainty in the velocity of light, which affects all systems. Mount angular measurements are recorded but are considered as a secondary measurement since they are dependent on manual tracking.

2.2.1 Laser Data Preprocessing

The OSB personnel were responsible for laser data preprocessing. The preprocessor program accomplishes the following functions:

- Converts the recorded time of observation to the time when the laser pulse was at the spacecraft.

- Computes the range to the satellite from the round-trip time interval values and calibration values.
- Corrects the measured elevation angle for refraction.
- Corrects the computed range for refraction.
- Edits the data based on a five-sigma rejection criterion.
- Reformats the acceptable data points into the required Geodetic Satellite Data Service (GSDS) format and outputs the data on a magnetic tape, with a density of 1 observation per second.

Preprocessing details are contained in Reference 14 and Reference 15. The authors received the WICE laser data from GSDS and conducted this intercomparison study with no additional preprocessing.

222.2 Laser System Calibration

For angle calibrations, a special boresight feature is incorporated in the collimating optics for the transmitted beam, which allows the laser transmitter to be aligned parallel to the opt-mechanical axis of the tracking pedestal. Boresighting is accomplished by firing the laser through a separately attached focusing lens onto a piece of aluminum foil in its focal plane. The reflex viewer, which forms the boresight function on the collimating optics, is then inserted in the optical path, and its cross-hairs are adjusted to coincide with the hole formed in the foil by the focused laser beam. With the focusing lens removed, the reflex viewer is directed along the laser beam and can be used to bring the laser optical axis parallel to the other optical systems on the tracking pedestal.

For range calibrations, the total delay in signal due to telescope optical path length and delay through the photomultiplier tube is measured over a geodimeter calibrated range (3274.98 meters at Wallops) before and after each pass. See Reference 14.

2.2.3 Laser System Timing

The laser data control unit generates all the control signals for operation of the laser and receiver systems. In addition, the unit maintains system time with respect to an external time source such as WWV or, as in the case of WICE, to the Wallops station master clock. This is accomplished by setting the laser control unit. A 1-MHz oscillator, acting as a secondary time standard, is counted to one pulse per second through phase shift and delay circuits for synchronization with the external timing standard. At WICE the laser 1-pps signal is synchronized to about $\pm$0.05 millisecond prior to each pass with the master clock cable signals adjusted for a cable delay bias and the current delay between the Ce standard and the TODG.

The 1-pps signal is then used as the on-time generated pulse throughout the entire data control unit and operates a binary coded decimal (BCD) time code generator whose output is displayed visually as well as recorded through the data select gates for correction with measured range. The rotation prism Q-switch cannot maintain exact synchronism with the on-time pulse, and therefore, the laser may fire from 8.5 to 11 milliseconds after the command time. An uncertainty of this magnitude in the time of observation is not compatible with the accuracy requirements, so a delay time interval counter was incorporated in the data control unit to accurately measure the time of firing with respect to on-time. This counter is started by the on-time and stopped by a signal from the laser beam sample unit, giving the absolute time at which the laser fires to within 100 microseconds. The output of the delay counter is stored and transferred to the data select gates in parallel with the range-time-interval measurement for recording. This value is used in the preprocesser to correct the data time tag.

2.2.4 Laser System Tracking Constraints

The GSFC laser located at Wallops had the following tracking constraints:

- Nighttime at the station (sun 10° below the horizon).
- Satellite maximum elevation angle above 30°.
- Satellite sunlit or lamp flashing for visual acquisition.
- One safety operator at laser station to make visual observation for low-flying aircraft.
- An operational surveillance radar to verify that there were no aircraft within a 14-nautical-mile range.

2.3 SECOR

The SECOR system, developed by the CUBIC Corporation provides a highly accurate modulation ranging multi-lateration system with inherent ionospheric range error estimation and correction. SECOR was operated for WICE and the data preprocessed by the Army Map Service (AMS).

The system utilizes carrier frequencies of 420.9 MHz up and 224.5 and 449.0 MHz down. The difference in measured range on the two (2:1 related) down frequencies provides the ionospheric error estimate. Range is measured by a series of sine wave modulation tones starting with 585.533 KHz and ranging down to 20 Hz for ambiguity resolution. System resolution is 0.25 meter. The geometry is pure ranging multilateration, each ground station interrogating the transponder sequentially and utilizing only the downcoming response to its own interrogation.

2.3.1 SECOR Data Preprocessing

AMS personnel were responsible for SECOR data preprocessing. The preprocessor program accomplishes the following functions:

- Computes the time of observation, which is defined as the time when the pulse was at the spacecraft.
- Makes ambiguity corrections to the edited range measurements.
- Applies calibration values to the edited range measurements.
- Applies tropospheric refraction to the range measurements.
- Uses the difference between ranges measured on the low- and high-frequency carriers from the spacecraft to compute a correction for retardation due to the ionosphere. If

$$M_1 = \text{measured range at } f_1 = 224.5 \text{ MHz}$$
$$M_2 = \text{measured range at } f_2 = 449.0 \text{ MHz}$$

then, since the ionospheric range errors are to first order proportional to Kf^{-2}

$$M_1 = R + Kf_1^{-2}$$
$$M_2 = R + Kf_2^{-2}$$

which can be solved for

$$R = \frac{f_1^2 M_1 - f_2^2 M_2}{f_1^2 - f_2^2}$$

and

$$K = \frac{M_1 - M_2}{f_1^{-2} - f_2^{-2}}$$

or

$$\Delta R_2 = \text{ionospheric error on } f_2$$
$$= M_2 - R$$
$$= Kf_2^{-2}$$
$$= \frac{M_1 - M_2}{\frac{f_2^2}{f_1^2} - 1}$$

The range is corrected for this value, and the ionospheric correction value is included in the output.

- Reformats the data into the required GSDS format and outputs the data on a magnetic tape, with a density of 1 observation per 4 seconds.

2.3.2 SECOR System Calibration

In the calibrate mode, the calibration oscillator generates 196.4 MHz. This is fed to a mixer mounted above the vertical axis of the WICE station dualreflector antenna system and between the up-link and down-link reflectors. A 420.9 MHz ground station up-link carrier frequency is radiated, from the up-link antenna to the mixer, to produce 224.5 MHz and its second harmonic, 449.0 MHz, which are the spacecraft down-link carrier frequencies. These are reradiated to the down-link antenna, providing a closed-loop method of determining approximate zero-set of the range servos prior to each pass. All components in the ground station are inside the calibration loop.

A refinement of the zero-set is made by air link calibration prior to each tracking pass and immediately after each tracking pass. This utilizes a mixer as above and a discone antenna which is 28 meters from the SECOR survey reference mark, and is fed through a cable connected to the ground station.

The difference between the 28-meter surveyed range to the discone and the measured range is recorded on calibration sheets, for both the high- and low-frequency channels, for both precalibration and postcalibration measurements. These calibration numbers are used in the preprocessor to correct the range data.

2.3.3 SECOR System Timing

The WICE SECOR station has a rubidium clock. The rubidium clock was used to operate the time code generators which record UTC time on the magnetic tape with a resolution of 1 millisecond each time the digital servos record the range on the tape.

The Wallops Island range time was derived from an HP 5060A cesium clock, set to UTC (NAVOBS). This clock was periodically transported to the SECOR site in order to check the rubidium clock. The offset between the rubidium clock and UTC (NAVOBS), as recorded on the data logs, was always between 5 and 15 microseconds during the WICE operation.

2.4 TRANET

The TRANET system transmits a set of accurately determined frequencies from the spacecraft and provides one-way doppler measurements to the ground station. TRANET utilizes three harmonically related transmitted frequencies of approximately 162, 324, and 972 MHz to provide ionospheric corrections and, as well, corrected data (doppler frequency) from any two of the three. TRANET was operated during WICE by University of Texas personnel under the direction of the Johns Hopkins Applied Physics Laboratory (APL) and the Naval Air Systems Command. The quantity measured by a TRANET tracking system is the doppler frequency as a function of time.

2.4.1 TRANET Data Preprocessing

The Naval Weapons Laboratory (NWL) personnel were responsible for the TRANET data preprocessing after collection of the data by APL. The TRANET data underwent the following preprocessing: (Ref. 15)

- First-order ionospheric refraction error estimates and corrections are made by analog techniques, using equipment at the tracking station. This correction is based on the assumption that the ionospheric doppler error varies inversely with the carrier frequency so that the corrected doppler shift and the doppler error referred to f_1 are given by

$$f_{D_1} = \frac{f_1 f_2 f_{D_2} - f_1^2 f_{D_2}}{f_2^2 - f_1^2}$$

$$\Delta f_{I_1} = \frac{f_2^2 f_{D_1} - f_1 f_2 f_{D_2}}{f_2^2 - f_1^2}$$

- The time of observation is computed. This is defined as the observed time, at the station, of the midpoint of the doppler integration interval. The calibration value (offset of the TRANET station clock from the Wallops Island cesium clock) is used to correct the observation time to UTC (NAVOBS).
- The observation frequency is corrected for the error in the station frequency standard determined from VLF comparisons.
- A spacecraft reference frequency (base frequency) is computed for the pass.
- The data are edited based on a 2.5-sigma rejection criterion.

- The remaining observations are aggregated in groups of eight, covering a 32-second interval. A smoothed frequency value is calculated by fitting a straight line to the residuals in the 32-second interval and evaluating the fit at the central time of the interval. The residual corresponding to the fit at the central time is then added to the computed frequency for that time. These data are run through a reformat pregram which arranges the filtered data into the format required by the GSDS. All smoothed frequency values and the base frequency for each pass are scaled to 108 megacycles by multiplying by $\frac{108 \times 10^6}{fe}$, where fe is the nominal equivalent frequency obtained from a table and approximates the frequency out of the station refraction corrector unit.

The TRANET are the only type of data which undergo mathematical smoothing in these intercomparisons.

The WICE TRANET data was further processed at Goddard through the following additional preprocessing steps prior to intercomparisons with the other systems.

- Conversion of the recorded time of the observation from observed time at the station to the time the signal was at the satellite by subtracting one-half of the round trip time.

- Conversion to range rate values in meters/sec by the following

$$\dot{R} = \frac{c\,(F_B - F_M)}{F_M}$$

where F_B = Base frequency received from NWL

F_M = Smoothed measured frequency received from NWL

c = Velocity of light

$= 2.997925 \times 10^8$ m/s

- Correction for tropospheric refraction, using the formula

$$\Delta\dot{R}_T = -\frac{8432.336\, N_s \dot{E} \operatorname{Cos} E}{(\operatorname{Sin} E + .026)^2}$$

$\Delta \dot{R}_T$ = correction (cm/sec) to add to $\dot{R}$

N_S = ground refractivity, $(\mu - 1)$

E = elevation angle

$\dot{E}$ = elevation angle rate (radians/sec)

2.4.2 TRANET System Calibration

The station frequency error which appears in the doppler data header in the teletype to APL is the departure of the frequency of the station standard as determined from a known (VLF) reference frequency. This known correction is applied, in the NWL preprocessing program, to the frequency measurements.

A nominal value of the satellite oscillator frequency is associated with each spacecraft but is modified for each pass as follows. First, NWL computes O-C's by comparing the VLF corrected doppler frequency measurements with the doppler frequencies predicted from a reference orbit. The reference orbit is determined with previous doppler data from the entire TRANET network. The O-C's are then used to compute an estimated frequency bias for each pass. The spacecraft oscillator nominal frequency corrected for this bias is called the base frequency and is included, as an additional number, with the frequency measurements submitted to the GSDS for each pass.

Since the determination of the base frequency involves the entire TRANET network, the WICE TRANET data are influenced by this network. Data submitted from the other WICE systems are not influenced by any other stations.

2.4.3 TRANET System Timing

The station clock error accompanying the doppler data in the teletype to APL combines the station clock offset from the received Wallops Island pulse, the cable delay, and offset of the Wallops Island working clock (TODG) from the cesium clock. The doppler data submitted to GSDS are referenced to the Wallops Island cesium clock which is set to UTC (NAVOBS).

2.4.4 Three-Frequency Data

In addition to the above described "standard" TRANET data there were made available through the University of Texas, separately received and recorded three-frequency "Geoceiver" data. From this data it is possible to derive explicitly both the ionospheric corrected data and the ionospheric correction, per se, by the equations given above.

2.5 C-Band

Data were received from two C-band radars operated by Wallops Island, the AN/FPQ-6 and the AN/FPS-16. Both are pulsed radars capable of non-ambiguous range measurements of up to 32,000 nautical miles, and each provides azimuth and elevation angle measurements to the target. The FPQ-6 radar can also measure range rate ($\dot{R}$) if used with a coherent transponder or if the reflected signal from the spacecraft is strong enough for skin tracking. A passive retro-directive Van Atta array on GEOS-2 makes it possible for the FPQ-6 radar to skin-track this spacecraft.

Two C-band beacons were installed in GEOS-2. Beacon #1 has a 0.7-μsec fixed nominal delay, and beacon #2 has a 5-μsec fixed nominal delay.

The FPQ-6 radar's subsystems may be functionally grouped under signal detection (transmitter, antenna, and receiver), target acquisition, target tracking (range and angle servos), data processing, and system control. An ultrastable frequency-synthesizer-multiplier chain, power amplifier, and hard-tube modulator form the C-band transmitter. The antenna comprises a solid-surface 29-foot parabolic reflector illuminated by a monopulse, polarization-diversity cassegrainian feed. This structure is supported by a 2-axis (azimuth-elevation) pedestal featuring a low-friction hydrostatic azimuth bearing, anti-backlash drive gearing, and precision single-space 20-bit angle-shaft encoding subsystem. The angle, or antenna-positioning, subsystems are high torque-to-inertia electrohydraulic servo loops. Tracking signals are supplied to the antenna-positioning and ranging servos by a low-noise, broad-band, 3-channel receiver subsystem. An all-electronic digital ranging subsystem affords unambiguous range coverage to 32,000 nautical miles at high-pulse-repetition rates, with a granularity of 2 yards. The data system contains a 4096-word coincident-core, bus-organized, stored-program, militarized computer (RCA, FC-4101).

The FPS-16 radar is very similar to the FPQ-6 except that it has a 17-bit angle encoder and a 12-foot parabolic reflector and does not have a computer and skin track capability.

2.5.1 C-Band Data Preprocessing

The following preliminary preprocessing is done by Wallops Island:

The on-site RCA 4101 computer program for the AN/FPQ-6 was used to apply the static corrections (pedestal mislevel, droop, nonorthogonality, encoder bias, encoder nonlinearity, and skew) to the raw FPQ-6 data, but not to the FPS-16 data. Dynamic lag corrections calculated by the 4101 program are recorded, but are not applied to the data. The 4101 FPS-16 raw data tapes were processed through the Wallops preprocessing program which applies a time tag correction to the data, converts the data from radar bits to range in feet and azimuth and elevation in decimal degrees, and reformats the data from 4101 format to the standard GEOS-B radar data format, sometimes called the modified Calsat format.

WICE-C-band data in the modified Calsat format were sent to the Principal Investigator, GEOS OSII. These data were then additionally preprocessed by the WICE-C-band preprocessor program at Goddard, which does the following:

- Computes the time of observation, which is defined as the time when the pulse was at the spacecraft.
- Applies tropospheric refraction corrections to both the range and angle measurements.
- Reformats the data to a format compatible with the GEOS data adjustment program (GDAP). (Editing is done by hand after residuals are obtained with GDAP against the laser reference orbit.)
- Selects every Nth point (one per second).
- Applies range bias corrections derived from the appropriate nominal beacon delay and from the pre- and post-pass range target measurements.

2.5.2 C-Band System Calibration

For pre- and postmission calibration, data tape recorders are run for approximately 10 seconds (at 10 samples/second, this gives approximately 100 samples), recording each of the following:

- Selected AGC values.
- Boresight tower (BST) normal - Antenna electrically locked to the BST in azimuth and elevation.
- Boresight tower plunged - Same set-up as for BST normal, except the antenna is in the plunged mode.
- Range target, skin gate - (If transponder track is planned, the proper delay compensation should be set into range system prior to this step.) Lock on range target in skin gate. Range displays and recordings should read the surveyed range to the range target.
- Range target, beacon gate - Range displays and recordings should read the surveyed range to the range target minus the proper delay compensation.

2.5.3 C-Band System Timing

The received pulse from the Wallops master clock is used by the C-band systems to time-tag the range, azimuth, and elevation data. The circuitry and cable transmission delays bias the time tag by +5.90 milliseconds for the FPQ -6 and +1.05 milliseconds for the FPS-16. These known biases are accounted for in the Wallops program by adding them to the recorded data time tags to give UTC time.

The delay between the Wallops Ce Standard and TODG (200 $\pm$ 100 µsec) has not been included thus far in the C-band data time tag corrections. However, these variations are measured and recorded daily at the master site by direct comparison of the TODG oscillator and the cesium beam standard, so the proper correction to the time tag can be applied at some future date.

2.6 Cameras

Data were taken on GEOS-2 flashes from four BC-4 cameras operated by Wallops Island and one PTH-100 camera operated by Goddard. These data were utilized in addition to the laser data as a primary reference in the derivation of GEOS reference orbits.

2.7 Meteorological Instrumentation

Ground measurements consisting of Temperature, Pressure, and Relative Humidity were recorded from measurements at the FPQ-6 radar site for each pass. Estimated accuracy of these measurements is

- Pressure $\pm$ .01 " Hg
- Temperature $\pm 1.0^{\circ}$F
- Relative Humidity $\pm$ 1% to $\pm$ 3%

Radiosondes were released for P,T, and RH profiles within 10 minutes of the start of each pass. Altogether some 93 such profiles and associated ground level measurements are available. These have been reduced to refractivity, ray traced, and utilized as the basis for various comparative studies discussed in section 4.

2.8 Ionospheric Soundings

Routine periodic (generally 15 minute) bottomside ionospheric soundings were available throughout the WICE experiment from stations at Wallops Island, Ottowa, and Grand Bahama.

In addition, near coincident Alouette 1 and 2 topside soundings were available for some passes at randomly related time and positional (Point-of-Closest-Approach) differences relative to the GEOS-2 passes. In order to select reasonably "coincident" passes a somewhat arbitrary measure of correlation was defined in terms of the expected time and positional correlation scales and discrepancies as follows:

$$\rho = \exp(-\Delta T/2)\exp(-\Delta R/3000)$$

where ΔT = time difference of POCA, hours

ΔR = distance between POCA's, miles advanced or retarded to common time at sun line rate. Differences are between GEOS-2 and either Alouette 1 or Alouette 2.

17 passes were thus identified having $\rho > 0.4$ and these were taken as the standard ionospheric test cases for future analyses. These are identified in Table 2-2.

TABLE 2-2

ALOUETTE-GEOS 2 COINCIDENCES

WICE ION. PASS #	DATE MM DD	TIME HH MM	ρ
1	0403	0143	0.41
2	0405	0222	0.79
3	0410	0207	0.85
4	0412	0245	0.55
5	0417	0231	0.55
6	0422	1743	0.58
7	0524	0320	0.99
8	0525	0339	0.92
9	0529	0306	0.71
10	0530	0325	0.69
11	0604	0312	0.49
12	0605	0331	0.47
13	0611	1715	0.70
14	0613	1753	0.66
15	0618	1739	0.65
16	0621	0458	0.56
17	0625	0425	0.75

3. RAY TRACING

3.1 REEK Program

Since it is used as a standard in many of the refraction comparisons to be used in ensuing sections we describe in this section the basic ray-trace program, REEK (Ref. Trimble 1970), used in these studies and later some investigations of fine points with regard to its use.

The problem addressed is that of determining the phase path, its bending, and phase path length in a spherically symmetrical refractive medium with arbitrarily specified refractive index vs height profile (assumed isotropic).

REEK solves the differential equations for the phase path (wavefront normals) in the form:

$$\frac{d\theta}{ds} = \frac{\cos\varphi}{r+h} \qquad (3.1\text{-}1)$$

$$\frac{dh}{ds} = \sin\varphi \qquad (3.1\text{-}2)$$

$$\frac{d\delta}{ds} = \frac{1}{n_p}\frac{dn_p}{dh}\cos\varphi \qquad (3.1\text{-}3)$$

$$\frac{d\rho}{ds} = n_p \qquad (3.1\text{-}4)$$

$$\varphi = \theta + \delta$$

where (see Figure 3-1)

- s = geometric path length
- θ = earth central angle subtended by path
- ρ = effective radio phase path length
- h = height
- δ = elevation angle of ray relative to horizontal at takeoff point
- n_p = phase refractive index
- φ = local elevation angle of ray

These equations are solved by numerical methods, subject to the following boundary conditions:

$$\left.\begin{aligned} \theta(0) &= 0 \\ h(0) &= 0 \\ \rho(0) &= 0 \end{aligned}\right\} \quad \text{starting at ground receiver}$$

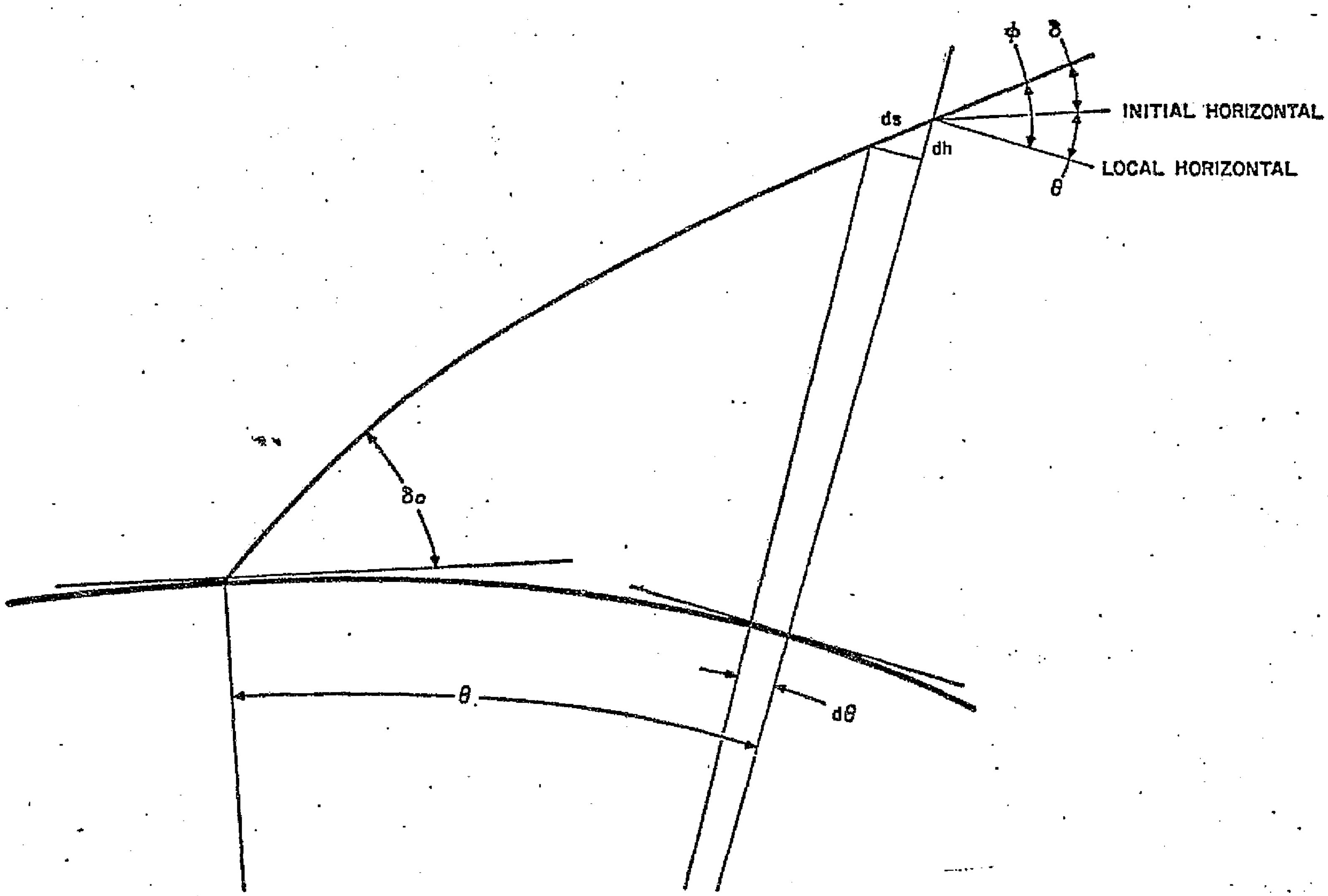

FIGURE 3.1-1

RAY TRACING GEOMETRY

$$\left.\begin{aligned} \theta(s_1) &= \theta_t \\ h(s_1) &= h_t \end{aligned}\right\} \quad \text{target coordinates} \tag{3.1-5}$$

The last two are equivalent to saying that for some s_1, initially unspecified, the ray should pass through the prescribed target coordinates. REEK inputs are in terms of either true or apparent elevation angle or range. In the case of apparent inputs the solution is straightforward starting the ray with initial conditions corresponding to apparent elevation angle and integrating until apparent range is reached. In the case of true inputs, the program uses a fast converging iterative method to find the initial ray angle corresponding to the specified end point coordinates.

To achieve maximum numerical accuracy, the equation for ρ, given in eq. 3.1-4 is decomposed by defining

$$\varepsilon_\rho \triangleq \rho - R \tag{3.1-6}$$

where ε_ρ = total phase path error

R = true range

$$\varepsilon_\rho = \underbrace{(s - R)}_{\varepsilon_B} + \underbrace{(\rho - s)}_{\varepsilon_R} \tag{3.1-7}$$

where the first term is defined as

$$\varepsilon_B \triangleq s - R = \text{phase path bending error}$$

$$\varepsilon_R \triangleq \rho - s = \text{phase path retardation error}$$

and both ε_B and ε_R are small quantities and can therefore be numerically integrated more accurately. Note that the solutions for the bending and retardation terms could be written, once the path (P) is found, by solution of eqs.(3.1-1) - (3.1-3)

$$\varepsilon_B = \int_P ds - R \tag{3.1-8}$$

$$\varepsilon_R = \int_P (n_p - 1)\, ds \tag{3.1-9}$$

One minor modification was incorporated in the REEK subroutine for the present program. In the original version, refractivity in or above the ionosphere was extrapolated linearly which in some cases resulted in refractivity going through zero to the opposite sign. In order to improve the accuracy and eliminate any such problem, the routine was changed to use exponential interpolation or extrapolation above the top of the ionosphere (Ref. 21).

3.2 Straight Path Approximation

For some purposes it is reasonably accurate to ignore bending and approximate the ray path by the geometrical straight line from transmitter to receiver. The computations under this approximation are greatly simplified. In order to gain some understanding of the limitations of this approximation and for other uses to be developed later it is useful to consider a simplified ionospheric model for which the exact and straight line approximate solutions can be written analytically.

For this purpose the ionosphere is modelled as a simple planar uniform slab as shown in Figure 3.2-1 where

h = height of satellite

τ = thickness of ionosphere slab

N = refractivity (phase) of ionospheric slab = $n - 1$

E = $90^{\circ} - \varphi$ = elevation angle geometric line-of-sight.

The exact analytic solution for bending and range errors can be developed for this model (Ref. 6). If we let

R_x denote geometrical path length of some path x

ρ_x denote refractivity integral along some path x

S subscript, denotes straight path

B subscript, denotes bent path

p,g subscript, denote phase or group respectively.

Then we can define four types of "range" of interest

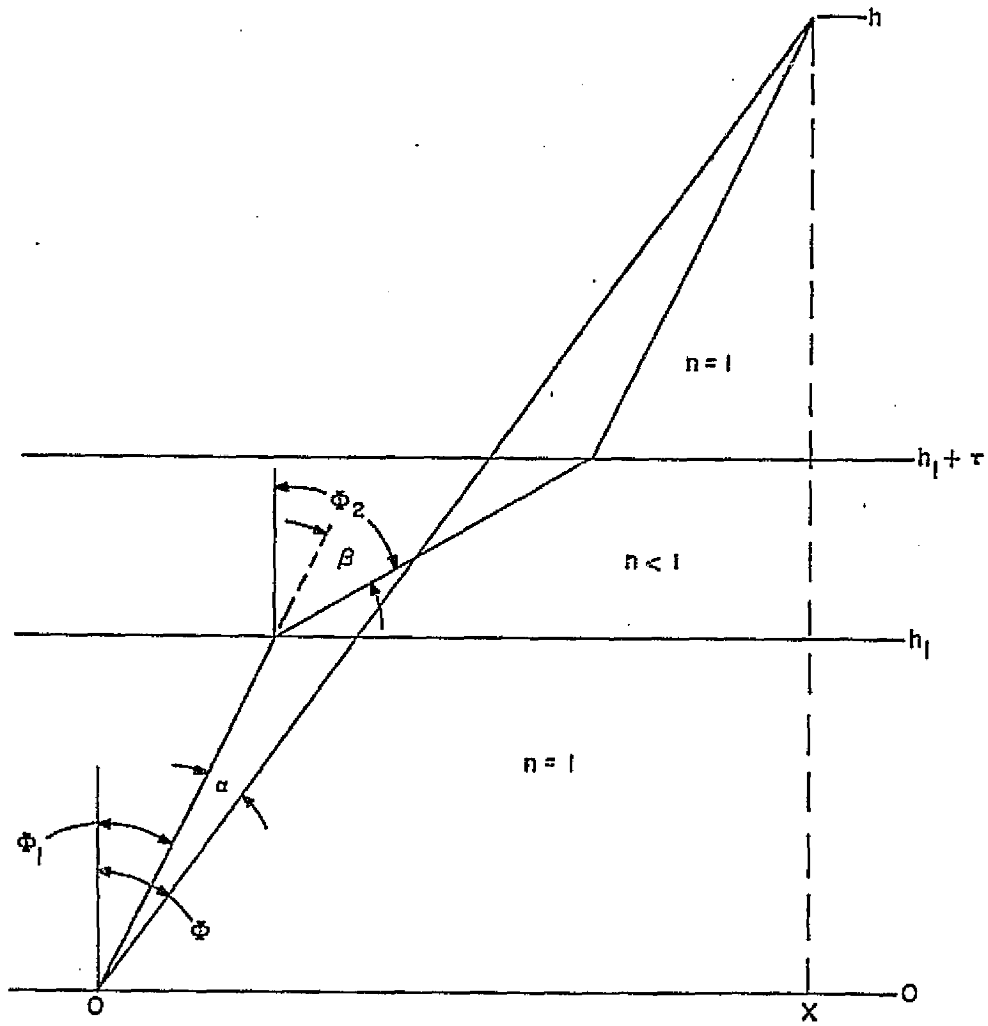

$\Phi_1 = \Phi - \alpha$

$\Phi_2 = \Phi_1 + \beta$

$\Phi_2 = \Phi - \alpha + \beta$

FIGURE 3.2-1

IDEALIZED IONOSPHERE
STRAIGHT AND BENT PATHS

$$R = \int_S ds = \text{true geometrical range}$$

$$\rho_{p_S} = \int_S n_p \, ds = \text{radio range using the phase refractivity integral along the straight path}$$

$$R_{B_p} = \int_{B_p} ds = \text{Geometrical length of the bent phase path}$$

$$\rho_p = \rho_{p_{B_p}} = \int_{B_p} n_p \, ds = \text{radio-range using the phase refractivity integral along the bent phase path. This is what the measuring system actually senses.} \qquad (3.2\text{-}1)$$

$\rho_{p_{B_p}}$ is, of course, the actual measured radio range while ρ_{p_S} is an often used approximation. R_{B_p} is equivalent to s, the variable of integration in the REEK formulation

Phase Path

From Snell's law and the geometry, approximate solutions for the bending angles defined in Figure 3.2-1 may be developed as power series in N:

$$\beta = -N \tan\Phi + N^2 \tan\Phi \left[1 - \frac{\tan^2\Phi}{2} - \frac{T}{h}\left(1 + \tan^2\Phi\right)\right] + O_3 \qquad (3.2\text{-}2)$$

$$\alpha = -\frac{T}{h} N \tan\Phi + N^2 \frac{T}{h} \tan\Phi \left[1 + \frac{3}{2}\tan\Phi - \frac{T}{h}\left(1 + 2\tan^2\Phi\right)\right] + O_3 \qquad (3.2\text{-}3)$$

where $O_j = O(N^j)$ denotes neglected terms of order N^j and higher.

Then for the various path integrals as defined

$$R = h\sec\Phi \tag{3.2-4}$$

$$\rho_{p_S} = R + N_p \tau \sec\Phi \tag{3.2-5}$$

$$R_{B_p} = R + \frac{N_p^2 \tau}{2}\left(1 - \frac{\tau}{h}\right)\tan^2\Phi \sec\Phi + O_3 \tag{3.2-6}$$

$$\rho_{p_{B_p}} = R + N_p \tau \sec\Phi - \frac{N_p^2 \tau}{2}\left(1 - \frac{\tau}{h}\right)\tan^2\Phi \sec\Phi + O_3 \tag{3.2-7}$$

It is interesting to note that the error due to ignoring bending is

$$\begin{aligned}(\rho_{p_{B_p}} - \rho_{p_S}) &= -(R_{B_p} - R) \\ &= -\frac{N_p^2 \tau}{2}\left(1 - \frac{\tau}{h}\right)\tan^2\Phi \sec\Phi\end{aligned} \tag{3.2-8}$$

i.e., the bending reduces the measured radio path length, $\rho_{p_{B_p}}$, relative to the straight path integral by just the same amount that it increases the geometrical path length, and this reduction or increase is strictly a second order, N^2, term. The N^2 dependent term may legitimately be called a bending term since it occurs only in connection with the bent paths and reduces to zero for a case of normal incidence ($\Phi = 0$) where there is no bending.

Group Effects

It is possible to carry one interesting step further and examine group effects in the same model for, quite generally, the group measured range is related to the phase measured range by

$$\rho_g = \frac{d}{df}(f \rho_p) \tag{3.2-9}$$

For the purposes of this example we will assume that the ionospheric refractivity follows a perfect f^{-2} dispersion law. Accordingly

$$N_p = -Kf^{-2} \tag{3.2-10}$$

and from (3.2-7), recognizing that $\rho_p \equiv \rho_{p_{B_p}}$

$$\boxed{\rho_g = R - N_p \tau \sec\Phi + \frac{3}{2} N_p^2 \tau (1 - \frac{\tau}{h}) \tan^2\Phi \sec\Phi + O_3} \qquad (3.2\text{-}12)$$

Note, interestingly, the same result is obtained if we were to integrate the group refractivity along the phase bent path, as is commonly done, for example in REEK, i.e.,

$$\begin{aligned}
\rho_{g^{B_p}} &= \int_{B_p} n_g \, ds \\
&= \int_{B_p} (1+N_g)\, ds \\
&= \int_{B_p} (1-N_p)\, ds \\
&= R - N_p \tau \sec\Phi + \frac{3}{2} N_p^2 \tau (1 - \frac{\tau}{h}) \tan^2\Phi \sec\Phi + O_3 \qquad (3.2\text{-}13)
\end{aligned}$$

which is identical to (3.2-12).

Similarly we can derive

$$\begin{aligned}
\rho_{g^S} &= \frac{d}{df}(f\rho_{p^S}) \\
&= R - N_p \tau \sec\Phi \qquad (3.2\text{-}14)
\end{aligned}$$

and thus the difference between the straight and bent path computations is

$$\boxed{\rho_{g^S} - \rho_{g^B} = -\frac{3}{2} N_p^2 \tau (1 - \frac{\tau}{h}) \tan^2\Phi \sec\Phi} \qquad (3.2\text{-}15)$$

This difference is so small that it can often be ignored for practical purposes. In terms of the ratio of errors computed in the two ways

$$\frac{\Delta R_{g^B}}{\Delta R_{g^S}} = \frac{\rho_{g^B} - R}{\rho_{g^S} - R}$$

$$\boxed{= 1 - \frac{3N_p}{2} (1 - \frac{\tau}{h}) \tan^2\Phi} \qquad (3.2\text{-}16)$$

To illustrate the error in the straight path assumption with a numerical example for the ionosphere, consider a case where

$$\tau = 293.57 \text{ km}$$
$$h = 1333 \text{ km}$$
$$f = 434 \text{ MHz (SECOR effective two-way frequency)}$$
$$f_o = 5.653 \text{ MHz} = \text{vertical incidence critical frequency}$$

so

$$N = -\frac{1}{2}\left(\frac{f_o^2}{f^2}\right)$$
$$= -84.84 \times 10^{-6}$$

Then as a function of Φ, we have from equation (3.2-16)

Elevation Angle at Ionosphere E_i, Degrees	$\Delta R_{g_B}/\Delta R_{g_S}$	
90	1	← (vertical ray - no bending)
45	1.000099	
20	1.000749	

There is no need to consider E_i less than 20^o, since the elevation angles in the real spherical ionosphere cannot be much less.

As a further check of the straight path assumption in a less idealized case a numerical comparison of the straight and bent path integrals for a spherical earth was carried out for a Chapman ionosphere with a maximum refractivity ($N_{max} = -84.84 \times 10^{-6}$) and the satellite at 1333 km. The straight path integral was carried out by a specially developed straight line raytrace program using a simple trapezoidal integrator and the bent path integral was carried out by the REEK raytrace program, modified for group range errors. The resulting differences between the outputs of these two programs are presented in Table 1. The difference, at most, is 0.11 meter out of 73 meters total refraction, or 0.15%, and is in reasonable agreement with the simple theory of the difference, equations (3.2-15,16), at low elevation angles, but is dominated at the higher elevation angles by a bias of about 0.04 m, presumably due to difference in the REEK and straight line integration formulas. These results are taken as confirming the approximate equations (3.2-15 and (3.2-16).

Table 3.2-1. Difference Between Straight Line Raytrace (ΔR_{g_S}) and REEK Raytrace (ΔR_{g_B})

Elevation (degrees) ($E = 90 - \phi$)	ΔR_{g_B} (meters)	$\Delta R_{g_S} - \Delta R_{g_B}$ (meters)	
		Numerical	Theoretical (eq. 3.2-15)
0.1	73.336	- 0.1140	- 0.0621
1	73.245	- 0.1122	- 0.0618
10	65.812	- 0.0715	- 0.0432
20	52.960	- 0.0424	- 0.0199
40	35.911	- 0.0355	- 0.0039
60	28.311	- 0.0395	- 0.0008
80	25.360	- 0.0428	- 0.000069
89	25.027	- 0.0434	- 0.0000006

The above is based on a spherical earth and a Chapman profile where

$$N = N_{max} \exp(1 - z - e^{-z})$$

$$z = \frac{h - h_{max}}{H_s}$$

$$N_{max} = -84.84 \times 10^{-6}$$

$$h_{max} = 375 \text{ km}$$

$$H_s = 108 \text{ km}$$

$$h_{sat} = 1333 \text{ km}$$

The figures in the theoretical column are based on equation (3.2-15) corrected for angle of incidence at 375 km, and using

$$\tau = 108\, e = 293.57 \text{ km}.$$

For the troposphere with

$$\tau = 7 \text{ km}$$
$$h_s = 1333 \text{ km}$$
$$N = 350 \times 10^{-6}$$

we have from equation (3.2-15) (using the positive sign for N_p in the troposphere)

Elevation Angle E_t, degrees	ΔR_{g^B} (meters)	$\Delta R_{g^B} - \Delta R_{g^S}$ (meters) (eq'n. 3.2-15)	$\frac{\Delta R_{g^B}}{\Delta R_{g^S}}$
2	100.26	30.06	.7001
3	55.71	8.90	.8402
4	38.87	3.75	.9035
5	30.02	1.91	.9361
10	14.34	.23	.9834
20	7.19	.03	.9960

Thus for accuracy of the order of 2% or .2 m which is near the limit of correction accuracy for the troposphere the straight line assumption is limited to elevation angles of 10^0 or greater. This is a severe limitation on the applicability of any approach ignoring bending in the troposphere.

3.3 Group vs Phase Effects

Basic Relations

In the ionosphere, the index of refraction is a function of frequency, i.e., dispersive and modulation or group effects travel at a different velocity and are subject to different overall delays than phase effects.

In general, between any two points in a linear network, the group and phase delays are related by the classical relation

$$\tau_g = \frac{d}{df} (f \tau_p) \tag{3.3-1}$$

which may be taken as defining the group delay.

Since inferred range (group or phase) is proportional to τ ($\rho = \tau c$), then, irrespective of the inhomogeneity or path taken in the intervening medium, the same relation holds between group and phase range

$$\rho_g = \frac{d}{df}(f \rho_p) \tag{3.3-2}$$

In principal, this provides a precise basic means of determining group range error from any accurate ray tracing program by numerical differentiation of the terminal, i.e., end-to-end phase range error results as a function of frequency. In practice, however, this involves several times as much computation as a single ray trace and is subject to the numerical problems characteristic of numerical differentiation so a more direct means is desirable for routine work.

For the ionosphere at UHF and higher frequencies it is a fair approximation (with error to be discussed later) to ignore magneto ionic and collision effects and take the refractive index in the form

$$n_p \approx \sqrt{1 - \frac{f_o^2}{f^2}} \tag{3.3-3}$$

where f_o^2 = local plasma frequency

$$= \frac{e^2}{4\pi^2 m \epsilon_o} N_e$$

$$= \frac{10^{-7} c^2 e^2}{\pi m} N_e$$

$$= 80.614 N_e \tag{3.3-4}$$

Consequently

$$n_g \approx \frac{d}{df}(f n_p)$$

$$\approx \frac{1}{n_p} \tag{3.3-5}$$

But since $n_g = 1+N_g$, $n_p = 1+N_p$ with N_g, N_p small in the region of interest,

$$N_g \approx -\frac{N_p}{1+N_p} \tag{3.3-6}$$

$$\approx -N_p \tag{3.3-7}$$

$$\approx \frac{f_o^2}{2f^2}$$

The difference between these alternative approximations is in any case significantly less than the error in either of them due to neglect of the longitudinal magneto-ionic term.

The deviations from these simple approximate relationships may be significant in at least two respects:

1) The $1/f^2$ term is subject to higher order corrections the most significant of which adds an f^{-3} dependence proportional to the main term times the ratio of longitudinal gyro frequency to carrier frequency, or as much as 2% correction at 100 MHz (Ref. 6).

2) Bending, ignored in the above analysis, introduces an f^{-4} dependence which may amount to $\approx 0.8\%$ of the main term at 100 MHz (Ref. 6).

It is estimated that the simple relation

$$\varepsilon_g = -\varepsilon_p \tag{3.3-9}$$

is accurate to within a fraction $(2/f_{MHz})$ for frequencies above 100 MHz which is useful for many purposes.

It is worthy of note that while ray tracing programs such as REEK are capable of taking into account the f^{-4} bending term quite accurately, the much more significant f^{-3} term ($\approx 2\%$ at 100 MHz) cannot be treated by any of the known operationally practical ray trace programs because that term is inherently anisotropic and birefringent, i.e., allows two, generally coupled, magneto-ionic modes, and requires a considerably more complex treatment dependent on antenna polarizations among other things.

REEK Group Option

The REEK ray trace program includes an option for group range error computed as follows: Recall from section 3.1 that REEK computes the total retardation on the basis

$$\epsilon_p = \epsilon_{R_p} + \epsilon_{B_p} \tag{3.3-10}$$

where ϵ_{R_p} = phase retardation error

$$= \int_p (n_p - 1)\, ds \tag{3.3-11}$$

ϵ_{B_p} = phase bending error

$$= \int_p 1\, ds - R \tag{3.3-12}$$

p = the phase path.

For the group option REEK takes

$$\epsilon_g = \epsilon_{R_g} + \epsilon_{B_g} \tag{3.3-13}$$

where $\epsilon_{R_g} = \int_p (n_g - 1)\, ds$

$$\epsilon_{B_g} \triangleq \epsilon_{B_p} = \int_p 1\, ds - R \tag{3.3-14}$$

$$n_g - 1 = N_g = -\frac{N_p}{1 + N_p} \tag{3.3-15}$$

whereas

$$\epsilon_{B_g} = \epsilon_{B_p}$$

That is the group retardation is computed by integration along the phase path, in effect REEK computes

$$\rho_B = \int_p n_g\, ds \tag{3.3-16}$$

Proof of the Group Option Procedure

This can be justified hueristically on the following basis:

Starting with the phase range as a function of frequency

$$\rho_p(f) = \int_{\bar{P}(f)} n_p(f)\, ds \tag{3.3-17}$$

where $\bar{P}(f)$ the path, is, by Fermat's principle, an extremal. In other words, considering an arbitrary path deformation, $\bar{\delta}(s)$ (subject to the constraint that the deformed path still passes through transmitter and receiver) then if $\bar{P}' = \bar{P}+\lambda\bar{\delta}$ where λ is an arbitrary multiplier, then the integral over the deformed path

$$\rho' = \int_{\bar{P}+\lambda\bar{\delta}} n_p ds \tag{3.3-18}$$

must satisfy

$$\left.\frac{\partial\rho'}{\partial\lambda}\right|_{\lambda=0} = 0 \tag{3.3-19}$$

for any $\bar{\delta}$ satisfying the end constraints (i.e., $\bar{\delta} = 0$ at the ends).

Now the group range is given exactly from (3.3-17) by the general relation

$$\rho_g(f_o) = \frac{d}{df}(f\rho_p(f)) \tag{3.3-20}$$

Expanding the path $(\bar{P}(f)$ about f_o we can write

$$\bar{P}(f) = \bar{P}(f_o) + (f-f_o)\frac{d\bar{P}(f)}{df} + O(f-f_o)^2 \tag{3.3-21}$$

whence, denoting $f-f_o$ by λ,

$$\rho_g(f_o) = \int_{\bar{P}(f_o)} \left.\frac{d}{df}(fn_p(f))\right|_{f_o} ds + \frac{d}{d\lambda} \left. \int_{\overbrace{\bar{P}(f_o)+\lambda\frac{d\bar{P}(f)}{df}+O(\lambda^2)}} fn_p(f_o)\, ds \right|_{\lambda=0} \tag{3.3-22}$$

but since the path variation $\frac{d\bar{P}(f)}{df}$ inherently satisfies the end conditions, that is, it is an allowed variation of the form $\bar{\delta}(s)$, the path variation of the integral, i.e., the second term above must vanish identically by the extremal principal (eq. 3.3-19) and we have just

$$\rho_g(f_o) = \int_{\bar{P}(f_o)} n_g(f_o)\, ds \tag{3.3-23}$$

i.e., we have the interesting result that the group range is given by the integral of the group refractivity along the phase path. This may be taken as a definition of the group path and in this sense it may be said that the group path is identical to the phase path in any such arbitrarily inhomogeneous dispersive (but isotropic) medium.

Numerical Tests of the Group Option

As a check on these group-phase relationships a numerical comparison was carried out (Ref. 6) between the REEK derived group range correction as described previously and the theoretically exact procedure of deriving group range error by numerical differentiation of REEK derived phase range error as a function of frequency. For these tests a hypothetical Chapman ionosphere was assumed leading to an assumed refractivity profile of the form

$$N(h) = N_{max} \exp(1 - z - \exp(-z)) \tag{3.3-25}$$

where
$$N_{max} = -\frac{16 \times 10^{-6}}{f^2_{GHz}}$$
$$z = (h - h_m)/H_s$$
$$h_m = 375 \text{ km}$$
$$H_s = 108.333 \text{ km}$$

The REEK phase range error was evaluated at $f = .136$, $.434$, and 2.0 GHz at various elevation angles.

In view of the assumed f^{-2} refractivity dependence it can be shown by the Poincare expansion theorem (Ref. 4, Lefschetz) that any integro-differential function thereof such as ε_p has an expansion in powers of f^{-2}:

$$\begin{aligned} \varepsilon_p(f) &= a_1 f^{-2} + a_2 f^{-4} \ldots \\ &\triangleq A_2 + B_4 \ldots \end{aligned} \tag{3.3-26}$$

where we define

$$A_2 \triangleq a_1 f^{-2}$$

$$B_4 \triangleq a_2 f^{-4}$$

In principle then we can solve for the phase ranging error, ε_p, in a ray tracing program such as REEK at several frequencies, then carry out a numerical fit to identify the frequency coefficients a_1, a_2 or A_2 and B_4 above, then differentiate by 3.3-2 to give the corresponding derived group error

$$\varepsilon_{g_{der}} = -A_2 - 3B_4 \tag{3.3-27}$$

For precise comparison with REEK group option results, however, it is necessary to take into account that REEK uses the approximation (3.3-15) or (3.3-6) for $N_g \left(N_{g_a} \approx -\dfrac{N_p}{1+N_p} \right)$ while for the f^{-2} three frequency REEK results the basic refractivities were scaled in the ratio f^{-2}, i.e., $N_p = Kf^{-2}$, corresponding to the approximation (3.3-7) ($N_{g_b} \approx -N_p$). Expanding (3.3-6)

$$\begin{aligned} N_{g_a} &\approx -N_p(1 - N_p \ldots) \\ &\approx N_{g_b} + N_p^2 = -N_p + N_p^2 \end{aligned}$$

So the range error difference on this account is equivalent to a term N_p^2 integrated over the path. That is

$$\varepsilon_{R_{g_a}} = \varepsilon_{R_{g_b}} + H_4$$

where for the Chapman profile as defined above this is approximately (plane earth approximation)

$$\begin{aligned} H_4 &\approx \int_p N_p^2 \, ds \\ &\approx N_{max}^2 \frac{e^2}{4} H_s \operatorname{Csc} E \end{aligned} \tag{3.3-28}$$

This is an f^{-4} term as it depends on N_{max}^2.

The corresponding derived group error is then

$$\varepsilon_{g_{der}} = -A_2 - 3B_4 - 3H_4$$

$$= -\varepsilon_p - 2B_4 - 2H_4 \qquad (3.3\text{-}29)$$

Which may be compared directly with the group option computed result. The comparison is shown in Table 3.3-1 in which the columns have the following significance

A ε_p = REEK phase ranging error, meters

B $2B_4$ = 2 x quadratic fit component of A

C $2H_4$ = 2 x refractivity approximation correction, per eqtn. (3.3-28)

D $\varepsilon_{g_{der}}$ = derived group error, eqtn. (3.3-29)

E REEK group option error, meters. Compare column D.

F , G REEK phase retardation and bending terms. In principle these should correspond to A_2+H_4 and B_4 respectively.

The check between the multi-frequency derived group error D and the REEK group option error E is very close (better than 0.06%) which would appear to be more than adequate for most applications. The difference though small appears to be systematic and numerically significant. Simple modifications of the REEK group option have been devised which reduce this error by about another order of magnitude in this case but the rationale and generality of such modifications is not clear and it is questionable whether they should be proposed for general use.

Elev. Deg.	Ⓐ ϵ_p REEK Phase	Ⓑ $2B_4$ = Bending Correction	Ⓒ $2H_4$ = Refractivity Correction	Ⓓ Derived Group = - Ⓐ - Ⓑ - Ⓒ	Ⓔ REEK Group	Ⓕ REEK Phase Retard ϵ_R	Ⓖ REEK Phase Bend ϵ_B
0.1	-747.178	-3.250	-0.439	750.867	751.299	-749.014	1.836
1.0	-746.213	-3.143	-0.439	749.794	750.222	-747.993	1.780
2.5	-741.331	-2.921	-0.436	744.688	745.098	-742.992	1.661
6.0	-715.839	-2.298	-0.421	718.558	718.891	-717.150	1.311
10.0	-669.932	-1.626	-0.394	671.952	672.181	-670.855	0.923
15.0	-603.126	-1.024	-0.355	604.505	604.631	-603.698	0.572
20.0	-538.671	-0.656	-0.317	539.644	539.705	-539.027	0.356
30.0	-435.220	-0.287	-0.256	435.763	435.774	-435.368	0.148
40.0	-364.859	-0.134	-0.214	365.208	365.208	-364.926	0.066
50.0	-318.131	-0.064	-0.187	318.382	318.380	-318.161	0.031
60.0	-287.435	-0.030	-0.169	287.634	287.632	-287.448	0.014
70.0	-268.078	-0.013	-0.158	268.248	268.246	-268.083	0.005
80.0	-257.372	-0.006	-0.151	257.529	257.526	-257.373	0.001
85.0	-254.794	-0.003	-0.150	254.947	254.945	-254.794	0.000
87.0	-254.249	-0.002	-0.149	254.401	254.390	-254.249	0.000
89.0	-253.977	0.000	-0.149	254.127	254.127	-253.977	0.000

In this table, errors are in meters and the following relations apply

$f = 136$ MHz $\qquad N_{max} = 0.865 \times 10^{-3}$

$h_{max} = 375$ km $\qquad H_s = 108.333$ km

TABLE 3.3-1

GROUP-PHASE COMPARISONS

3.4 Superposition

For analytic corrections the tropospheric and ionospheric corrections are generally treated as independent. In actuality the incidence angle for one is affected by the refraction error due to the other so that superposition should not be expected to hold, i.e.,

$$\Delta R_{total} = \Delta R_{trop} + \Delta R_{ion} + \varepsilon_{interaction} \qquad (3.4\text{-}1)$$

A short study was carried out to investigate the magnitude of the interaction error, $\varepsilon_{interaction}$. This was done for two different values of ionospheric refractivity, $-.001$ and $-.0001$. Even with the rather large maximum refractivity of $-.001$, corresponding to say, 100 to 400 MHz frequency, the interaction error is at most of the order of 2×10^{-3} of the total error at low elevation angles as can be seen in Table 3.4-1, where

$$\varepsilon_{int} = \Delta R_{tot} - (\Delta R_{ion} + \Delta R_{trop}) \quad .$$

The same thing done for range rate errors yields somewhat higher relative interaction terms ($\approx 3\%$), apparently resulting from the fact that the tropospheric and ionospheric errors are of more nearly comparable magnitude in range rate.

TABLE 3.4-1

SUPERPOSITION TESTS

NS = .000313   NI(MAX) = −.001

	RANGE ERRORS				RANGE RATE ERRORS			
EL (DEG)	ΔR_{ion} (Meters)	ΔR_{trop} (Meters)	ΔR_{tot} (Meters)	ϵ_{int} DIFR (M)	ΔRR_{ion} (CM/SEC)	ΔRR_{trop} (CM/SEC)	ΔRR_{tot} (CM/SEC)	ϵ_{int} DIFRR (CM/SEC)
0.10	829.8126	74.3268	905.8979	1.7584	00.0000	00.0000	00.0000	0.0000
0.15	829.7876	72.9693	904.4672	1.7102	0.2871	15.5816	16.4216	0.5529
0.25	829.7206	70.3416	901.6891	1.6268	0.3852	15.1146	15.9795	0.4797
0.40	829.5779	66.6763	897.7588	1.5046	0.5494	14.1084	15.1284	0.4706
0.60	829.3088	62.2213	892.8895	1.3594	0.7809	12.9296	14.1320	0.4214
1.00	828.5021	54.6030	884.2277	1.1226	1.1815	11.1572	12.6854	0.3467
1.50	826.9954	47.0038	874.8901	0.8910	1.7900	9.0281	11.0932	0.2751
2.50	822.3672	36.2022	859.1487	0.5793	2.8147	6.5692	9.5735	0.1895
4.00	811.6519	26.3918	838.3770	0.3333	4.5231	4.1411	8.7680	0.1038
6.00	791.3192	19.0849	810.5842	0.1801	6.8235	2.4521	9.3270	0.0514
10.00	736.7049	12.1096	748.8829	0.0684	10.1691	1.298[illegible]	11.4887	0.0208
15.00	658.9756	8.2814	667.2837	0.0266	13.6325	0.6714	14.3112	0.0073
20.00	585.4201	6.3113	591.7438	0.0123	15.5324	0.4160	15.9515	0.0030
30.00	469.6238	4.3405	473.9679	0.0036	15.8325	0.2371	16.0704	0.0008
25.00	522.0697	5.1257	527.2018	0.0064	16.0610	0.3006	16.3631	0.0015
40.00	392.1420	3.3828	395.5261	0.0013	14.7871	0.1828	14.9703	0.0004
50.00	341.1470	2.8410	343.9886	0.0006	12.7464	0.1354	12.8820	0.0002
60.00	307.8225	2.5143	310.3370	0.0002	10.2844	0.1008	10.3853	0.0001
80.00	275.3038	2.2119	277.5157	0.0000	6.1480	0.0572	6.2052	0.0000
89.00	271.6392	2.1787	273.8179	0.0000	1.7021	0.0154	1.7175	0.0000

NS = .000313   NI(MAX) = −.0001

EL (DEG)	ΔR_{ion} (Meters)	ΔR_{trop} (Meters)	ΔR_{tot} (Meters)	ϵ_{int} DIFR (M)	ΔRR_{ion} (CM/SEC)	ΔRR_{trop} (CM/SEC)	ΔRR_{tot} (CM/SEC)	ϵ_{int} DIFRR (CM/SEC)
0.10	82.2783	74.3268	156.7865	0.1814	0.0000	00.0000	00.0000	0.0000
0.15	82.2768	72.9693	155.4190	0.1729	0.0169	15.5816	15.6963	0.0978
0.25	82.2722	70.3416	152.7801	0.1663	0.0264	15.1146	15.1788	0.0378
0.40	82.2612	66.6763	149.0884	0.1809	0.0423	14.1084	14.2098	0.0591
0.60	82.2389	62.2213	144.6006	0.1404	0.0647	12.9296	13.0250	0.0306
1.00	82.1683	54.6030	136.8867	0.1155	0.1035	11.1572	11.2971	0.0364
1.50	82.0314	47.0038	129.1265	0.0913	0.1626	9.0281	9.2194	0.0288
2.50	81.6000	36.2022	117.8598	0.0576	0.2624	6.5692	6.8521	0.0205
4.00	80.5822	26.3918	107.0077	0.0337	0.4296	4.1411	4.5808	0.0101
6.00	78.6257	19.0849	97.7287	0.0181	0.6566	2.4521	3.1140	0.0052
10.00	73.3061	12.1096	85.4225	0.0069	0.9905	1.2988	2.2914	0.0021
15.00	65.6604	8.2814	73.9445	0.0027	1.3409	0.6714	2.0131	0.0007
20.00	58.3836	6.3113	64.6962	0.0012	1.5366	0.4160	1.9529	0.0003
25.00	52.0969	5.1257	57.2232	0.0006	1.5939	0.3006	1.8946	0.0002
30.00	46.8824	4.3405	51.2233	0.0004	1.5741	0.2371	1.8113	0.0001
40.00	39.1670	3.3828	42.5499	0.0001	1.4725	0.1828	1.6553	0.0000
50.00	34.0830	2.8410	36.9241	0.0001	1.2708	0.1354	1.4062	0.0000
60.00	30.7586	2.5143	33.2729	0.0000	1.0260	0.1008	1.1268	0.0000
80.00	27.5131	2.2119	29.7250	0.0000	0.6136	0.0572	0.6708	0.0000
89.00	27.1473	2.1787	29.3260	0.0000	0.1699	0.0154	0.1853	0.0000

4. ANALYTIC CORRECTIONS

This section summarizes the results of a series of studies of the relative accuracy and limitations of several proposed and operational analytic and semi-analytic refraction corrections.

4.1 Troposphere

Table 4.1-1 gives the principal characteristics of the various corrections considered here in terms of layer shape assumptions, measurements utilized, approximations to the integral, and correction quantities computed (R, E, $\dot{R}$). For the troposphere roughly 90 to 95% of the day-to-day variability is accounted for by the variation of Ns, the surface value of refractive index. Since this is readily measured in terms of pressure, temperature, and humidity it is not surprising to find that many of the practical formulations depend on Ns.

For long range prediction, worldwide statistics of N(z) are available (Ref. 22).

Reference 18 compared the results of the formulations listed in Tables 4.1.2, 4.1.3, 4.1.4 for elevation angle, range, and range rate with the corresponding results from REEK ray trace, assuming an exponential model atmosphere with surface refractivity $N_s = 313 \times 10^{-6}$ and scale height $H_s = 6951.25$ meters as per the CRPL standard troposphere.

The results of these comparisons are plotted in Figures 4.1, 4.2, and 4.3.

Each of the corrections for either angle, range or range rate is asymptotically of the same form at high elevation angles, namely,

$$\Delta E_{to} = N_s \operatorname{ctn} E$$

$$\Delta R_{to} = H N_s \csc E$$

$$\Delta \dot{R}_{to} = -H N_s \dot{E} \csc E \operatorname{ctn} E$$

TABLE 4.1-1

TROPOSPHERIC CORRECTIONS

METHOD	LAYER MODEL	INPUT PARAMETERS (MEASUREMENTS)	INTEGRAL	R, E, $\dot{R}$
RAYTRACE				
REEK (Typical of Class)	NONE	N(h)	RAYTRACE	R, E
SEMI-ANALYTIC				
MOMENTS	NONE	$M_n(h) = \int_0^{h_s} h^n N(h)\, dh$	ANALYTIC SERIES	R, E, $\dot{R}$
REGRESSION				
NBS STD.	NONE	$N_s, \frac{dN_s}{dh}$	TABLE, LOOK UP	R
NBS CAPE CANAV.				R
WALLOPS		N_s, P, T, H		R
NBS BEAN ∉ CAHOON		N_s		E
ANALYTIC				
HOPFIELD	BIQUARTIC	$N_{s_{dry}}, N_{s_{wet}}$	ANALYTIC	R
DC	EXPONENTIAL	N_s	ANALYTIC	R, E, $\dot{R}$
FREEMAN				
NO NAME				
GDAP				
C BAND				R, E
NAP-1				R, E, $\dot{R}$
SAO				R
AMS SECOR				R
APL TRANET				$\dot{R}$
NWL TRANET				$\dot{R}$

TABLE 4.1-2

RANGE REFRACTION CORRECTION EQUATIONS

Refraction Formulation	Range Refraction Correction ΔR ΔR (meters) = Obs − Corr.
GSFC DC	$\Delta R_{to}\left[\frac{8750}{H}\left(\frac{1}{\sqrt{1+0.000772\,\mathrm{ctn}^2 E}}\right)\right]$
GSFC DC	$\Delta R_{to}\,\frac{8750}{H}$
GSFC Freeman	$\Delta R_{to}\left(1-\frac{H}{R_s}\,\mathrm{ctn}^2 E\right)$
GSFC NONAME	$\Delta R_{to}\left[\frac{8432.336}{H}\left(\frac{1}{1+0.026\csc E}\right)\right]$
GSFC GDAP	$\Delta R_{to}\left[\frac{7200}{H}\left(\frac{2}{1+\sqrt{1+0.0045154\csc^2 E}}\right)\right]$
GSFC NAP-1	$\Delta R_{to}\left[\frac{2.7432}{HN_s}\left(\frac{2}{1+\sqrt{1+0.004\csc^2 E}}\right)\right]$
GSFC & SAO lasers	$\Delta R_{to}\left(\frac{2.1}{HN_s}\right)$
SAO lasers (after May 1968)	$\Delta R_{to}\left[\frac{2.238+533.5N_s}{HN_s\,(1+10^{-3}\cos E\csc^2 E)}\right]$
AMS SECOR	$\Delta R_{to}\left[\frac{2.7}{HN_s}\left(\frac{1}{1+0.0236\,\mathrm{ctn}\,E}\right)\right]$
Wallops C-band	$\Delta R_{to}\left(\frac{7600}{H}\right)$

where $\Delta R_{to} = HN_s \csc E = H\Delta E_{to} \sec E$ = first order correction.

TABLE 4.1-3

ELEVATION ANGLE REFRACTION CORRECTION EQUATIONS

Refraction Formulation	Elevation Angle Refraction Correction ΔE ΔE (radians) = Obs − Corr.
GSFC DC	ΔE_{to}
GSFC Freeman	ΔE_{to}
GSFC NONAME	$\Delta E_{to}\left(\frac{1}{0.93 + 0.0164 \operatorname{ctn} E}\right)$
GSFC GDAP	$\Delta E_{to}\left(\frac{2}{1 + \sqrt{1 + 0.0045154 \csc^2 E}}\right)$
GSFC NAP-1	$\Delta E_{to}\left[\frac{0.000350}{N_s}\left(\frac{2}{1 + \sqrt{1 + 0.004 \csc^2 E}}\right)\right]$
Wallops C-band	ΔE_{to}

where $\Delta E_{to} = N_s \operatorname{ctn} E$ = first order correction.

TABLE 4.1-4

RANGE RATE REFRACTION CORRECTION EQUATION

Refraction Formulation	Range Rate Refraction Correction, $\Delta\dot{R}$ $\Delta\dot{R}$ (meters/sec) = Obs − Corr.
GSFC DC	$\Delta\dot{R}_{to}\left[\frac{8743.25}{H}\ \frac{1}{(1+0.000772\ \mathrm{ctn}^2 E)^{3/2}}\right]$
GSFC DC	$\Delta\dot{R}_{to}\left(\frac{8750}{H}\right)$
GSFC Freeman	$\Delta\dot{R}_{to}\left[1+\frac{H}{R_s}\ (1-3\csc^2 E)\right]$
GSFC NONAME	$\Delta\dot{R}_{to}\left[\frac{8432.336}{H}\ \frac{1}{(1+0.026\csc E)^2}\right]$
GSFC GDAP	$\Delta\dot{R}_{to}\left[\frac{7200}{H}\ \frac{2}{\sqrt{1+0.0045154\csc^2 E}+(1+0.0045154\csc^2 E)}\right]$
GSFC NAP-I	$\Delta\dot{R}_{to}\left[\frac{2.7432}{HN_s}\ \frac{2}{\sqrt{1+0.004\csc^2 E}+(1+0.004\csc^2 E)}\right]$
APL TRANET	$\Delta\dot{R}_{to}\ \frac{R_s}{H}\sin^2 E\ [f(E)]$
NWL TRANET	$\Delta\dot{R}_{to}\ \frac{2.3}{HN_s}$

where

$$f(E) = 1 + \frac{2R_s}{H_t^2}\sin E\left[\sqrt{H_t^2+2R_sH_t+R_s^2\sin^2 E} - R_s\sin E + (R_s+H_t)\ \ln\frac{R_s(1+\sin E)}{(R_s+H_t)+\sqrt{H_t^2+2R_sH_t+R_s^2\sin^2 E}}\right]$$

$$\Delta\dot{R}_{to} = -HN_s\dot{E}\csc E\ \mathrm{ctn}E = -\Delta R_{to}\dot{E}\ \mathrm{ctn}E = -H\Delta E_{to}\dot{E}\csc E = \text{first order correction}$$

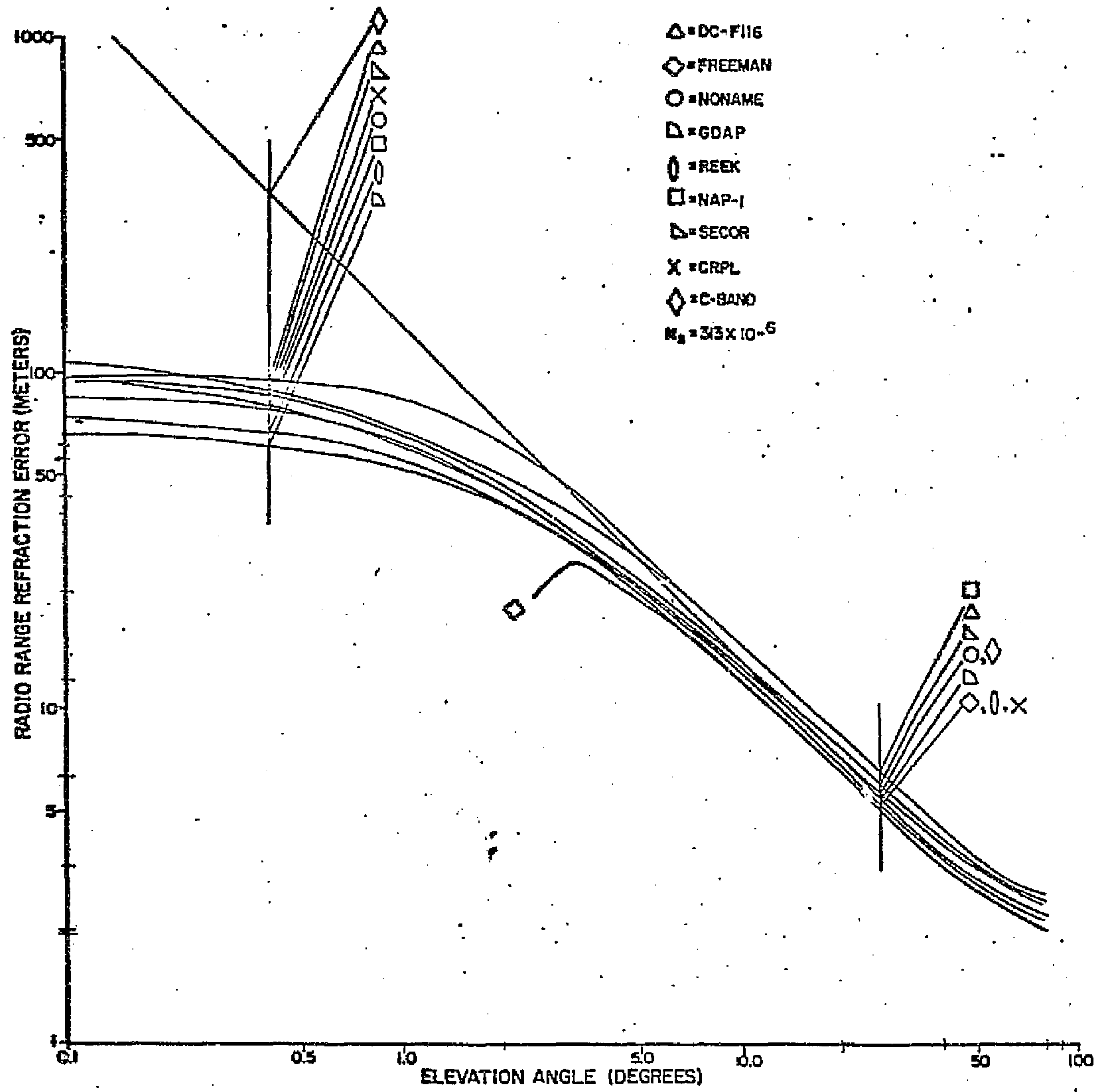

FIGURE 4.1

RANGE ERROR DUE TO TROPOSPHERIC REFRA TION

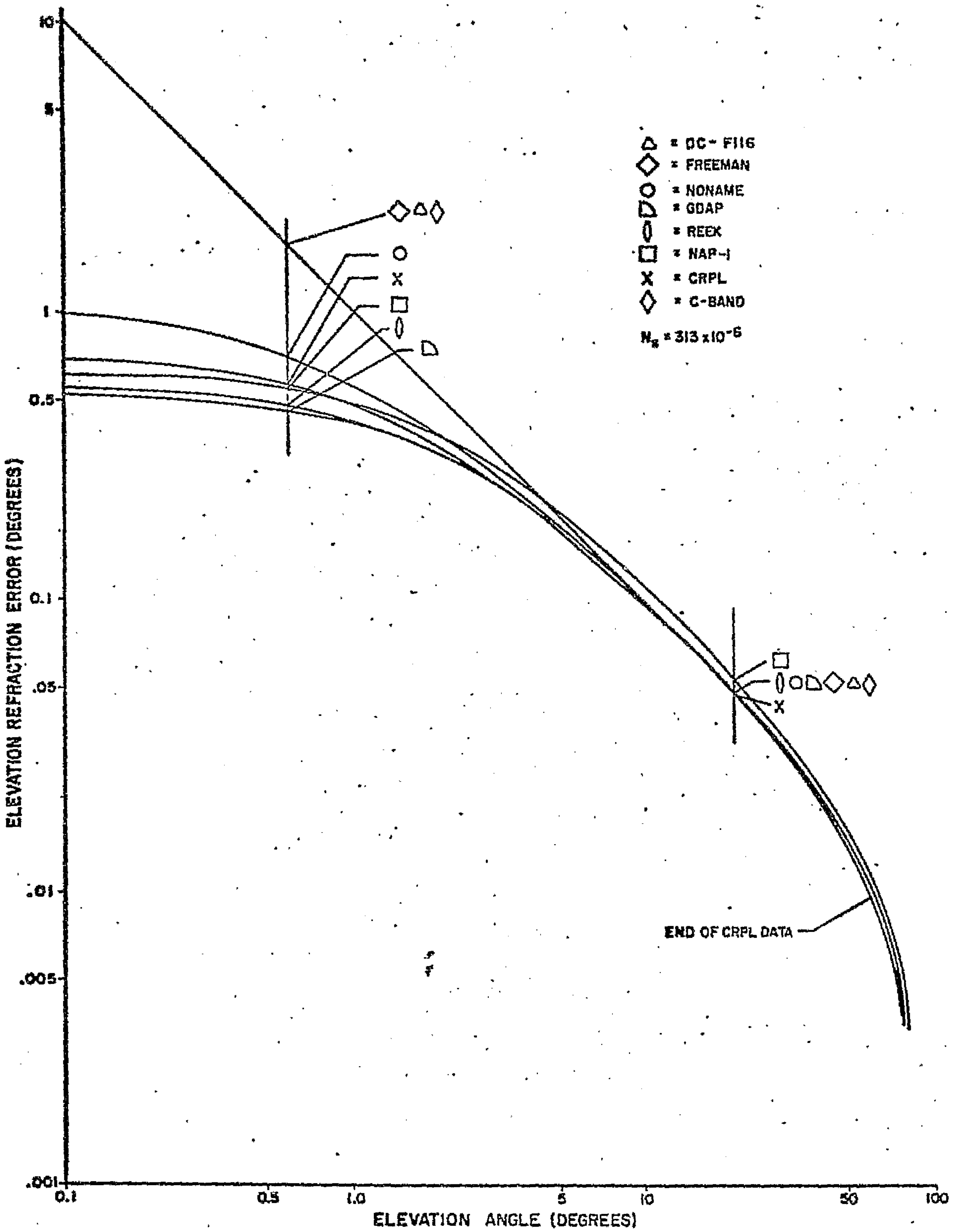

FIGURE 4.2

ELEVATION ERROR DUE TO TROPOSPHERIC REFRACTION

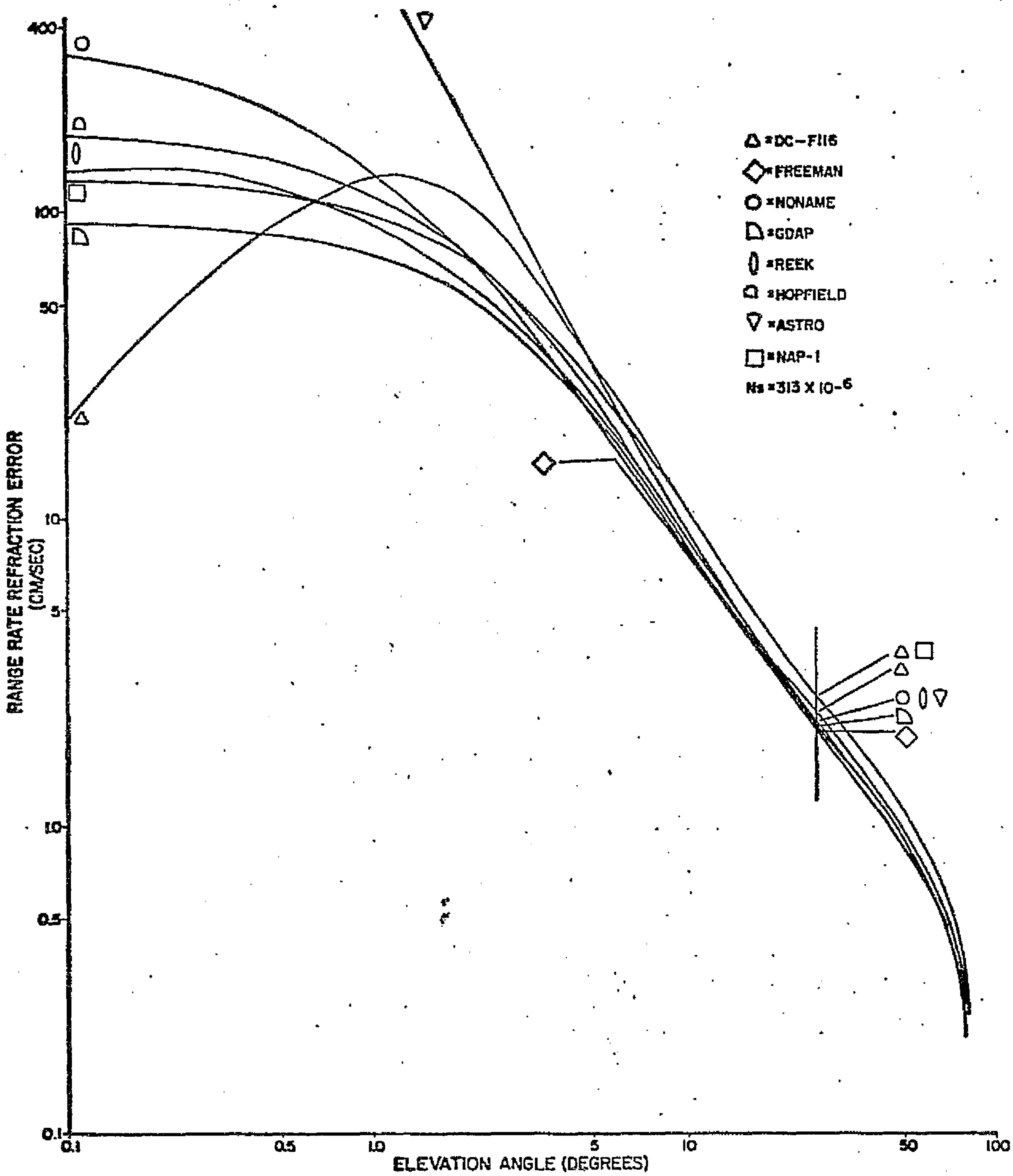

FIGURE 4.3

RANGE RATE ERROR DUE TO TROPOSPHERIC REFRACTION so it is as expected that all of the various corrections approach a quite accurate match to the REEK reference at high elevation angles, or at least could be brought into very close agreement by choice of scale factor, H. Significant differences appear below about 5^{o}, however. GDAP and NAP-1 (which are essentially identical) appear to offer consistently good approximations down to the lowest angles.

References 7, 8, and 19 as summarized in section 5 of this report derive series expansions of the elevation, angle, and range errors in terms of the successive moments of the distribution of refractivity vs height. It turns out that for range errors all the way to the horizon and for elevation and range rates errors down to about 2^{o} elevation, the moment expansion utilizing the first three (0^{th}, 1^{st}, 2^{nd}) moments provides quite a good analytic correction, midway in accuracy between those corrections depending only on N_s and the REEK correction based on the entire profile. This is plotted for comparison in chapter 5, Figures 5.7, 5.8, 5.9.

Hopfield (Ref. 31) has proposed a bi-quartic model for the tropospheric refractivity:

$$N(h) = N_{o_d}\left(\frac{h_{t_d} - h}{h_{t_d}}\right)^4 + N_{o_w}\left(\frac{h_{t_w} - h}{h_{t_w}}\right)^4$$

where N_{o_d} = surface value of the "dry" terms of refractivity

$$= \frac{77.6\,P_o}{T_o}$$

h_{t_d} = associated dry term scale height

N_{o_w} = surface value of "wet" term of refractivity

$$= \frac{77.6\,(4810\,e)}{T^2}$$

h_{t_w} = associated wet term scale height

Both limited to zero above where they go to zero at h_{t_d} and h_{t_w}

This bi-quartic form fits experimental data quite well over the most important part of the troposphere (obviously not around h_{t_d} or h_{t_w}) and the resulting straight-line refraction integral can be carried out analytically (Ref. 31) yielding:

$$\Delta\rho_i = \sum_{i=1}^{2} 10^{-6} N_{o_i} \Big[-\ell_1 + \frac{4}{h_{t_i}^4} \Big\{ \frac{1}{3} r_o^2 \ell_1^3 - \frac{2}{15} \ell_1^5 - \frac{3}{4} r_o r_{t_i} \ell_1 (\ell_1^2 + \frac{1}{2} \ell_2^2)$$

$$+ r_{t_i}^2 \ell_1^3 - \frac{1}{2} r_{t_i}^3 r_o \ell_1 - \frac{1}{3} r_{t_i}^2 \ell_{3_i}^3 + \frac{2}{15} \ell_{3_i}^5$$

$$+ \frac{3}{4} r_{t_i}^2 (\ell_{3_i}^3 + \frac{1}{2} \ell_{3_i} \ell_2^2) - r_{t_i}^2 \ell_{3_i} (\ell_{3_i}^2 - \frac{1}{2} r_{t_i}^2)$$

$$+ \frac{1}{2} r_{t_i} \ell_2^2 (\frac{3}{4} \ell_2^2 + r_{t_i}^2) \ln \frac{r_o + \ell_i}{r_{t_i} + \ell_{3_i}} \Big\} \Big]$$

where

r_o = radius of earth

h_{t_i} = height of top of layer

r_{t_i} = $r_o + h_{t_i}$ = radius of top of layer

$\ell_1 = r_o \sin E$

$\ell_2 = r_o \cos E$

$\ell_{3_i} = (r_{t_i}^2 - \ell_2^2)^{1/2}$

E = elevation angle of ray at $h = 0$, $r = r_o$

$$i = \begin{cases} 1 & \text{dry term} \\ 2 & \text{wet term} \end{cases}$$

Actually this closed form is difficult to compute since the individual terms in brackets are of order $(r_o/h_t)^5$, typically 10^{14}, larger than their sum! While this is well within capabilities of some computers in double precision, it would be highly desirable to find simplifications of this formula which would make it more readily available on more modest computing equipment. Reference 11 treats the problem of alternate ways of computing this including two very efficient series expansions derived by Yionoulis (Ref. 32) and straight-forward numerical integration. Best results were obtained with simple numerical integration; using a Simpson formula gave 5-place accuracy with 20 points for $E > 2^{\circ}$, 80 points down to 0.6° and 160 points below 0.6°.

Finally a series of comparisons was carried out with 85 actual radiosonde profiles measured during WICE. 5 methods were compared

- REEK raytracing (including bending) of the actual profiles (taken as the standard of comparison
- Hopfield's model
- The NBS "Standard Sample" regression model
- The NBS "Cape Canaveral Sample" regression model
- A special regression model based on P_o, T_o, H_o derived for the WICE sample.

A few words of explanation of the latter three models will be in order. The NBS regression models are those derived by Thayer and Bean (Ref. 33) and are of the form

$$\Delta R = A(E) + B(E)\,\Delta N$$

where $A(E)$ and $B(E)$ coefficients are functions of elevation angle, E, established by least-squares regression fit to a sample of actual data and published in Ref. 33

$\Delta N = N_o - \overline{N}_o$

N_o = ground level measured refractivity

$\overline{N}_o$ = average value of N_o over the sample

ΔR = predicted range refraction error.

Two sets of coefficients were found, one the so-called "standard sample", from a worldwide sample of 77 profiles; the second from 84 profiles all taken at Cape Canaveral.

These regression models were extended for the 85 profile WICE sample by considering various possible regressors of the form

$$\Delta R = \sum_i A_i f_i(P, T, H, E)$$

where H = Relative Humidity

E = partial pressure of water vapor

$f_i(\cdot)$ = various tentative functional combinations and transformations of the basic P, T, H, E measurements.

The various combinations tried and the resulting standard error of the regression fit for each case are given in Table 4-5.

TABLE 4-5

STANDARD ERROR OF REGRESSION FIT, METERS

Independent Variables (f_i)	Dependent Variables	
	$\Delta R(E = 12.173^{o})$	$\Delta R(E = 90^{o})$
$\Delta R(E = 90^{o})$	.032	---
T	.216	.046
E	.162	.035
N(P, T, H)	.149	.032
E, P	.154	.035
E, P, H	.147	.031
T, H	.159	.035
T, H, P	.148	.032
P/T, E/T^2	.148	.032

The particular case where $\Delta R(E = 90^{o})$ was used as the regressor (for lower elevation angle) is of some interest in indicating the possible residual error at other than vertical incidence if the integrated refractivity content (equivalent to $\Delta R(E = 90^{o})$) could be measured by some other means; the indication is clearly very encouraging to such a development. The upshot of these studies was to indicate that given the several ground level measurements (P, T, H or E) about the best and simplest predictor is N(P,T,H) alone, i.e., just the form of the NBS model, and this was the form used in the comparison. The coefficients resulting from the three regressions are compared in Table 4-6.

TABLE 4-6

REGRESSION COEFFICIENTS AT $E = 12.173^{\circ}$

	$A_{(m)}$	$B_{(m/N)}$
NBS Standard Sample	3.8929	.02149
NBS Cape Canaveral Sample	6.6595	.01377
WICE Sample	7.3483	.01100

$$\Delta R^{*} = A + B\Delta N$$

Finally the results of these various regression models along with the Hopfield bi-quartic model were compared with REEK ray tracings for the 85 WICE radiosonde samples. For this purpose the scale heights of the bi-quartic model were taken as $h_{dry} = 41.17$ km and $h_{wet} = 12.0$ km as recommended by Hopfield for the latitude of Wallops. The wet, dry, and total refractivity terms in all cases were taken from the ground level readings of the radiosonde.

The results are summarized in Table 4-7 for the case of $E = 12^{\circ}$.

TABLE 4-7

COMPARISON OF TROPOSPHERIC REFRACTION CORRECTORS VS REEK RAY TRACINGS ON 85 WICE PROFILES

Predictor	Std.Dev. of Prediction Errors (Meters) $E = 12^{\circ}$
Hopfield	.223
NBS "Standard Sample" Coefficients	.281
NBS "Cape Canaveral Sample" Coefficients	.258
Special Wallops Regression on N(P,T,H)	.149

It should be pointed out that the Special Wallops Regression is undoubtedly optimistic in its estimate of its own prediction error since, among other things, it was developed and tested on only a three-month segment of data (April, May, June 1968). In comparison with the NBS predictions it will be seen that the Hopfield formula is generally comparable, but slightly better in accuracy.

4.2 Analytic Corrections for the Ionosphere

Reference 20 presented a comparison of several commonly used analytic corrections for the ionosphere with REEK ray trace taken as a standard. The external characteristics of these algorithms are given in Table 4-8 in terms of layer model assumptions, input parameters, integral approximations and outputs.

Tables 4.9 - 4.11 give the actual formulations of the analytic corrections and the moment correction is discussed in section 5. For the comparisons shown in Figures 4.4 - 4.6 a Chapman-type ionosphere was assumed with $N_{max} = 10.67 \times 10^{-6}$, h_m = 364 km and H_s = 104.667 km, typical of daytime near solar maximum at f = 2GHz. The GEOVAP and Freeman formulations are not useful at low elevation angles and are in fact relatively poor at angles as high as 40^o - 50^o. All the other formulations listed in Tables 4.9 - 4.11 except NAP-3 act similarly at low angles in R, E and $\dot{R}$ and what differences do appear can largely be ascribed to the necessarily somewhat arbitrary choices involved in fitting the parameters of the various models to the particular Chapman model used as the basis of comparison.

In other words, a slightly different choice of h_m and H_s parameters would in these cases yield vary close agreement with the REEK ray trace results. The ionosphere is significantly different than the troposphere in that the minimum elevation angle in the ionosphere is of the order of 18^o - 20^o even for horizontal takeoff from the earth (E = 0), consequently the very low angle problem is never encountered in the ionosphere for the cases with which we are concerned.

Consequently the main difference between approaches is related simply to how much information about the actual ionosphere is actually input to the algorithm, or how well the modelled ionosphere matches the real.

Moment series comparisons with idealized and actual ionospheres are given in section 5. The match is very close as would be expected from the fact that the moments themselves approach a complete description of the actual layer and the very low angle convergence question is moot for the ionosphere for the reasons discussed above.

TABLE 4.8

IONOSPHERIC CORRECTION ALGORITHMS

METHOD	LAYER MODEL	INPUT PARAMETERS (MEASUREMENTS)	INTEGRALS	R, E, $\dot{R}$
<u>RAYTRACE</u>				
REEK	NONE	N(h)	FULL RAYTRACE	R, E
<u>SEMI-ANALYTIC</u>				
MOMENTS	NONE	MOMENTS	ANALYTIC SERIES	R, E, $\dot{R}$
<u>ANALYTIC</u>				
DC	CHAPMAN	N_{max}, H_s, h_{max}	ANALYTIC	R, E, $\dot{R}$
DODS				
Freeman				
GEOVAP				
GPRO (GDAP)	PARABOLIC			
NAP-3	Parabolic Bottom Exponential Top	y_m = bottom scale ht k = topside scale h_m = height of max N_{max}		

TABLE 4.9

RANGE REFRACTION CORRECTION FORMULAS

Refraction Formulation	Range Refraction Correction ΔR ΔR (meters) = $R - R_c$
GSFC DC ¢ DODS ($E < 10^0$)	$\frac{4}{5}\Delta R_{io}\left\{\frac{\sin E}{\left[1-\left(\frac{R_e \cos E}{R_e+h_m}\right)^2\right]^{1/2}}\right\}$
GSFC DC ¢ DODS ($E > 10^0$)	$\frac{4}{5}\Delta R_{io}$
GSFC Freeman	$\Delta R_{io}\left[1-\left(\frac{H+h_m}{R_e}\right)\text{ctn}^2 E\right]$
GSFC GPRO (GDAP)	$\frac{-8 H_g N_{im} \csc E_1}{1+\left[1+\frac{25 H_g \text{ctn}^2 E_1}{3(R_e+h_m-3H_g}\right]^{1/2}}$
NAP-3	$\frac{-N_{im}\left[\frac{9}{16K}\left(1-e^{-(h_s-h_m-\frac{y_m}{2})K}\right)+\frac{459}{480}y_m\right]}{\left[1-\left(\frac{R_e}{R_e+R_h}\right)^2\cos^2 E\right]^{1/2}}$
GEOVAP	ΔR_{io}

$$\Delta R_{io} = -N_{im} He^{1} \csc E = -M_o \csc E$$

TABLE 4.10

RANGE RATE REFRACTION CORRECTION FORMULAS

Refraction Formulation	Range Rate Refraction Correction $\Delta\dot{R}$ $\Delta\dot{R}$ (meters/sec) = $\dot{R} - \dot{R}_c$
GSFC DC ∉ DODS ($E < 10^o$)	$\frac{4}{5}\Delta\dot{R}_{io}\left(\frac{R_e}{R_e+h_m}\right)^2 \sin^3 E\left[1-\left(\frac{R_e\cos E}{R_e+h_m}\right)^2\right]^{-3/2}$
GSFC DC ∉ DODS ($E > 10^o$)	$\frac{4}{5}\Delta\dot{R}_{io}$
GSFC Freeman	$\Delta\dot{R}_{io}\left[1+\left(1-\frac{3}{\sin^2 E}\right)\left(\frac{H+h_m}{R_e}\right)\right]$
GSFC GPRO (GDAP)	$\frac{-8N_{im}H_g\dot{E}_1 \operatorname{ctn} E_1 \csc E_1\left[1+\frac{1-4\beta_2^2}{(1+4\beta_2^2\operatorname{ctn}^2 E_1)^{1/2}}\right]}{\left[1+(1+4\beta_2^2\operatorname{ctn}^2 E_1)^{1/2}\right]^2}$
NAP-3	$-\frac{\dot{E}(\Delta R)\left(\frac{R_e}{R_e+R_h}\right)^2 \sin E\cos E}{1-\left(\frac{R_e\cos E}{R_e+R_h}\right)^2}$
GEOVAP	$\Delta\dot{R}_{io}$

$$\Delta\dot{R}_{io} = N_{im}He\ \dot{E}\operatorname{ctn} E\csc E = M_o\frac{d(\csc E)}{dt}$$

TABLE 4.11

ELEVATION REFRACTION CORRECTION FORMULAS

Refraction Formulation	Elevation Angle Refraction Correction ΔE ΔE (radians) $= E - E_c$
GSFC DC ⊄ DODS	$\frac{4}{5}\Delta E_{io}$
GSFC Freeman	ΔE_{io}
NAP-3	$\cos^{-1}\left[\frac{X_1 \cos\alpha - X_2}{\left(X_1^2 + X_2^2 - 2X_1 X_2 \cos\alpha\right)^{1/2}}\right]$

$$\Delta E_{io} = \frac{-N_{im} H e^1}{h_t} \operatorname{ctn} E = -\frac{M_o}{h_t} \operatorname{ctn} E$$

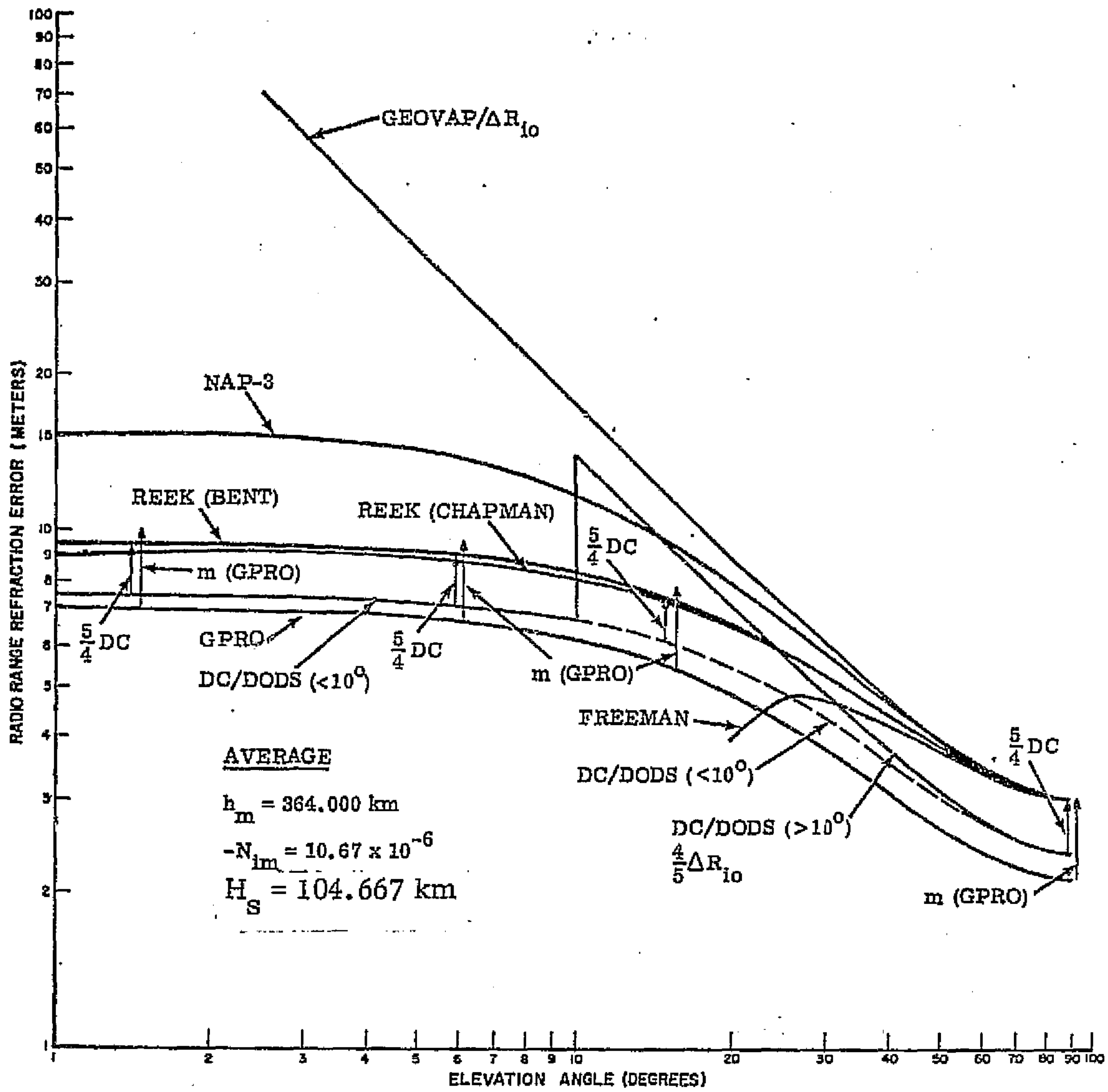

FIGURE 4.4

RANGE ERROR DUE TO IONOSPHERIC REFRACTION

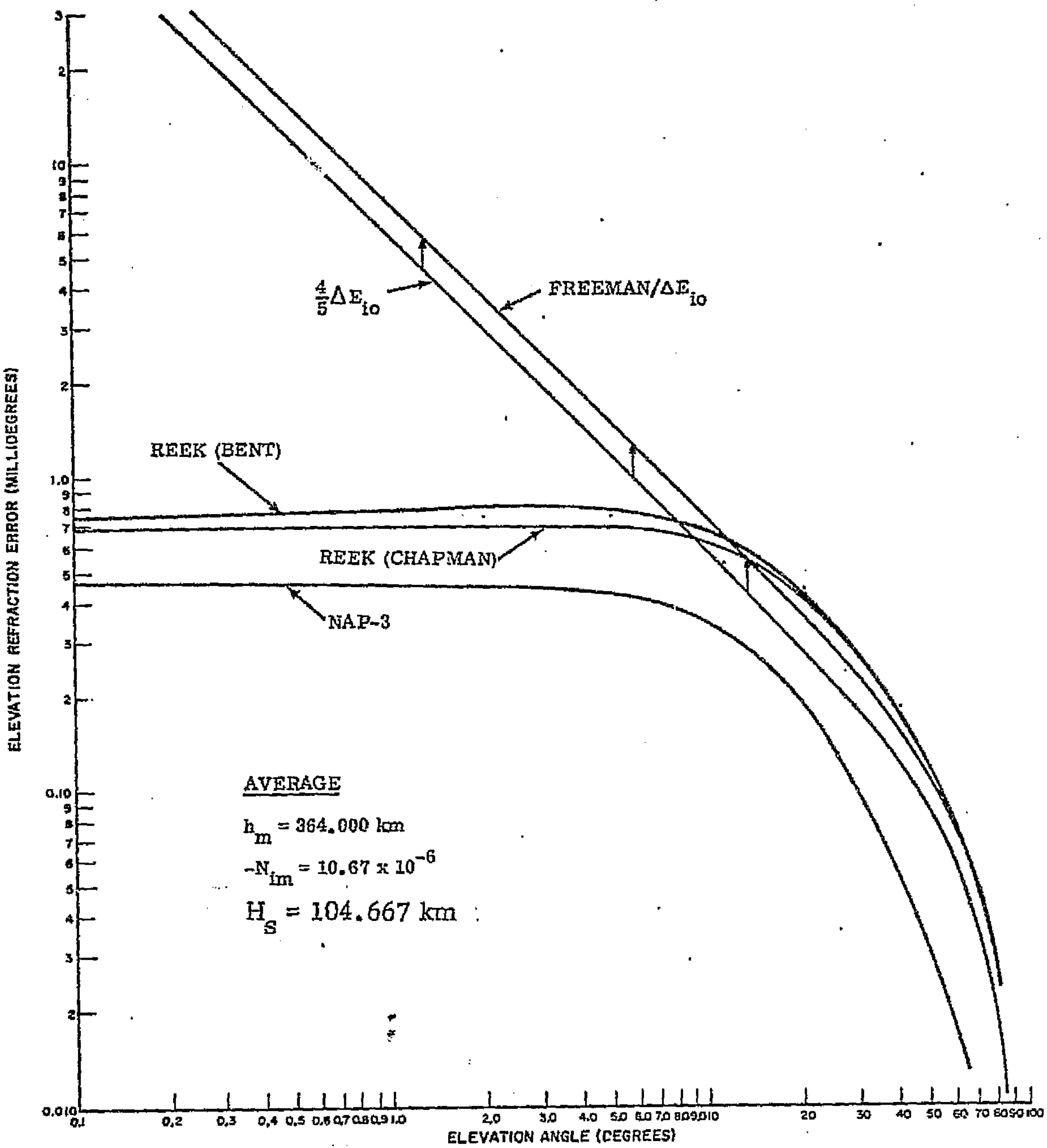

FIGURE 4.5
ELEVATION ERROR DUE TO IONOSPHERIC REFRACTION

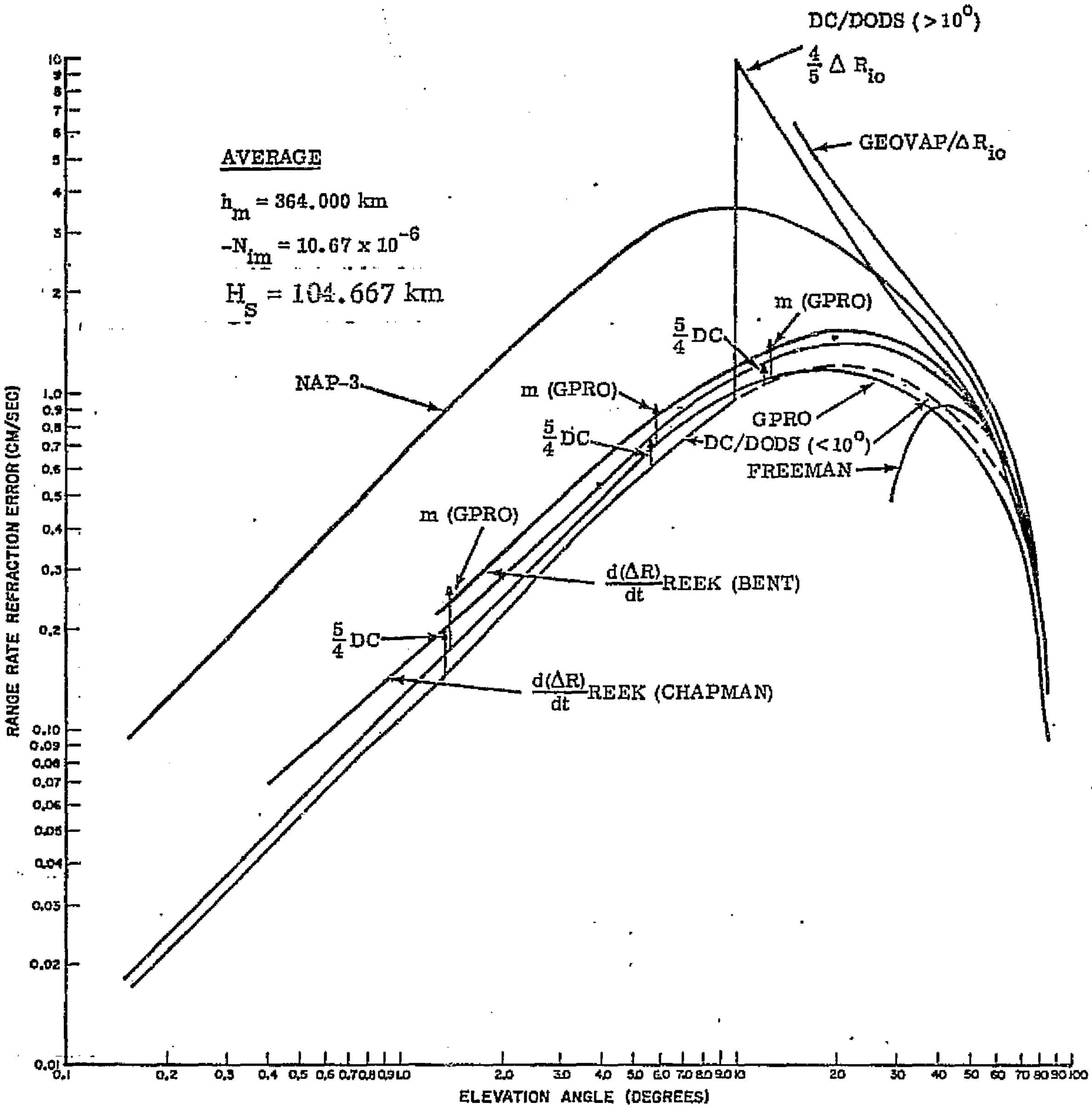

FIGURE 4.6

RANGE RATE ERROR DUE TO IONOSPHERIC REFRACTION

5. MOMENT EXPANSIONS

5.1 Introduction

The refractive range errors at a given frequency - (to a zero order approximation valid for plane earth) - are directly proportional to the total columnar refractivity content or zeroth order moment of the density profile and a simple function, csc E, of the elevation angle. For spherical earth, a first-order correction is available which depends only on the effective height, or first-order moment of the electron density profile.

These considerations lead one to consider the possibility of an expansion of the range error correction in terms of successive moments of the profile distribution, and in which the coefficients are elevation angle functions. If such a formulation is capable of providing sufficient accuracy in a reasonably small number of terms, it would have significant computational advantages over straightforward raytracing for the case where corrections at a large number of points (i.e., elevation angles) must be computed for the same ionosphere.

Freeman (Ref. 26) made a start in this direction for ionospheric range errors, but found relatively slow convergence. His expansion was in terms of moments about the ground level, $h = 0$. It can be reasoned that the expansion would necessarily be more rapidly convergent if moments were taken about a point in the ionosphere, such as the centroid. For example, it is clear, to the extent that the ionospheric density profile can be approximated by a thin shell at its centroid, that a single term in the moment expansion (the zeroth moment) would give an exact answer for the case of moments about the centroid, since all higher order moments are already zero for moments about the centroid, but not for moments about any other point.

This section summarizes further results on the moment expansion first derived under this project and reported in Refs. 7,8, and 19.

5.2 Moment Expansion Derivation

Based on the straight path assumption, discussed in section 3.2, the range error is approximated simply as

$$\Delta R = \int_{\substack{\text{straight}\\ \text{path}}} (n-1)\, ds$$

$$= \int \sec\Phi_o\, N(h)\, dh\,. \tag{5.2-1}$$

On a spherical earth (See Figure 5.1) this becomes

$$\Delta R = \int_0^{h_s} \sec(\Phi(h))\, N(h)\, dh \tag{5.2-2}$$

where $N(h) = n(h) - 1$

$\Phi(h)$ is the angle the straight line ray makes with the local vertical as it passes through height h.

From the spherical geometry shown in Figure 5.1, $\sec\Phi(h)$ is given by

$$\sec\Phi(h) = \left[1 - \left(\frac{a}{a+h}\sin\Phi_o\right)^2\right]^{-1/2} \tag{5.2-3}$$

Now, following the motivation discussed previously, we expand $\sec(\Phi(h))$ in a Taylor series in h about some arbitrary reference height, h_c, which will normally be chosen somewhere near the center of the refractive layer, thus

$$\sec(\Phi(h)) = \sec(\Phi(h_c)) + (h-h_c)\left[\frac{d}{dh}\sec(\Phi(h))\right]\ldots$$

$$= \sum_{m=0}^{\infty} \frac{(h-h_c)^m}{m!} \frac{d^m}{dh^m}(\sec\Phi(h)) \tag{5.2-4}$$

where the derivatives are to be evaluated at $h = h_c$.

Note that the geometrical factor is independent of h. This means that when we carry out the integral, equation (5.2-2), interchanging integral and

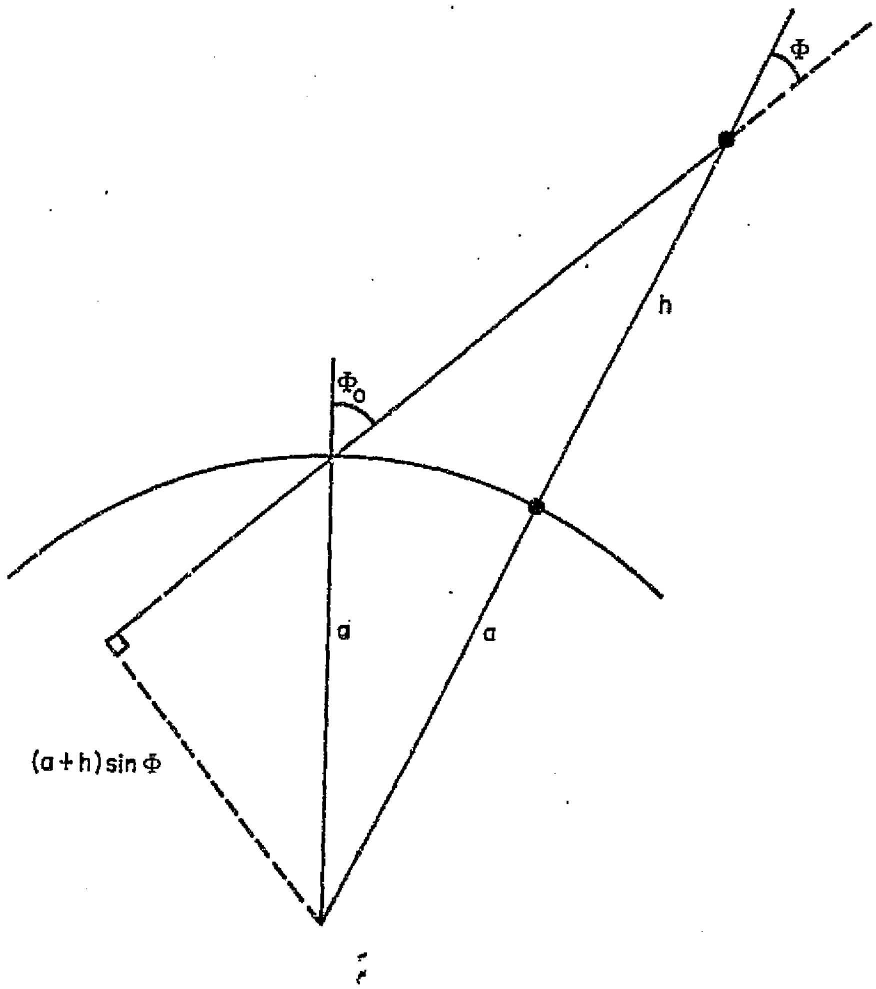

FIGURE 5.1
GEOMETRY OF THE STRAIGHT LINE PATH ANGLE

summation, the geometrical factors come out of the integrals and we have

$$\boxed{\Delta R = \sum_{m=0}^{\infty} G_m(E_o) M_m} \tag{5.2-5}$$

where $G_m = \frac{1}{m!} \frac{d^m}{dh^m} \sec(\Phi(h))\Big|_{h=h_c}$ are geometrical factors (5.2-6)

depending only on $\varphi(h = h_c)$, i.e., on φ_o and h_c.

$$M_m = \int_0^{h_s} (h - h_c)^m N(h)\, dh \tag{5.2-7}$$

= mth moment about h_c of refractivity distribution.

The moments adequately characterize the ionosphere or troposphere for refraction correction purposes, as will be shown.

5.3 Moment Expansion for Angle

The corresponding moment series for elevation angle errors can be derived from that for range from the general relation between range and angle errors derived in Ref. 13, namely

$$\Delta E = N_o \operatorname{ctn} E + \left(\frac{1}{a} + \frac{\sin E}{R}\right) \csc E \frac{\partial}{\partial E} \Delta R(E, h) \tag{5.3-1}$$

where a = radius of earth

R = range to target

$= \sqrt{(a+h_t)^2 - (a \cos E)^2} - a \sin E$

h_t = target height

N_o = ground level refractivity.

Using eq. (5.2-5) in eq. (5.3-1) gives the moment series for angle

$$\Delta E \approx N \operatorname{ctn} E + \left(\frac{1}{a} + \frac{\sin E}{R}\right) \csc E \sum_{m=0}^{\infty} G'_m(E) M_m(h_c) \tag{5.3-2}$$

where $G'_m(E) = \frac{d}{dE} G_m(E)$

The first few G' and G are given in Table 5.1.

TABLE 5.1

GEOMETRICAL FACTORS

$$C = (a\cos E)^2$$
$$r = a + h_c$$

m	G_m	G'_m
0	$\left(1 - \frac{C}{r^2}\right)^{-1/2}$	$-CG_o^3 \tan E/r^2$
1	$-CG_o^3/r^3$	$-\frac{G'_o}{r}\left[2 + \frac{3CG_o^2}{r^2}\right]$
2	$3/2\, CG_o^5/r^4$	$\frac{3}{2}\frac{G'_o}{r^2}\left[2G_o^2 + \frac{5CG_o^4}{r^2}\right]$
3	$\frac{1}{2r^5} C(-5G_o^7 + G_o^5)$	$\frac{1}{2}\frac{G'_o}{r^3}\left[2(-5G_o^4 + G_o^2) + \frac{C}{r^2}(-35G_o^6 + 5G_o^4)\right.$
4	$\frac{5C}{8r^6}(7G_o^9 - 3G_o^7)$	$\frac{5}{8}\frac{G'_o}{r^4}\left[2(7G_o^6 - 3G_o^4) + \frac{C}{r^2}(63G_o^8 - 21G_o^6)\right]$
5	$\frac{3C}{8r^7}(-21G_o^{11} + 14G_o^9 - G_o^7)$	$\frac{3}{8}\frac{G'_o}{r^5}\left[2(-21G_o^8 + 14G_o^6 - G_o^4) + \frac{C}{r^2}(-231G_o^{10} + 126G_o^8 - 7G_o^6)\right]$
6	$\frac{7C}{16r^8}(33G_o^{13} - 30G_o^{11} + 5G_o^9)$	$\frac{7}{16}\frac{G'_o}{r^6}\left[2(33G_o^{10} - 30G_o^8 + 5G_o^6) + \frac{C}{r^2}(429G_o^{12} - 330G_o^{10} + 45G_o^8)\right]$

5.4 Moment Expansion for Range Rate

The moment series for range rate is given simply by differentiating eq. (5.2-5)

$$\Delta\dot{R} = \dot{E} \sum_{m=0}^{\infty} G'_m(E) M_m(h_c) \qquad (5.4\text{-}1)$$

This assumes that the moments themselves are not changing, i.e., that the target is either well above the ionosphere or traveling at a constant level in the ionosphere and that the horizontal variations are negligible. This assumption also underlies the other refraction correction analytic developments discussed in this report. Note that the series here is identical to that for the elevation angle so the convergence behaviour is identical.

5.5 Convergence

Convergence of the moment series was considered in Ref. 8 for the specific case of tropospheric elevation angle where convergence difficulties had been noted. The general result gives a sufficient condition for convergence as

$$\cos E < \frac{a+h_c}{a} \sqrt{1 - \frac{H_s}{a+h_c}}$$

For example:

Ionosphere

assuming $a = 6380$ km

$h_c = 375$ km

$H_s = 108$ km

we find $\cos E < 1.05$

which is of course always satisfied, i.e., the series should always converge for the ionosphere.

Troposphere

using $a = 6380$ km

$h_c = 0$

$H_s = 6.95$ km

we find $E > 1.89^{\circ}$ for convergence.

We shall show examples indicating that the series does, in fact, diverge below about this value.

5.6 Tests of the Moment Expansion for Range

5.6.1 Ionosphere

Three types of test of the moment expansion have been carried out. Each involves comparison of the moment expansion against raytrace calculations by the REEK program for various ionospheric density profiles at the SECOR effective frequency of 434.2696 MHz.

In the first test (Ref. 7) a model ionosphere was postulated as a modified Chapman layer of reasonably representative thickness, height, and density. This was used mainly to explore the convergence properties of the range error expansion as functions of the expansion height, h_c, and order N. Figure 5.2 shows the residual error of the partial sum $\sum_{m=0}^{N_t} G_m(E_o)M_m$ to terms of order N_t for various N_t as a function of the expansion center h_c. Clearly the convergence is best for h_c at or slightly above the centroid height.

Figure 5.3 shows the residual range error as a function of the order N_t for expansion at the centroid compared to REEK ray traces through the first 4 of the 17 WICE ionospheric profiles described in section 6. This makes it clear that the convergence is far from uniform and that the expansion should be stopped on even order with $N = 2$ adequate.

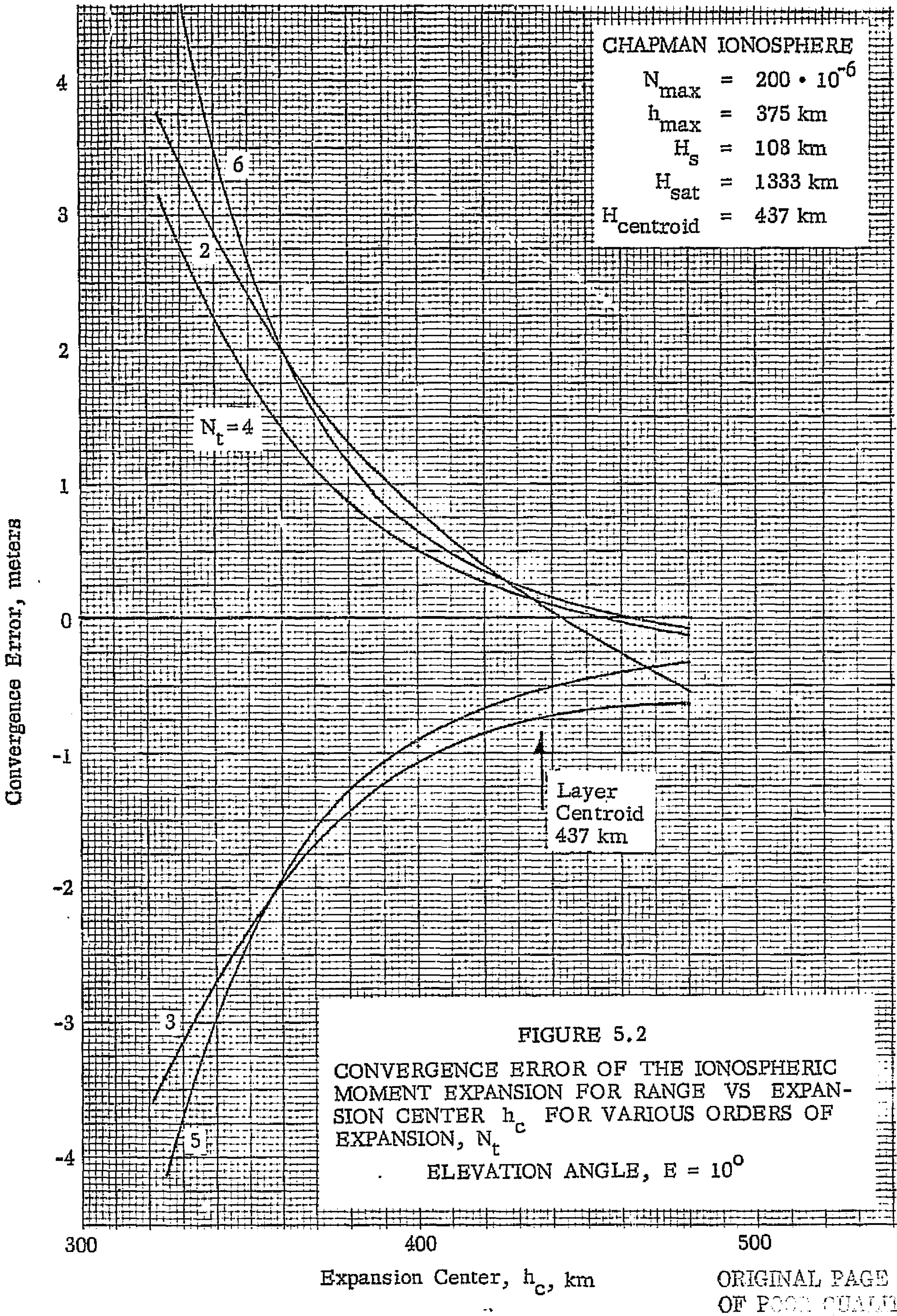

FIGURE 5.2

CONVERGENCE ERROR OF THE IONOSPHERIC MOMENT EXPANSION FOR RANGE VS EXPANSION CENTER h_c FOR VARIOUS ORDERS OF EXPANSION, N_t

ELEVATION ANGLE, $E = 10^{\circ}$

ORIGINAL PAGE IS OF POOR QUALITY

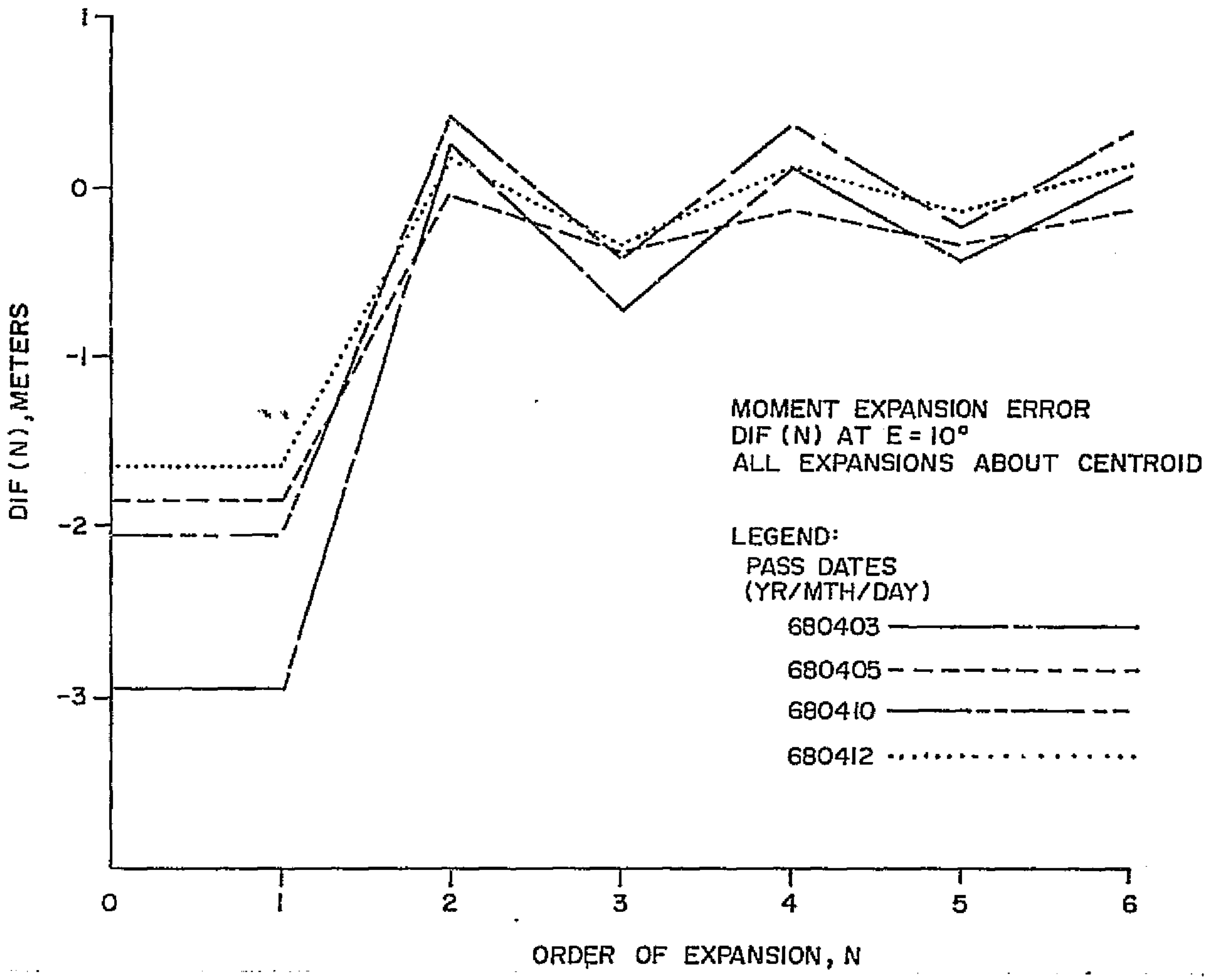

FIGURE 5.3

MOMENT EXPANSION ERROR DIF (N) at E = 10^0

ORIGINAL PAGE IS OF POOR QUALITY

The remaining test cases detailed in Ref. 7 were based on real profile data for 16 of the 17 WICE ionospheric data sets. These were analyzed in the same way with respect to partial sum convergence. The results were completely in consonance with the above findings for the Chapman layer and need not be repeated here.

Figures 5.4, 5.5 and 5.6 show the moment series range, elevation, and range-rate corrections for the same standard ionosphere used in Ref. 20 for comparison with other commonly used analytic approximations and the REEK raytrace as a standard. It can be concluded that the moment series to $N = 2$ provides a convenient and more accurate analytic approximate correction than any of the other commonly used analytic forms for ionospheric range, elevation, or range-rate tested here.

5.6.2 Troposphere

Tests of the moment expansion for tropospheric refraction error were carried out on an exponential tropospheric model using REEK Raytrace as a reference.

The results shown in Table 5.2 as a function of expansion order confirm the conclusion previously derived that the series for the troposphere becomes divergent for larger orders below about $E = 2.5^{\circ}$. The partial sum to 2 terms, however, provides a simple and reasonably accurate representation.

As additional tests the series to $N_t = 2$ for range, elevation and range-rate were calculated for the same standard troposphere used as a basis for comparing various analytic approximations in Ref. 18. The comparative results are plotted in Figures 5.7, 5.8, and 5.9. Agreement with the REEK ray traces is better for the moment expansion corrections than for the other commonly used analytic approximate correction forms tested here, at least down to about 2° elevation angle. Some of the analytic expressions are better than the moment expansions below 2° for tropospheric refraction corrections for elevation and range rate.

ORIGINAL PAGE IS
OF POOR QUALITY

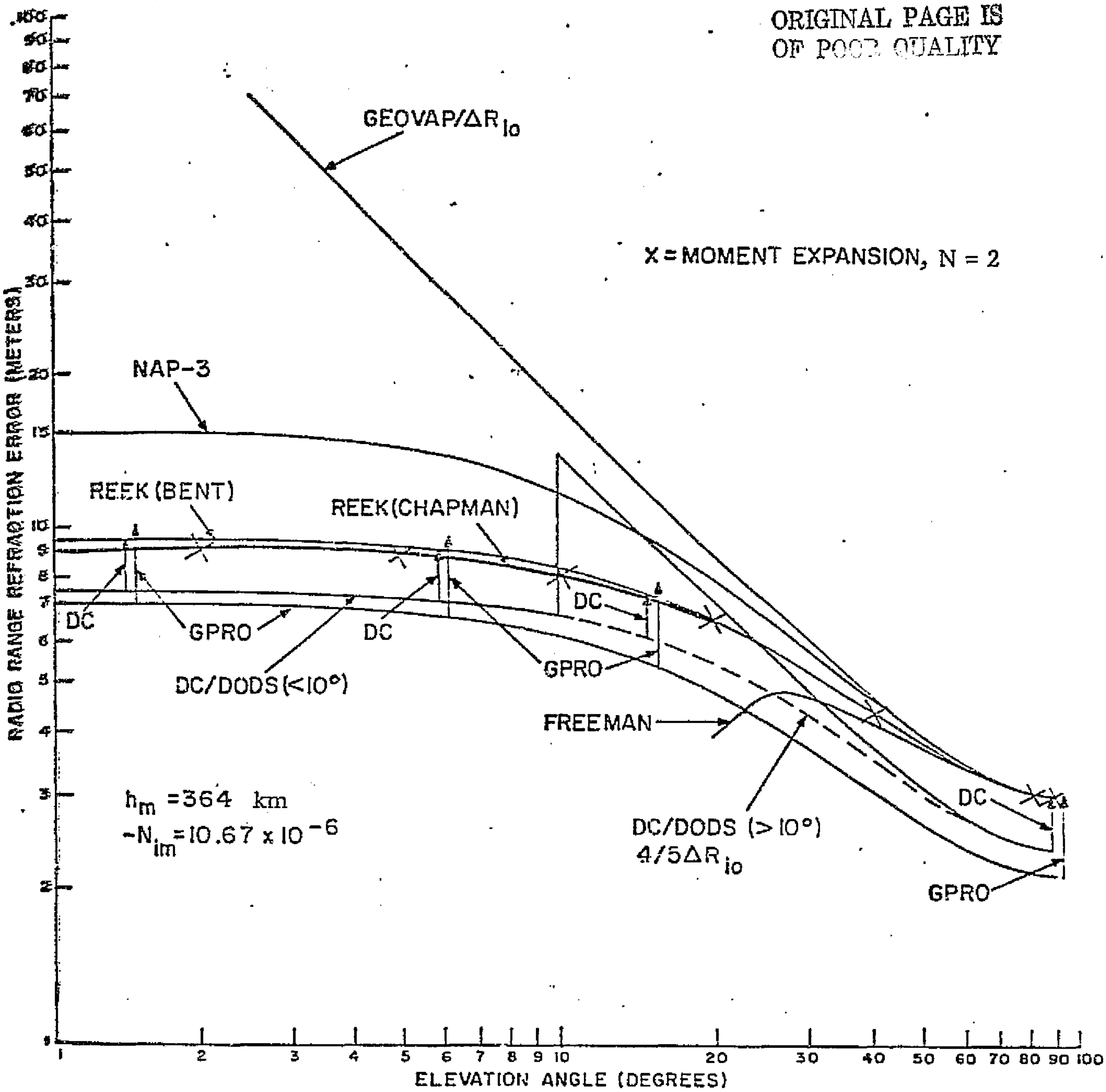

FIGURE 5.4

RANGE ERROR DUE TO IONOSPHERIC REFRACTION

ORIGINAL PAGE IS
OF POOR QUALITY

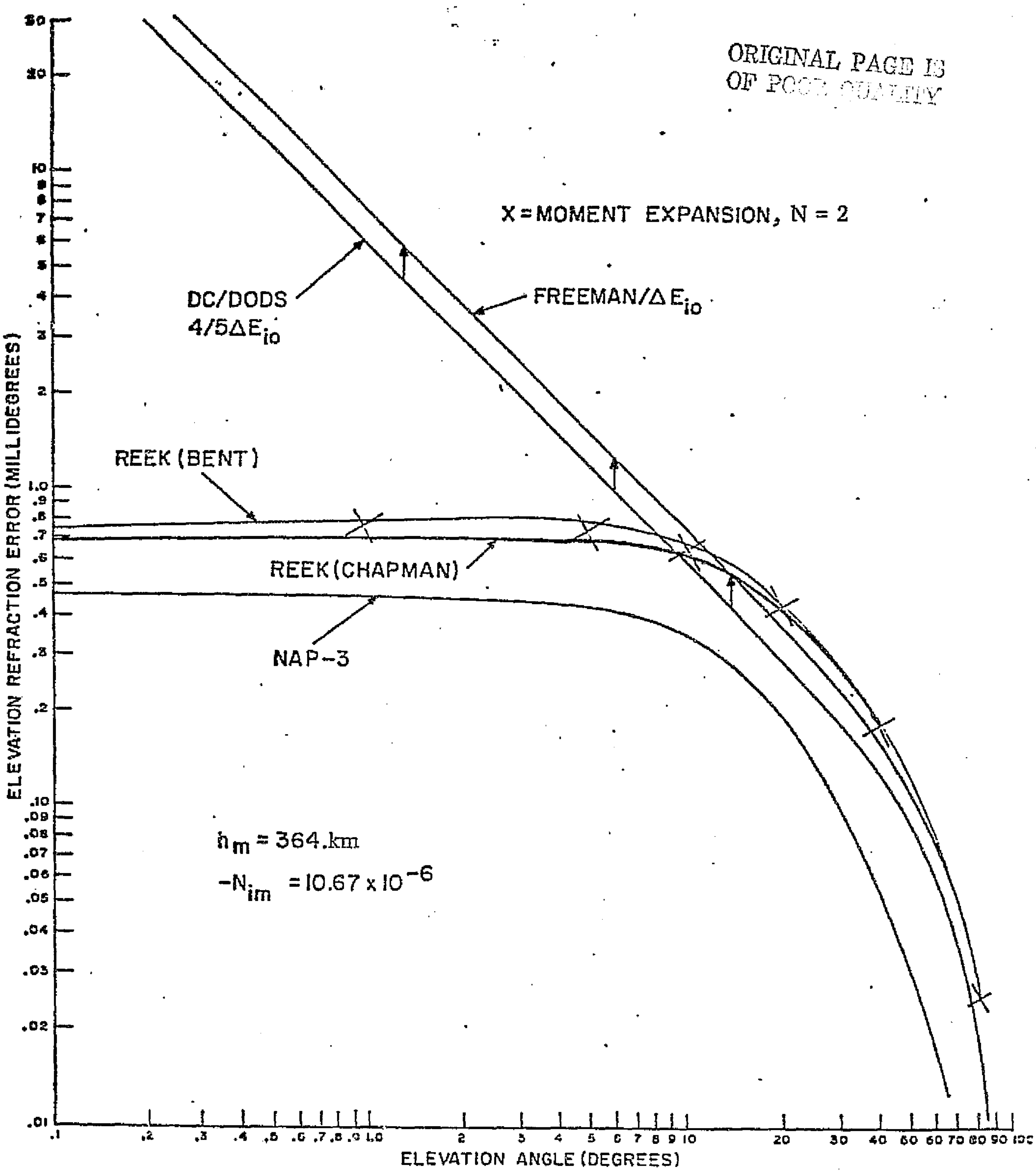

FIGURE 5.5

ELEVATION ERROR DUE TO IONOSPHERIC REFRACTION

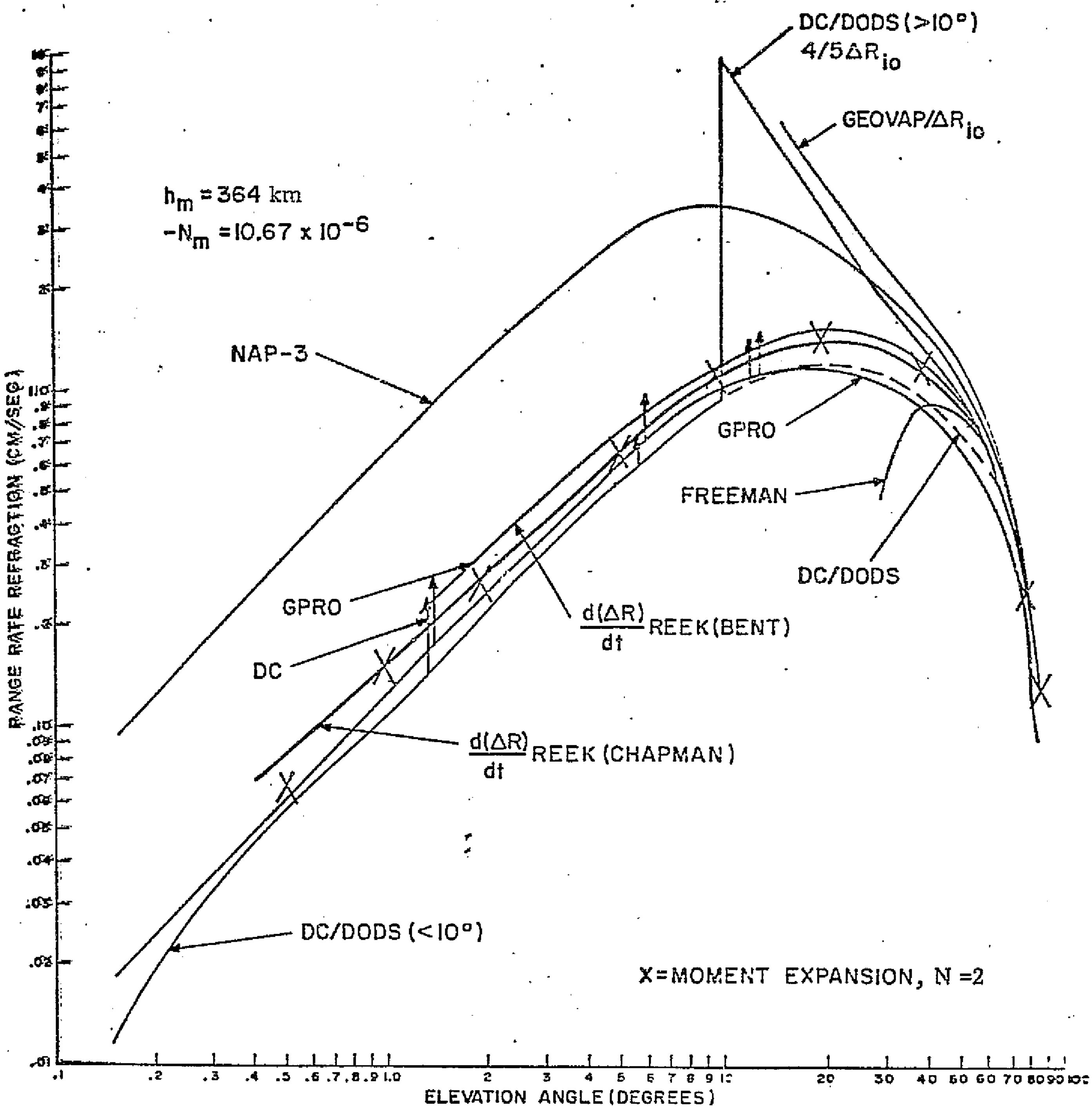

FIGURE 5.6

RANGE RATE ERROR DUE TO IONOSPHERIC REFRACTION

TABLE 5.2

TROPOSPHERIC RANGE ERROR

ΔR_T (m)

ELEV. Degs.	MOMENT EXPANSIONS TO ORDER: 0	1	2	3	4	5	REEK
0.1	46.609	46.609	64.023	35.035	149.033	351.920	---
0.5	45.842	45.842	61.868	36.062	134.230	283.065	63.6367
1.0	43.684	43.684	56.273	37.865	101.450	143.975	54.1222
2.0	37.359	37.359	43.113	36.961	52.501	8.640	40.7921
4.0	25.946	25.946	26.872	26.395	26.976	26.185	26.3309
5.0	22.028	22.028	22.435	22.284	22.417	22.287	22.1553
7.0	16.689	16.689	16.789	16.768	16.779	16.773	---
10.0	12.112	12.112	12.132	12.130	12.131	12.131	12.1028
20.0	6.310	6.310	6.310	6.310	6.310	6.310	6.3105
40.0	3.380	3.380	3.380	3.380	3.380	3.380	3.3811
80.0	2.209	2.209	2.209	2.209	2.209	2.209	2.2092
90.0	2.176	2.176	2.176	2.176	2.176	2.176	2.1756

TROPOSPHERIC MODEL: EXPONENTIAL

$N_s = 313 \cdot 10^{-6}$

$H_c = H_s = 6951$ m

ORIGINAL PAGE IS
OF PO[illegible]

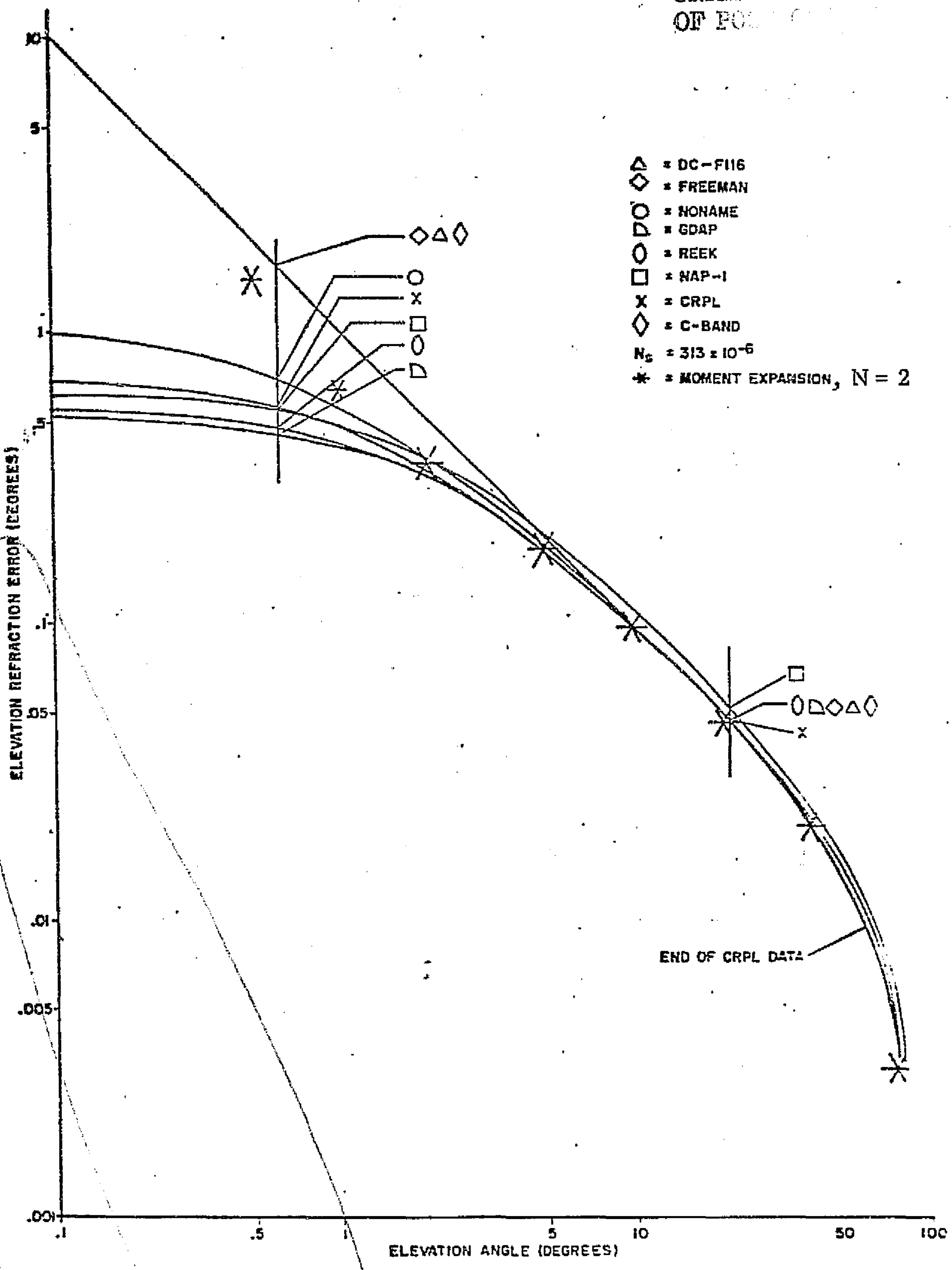

FIGURE 5.7

RANGE ERROR DUE TO TROPOSPHERIC REFRACTION

ORIGINAL PAGE IS
OF POOR QUALITY

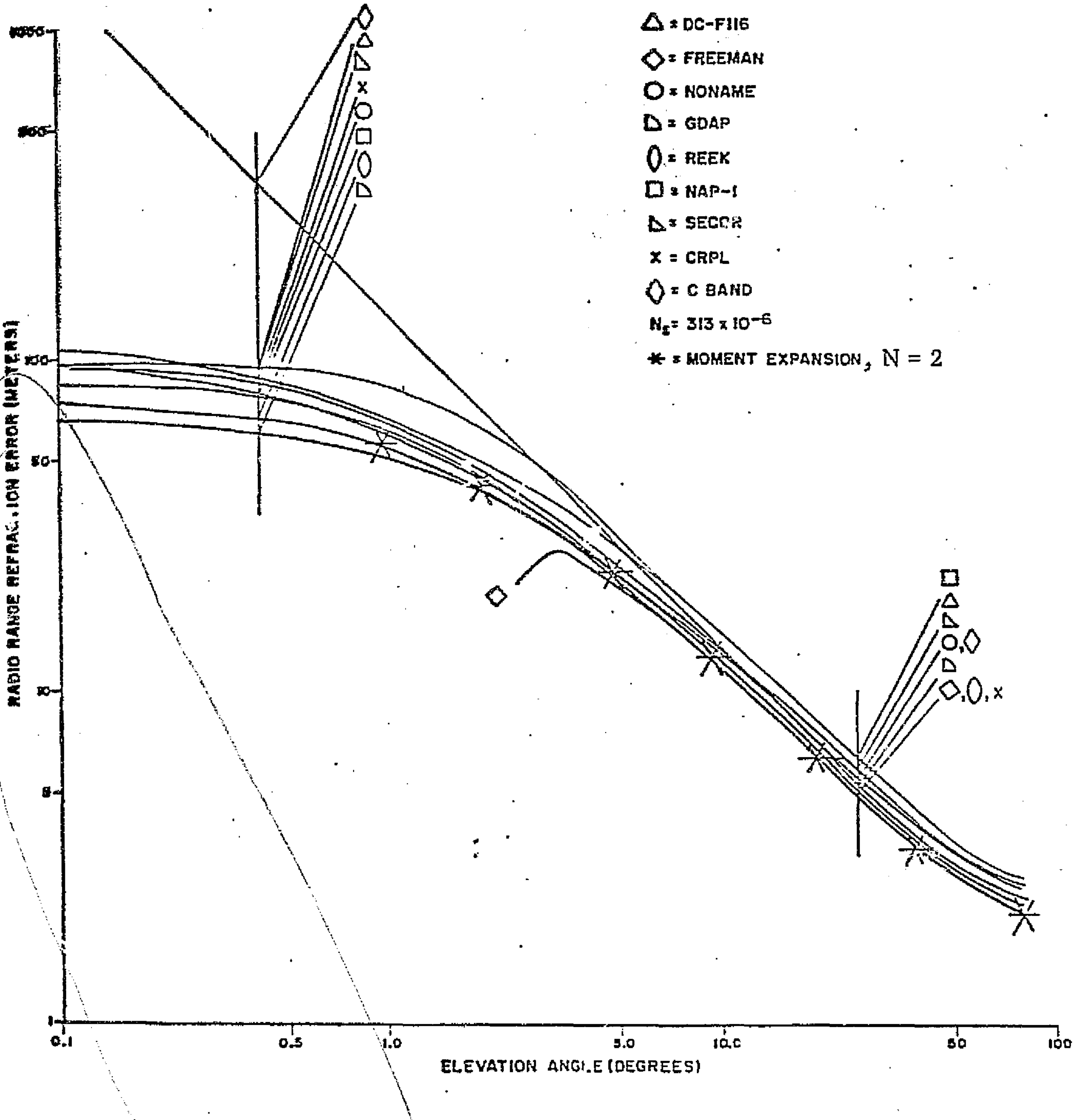

FIGURE 5.8

ELEVATION ERROR DUE TO TROPOSPHERIC REFRACTION

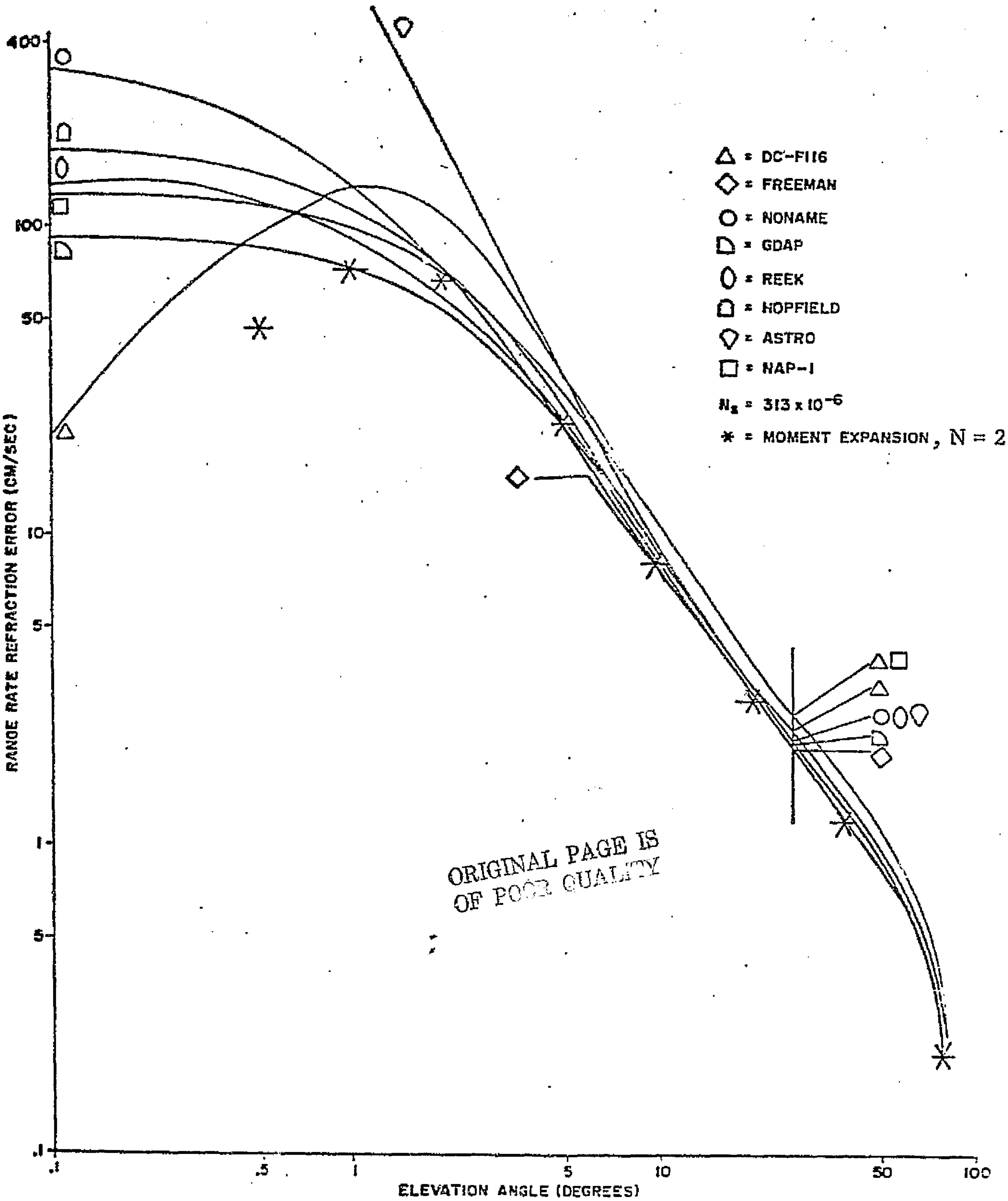

ORIGINAL PAGE IS
OF POOR QUALITY

FIGURE 5.9

RANGE RATE ERROR DUE TO TROPOSPHERIC REFRACTION

6. PROFILE DETERMINATIONS

Because of the predominant role of ionospheric errors in the systems under consideration, a considerable effort was devoted to a study of how well the ionospheric profile could be predicted or measured by available techniques, including bottomside and topside sounders and predictions. This section describes the techniques used for these predictions and their comparisons.

6.1 Jackson's Composite Profiles

The principal source of ionospheric profile data was that provided by John E. Jackson of GSFC for 16 of the 17 Alouette coincidences identified in Table 6.2a). These consisted of composite bottomside and topside profiles, based on true height reductions of bottomside ionosonde and topside Alouette data. In some cases these involved both Alouette 1 and Alouette 2 passes and in some cases both Ottowa and Grand Bahama Island bottomside soundings which provided a basis for estimation and incorporation of Latitudeinal gradients. Alouette 2 data by itself was of limited usefulness because of its low altitude ($\approx$530 km), only slightly above $h_{max}F_2$. Also some adjustment was necessary to the topside heights to account for the observations discussed elsewhere (Ref. 24) that topside ionosonde reduction apparently tends normally to estimate true heights that are too low and bottomside-topside composite profiles meshed straightforwardly tend to predict a total ionospheric content (or effective thickness) 2% to 15%, averaging about 5% too low. The details of how these various complications were handled are recorded in a series of GSFC memoranda and documents (Refs. 24 and 25). Suffice it to day here that these "Jackson composite" profiles represent what is believed to be the best product of skilled judgement based on available topside and bottomside soundings.

6.2 ESSA Bottomside Profiles

For comparison with these "Jackson composites" ESSA was asked to do an independent reduction of the associated bottomside-only profiles for six days for which good ionosonde data was available. ESSA further provided estimates of the entire ionospheric profile based on extrapolations of the bottom-side-only data using a modified Chapman layer fit.

6.3 Predictions from Radio Propagation Predictions

A method that has been in use at GSFC for some time utilizes radio propagation predictions as an indirect basis for estimating ionization density profiles. The origin of the method is unknown but it is discussed and refined in terms of its numerical parameters in Ref. 26, which is the form adopted for this sutdy. As a starting point the quantities

$$f_oF_2 = F_2 \text{ layer ordinary critical frequency}$$

and

$$M(3000)F_2 = 3000 \text{ km MUF factor}$$

or

$$EJF(0)F_2 = MUF(0)F_2 = \text{Estimated Junction Frequency or "Standard" Maximum Usable Frequency reflected from } F_2 \text{ layer at vertical incidence}$$

and

$$EJF(4000)F_2 = MUF(4000)F_2 = \text{same thing at 4000 km range}$$

are obtainable from predictions, e.g., Ref.27, either numerically or graphically. In the latter case, the EJF quantities are normally given in which case these are transformed to the former two quantities by (Ref. 27)

$$f_oF_2 = MUF(0)F_2 - \frac{f_H}{2}$$

and

$$M(3000)F_2 = \frac{EJF(4000)F_2}{1.1 \times f_oF_2}$$

where f_H = local magneto-gyro frequency

$$= \frac{eB}{2\pi m}$$

$$\approx 1.5 \text{ MHz at Wallops Island.}$$

In terms of these available predicted quantities, then, the layer refractivity is modelled by a modified Chapman shape

$$N(h) = N_m \exp(1 - z - e^{-z})$$

where $z = \dfrac{h - h_m}{H_s}$

with parameters related to the predicted quantities by

$$N_m = -\frac{1}{2}\left(\frac{f_oF_2}{f}\right)^2$$

$$h_m = 1393.1 \exp(-0.5014 \times M(3000)F_2)$$

(= height of layer maximum)

$$H_s = \frac{5}{3}\left[30 + .2(h_m - 200)\right] = \frac{h_m - 50}{3}$$

For future reference these equations will be called the Freeman prediction.

Note that under this model the total refractivity integral or zeroeth order moment is given by

$$\int N\,dh = M_o = N_m H_s e$$

where $e = 2.71828\ldots$

Two different sets of basic ionospheric predictions were compared under Freeman's method, the first using the "Basic Radio Propagation Predictions Three Months in Advance", published for the period of the tests by CRPL (now ESSA) and the second based on CCIR report #340, "Atlas of Ionospheric Characteristics", (Oslo 1966), using the relevant sunspot number R = 112. Both provide the same type of data but with slightly different numerical results.

6.4 ESSA Predictions

For some time ESSA has provided to GSFC monthly predictions of maximum refractivity N_m and h_m which are then used in a form equivalent to the above equations for minitrack corrections. The predictions are valid for the month but for simplicity are given at only 4 times during the day which are then interpolated linearly to the time of interest.

6.5 Comparisons in Terms of Moments

A convenient mode for comparison was available in terms of the moment expansion technique developed in section 5 whereby

$$\Delta R = \sum_{m=0}^{N} G_m(E_o) M_m$$

where M_m = m^{th} moment of refractivity profile distribution in height

$$= \int_{o}^{h_s} (h - h_c)^m N(h)\, dh$$

h_s = satellite height, taken as infinite for these comparisons

N = expansion order.

From section 5 it was found that the expansion to $N = 2$ suffices so that only the $N = 0, 1, 2$ terms need be considered.

The moment expansion has the merit for these purposes of explicitly separating the angular dependence from the profile shape dependence in the $G_m(E_o)$ and M_m terms, so makes possible a comparison of fundamental layer parameters independent of particular ray geometry, in terms of the first three moments, M_o, M_1, and M_2. Note that the dominant term, M_o, corresponds simply to the range error on a vertical ray or total refractivity integral. The first three geometrical coefficients, $G_o(E)$, $G_1(E)$, $G_2(E)$ are plotted in Figure 6.1.

The moment series comparison was carried out in detail for the "Jackson Composite" and "ESSA Bottomside" profiles in Ref. 28 for 6 days.

The ESSA profiles were given at 3 to 5 15 minute intervals, about the reference time taken as t_{PCA}, time of point-of-closest- approach.

The first 3 moments M_0, M_1, and M_2 were found by numerical integration for each adjacent time for each day, giving

$$M_{n,t,d}$$

$$n = \text{order} = 0,1,2.$$

$$t = \text{record index for day} = 1,2,\ldots T_d$$

$$T_d = 3 \text{ to } 5$$

$$d = \text{day} = 1,\ldots 6$$

For the purpose of this analysis the 3 to 5 data within ± 45 min of TCA for each day were averaged giving

$$\overline{M}_{n,d}$$

which were then compared with the corresponding moments for the Jackson composite profiles, denoted M^j, yielding the differences

$$DD_{n,d} = \overline{M}_{n,d} - M^j_{n,d}$$

The mean and standard deviation statistics of $DD_{n,d}$ were computed yielding the data of Table 6.1.

It is notable from the Table that the sample bias term is only of the order of 1/3 of the estimated standard deviation, in other words, the discrepancies between the two types of data do not appear to be significantly biased.

The significance of the various orders of moments in terms of the total range error discrepancy is shown in Figure 6.2 where the standard deviations above

ORIGINAL PAGE IS
OF PO...

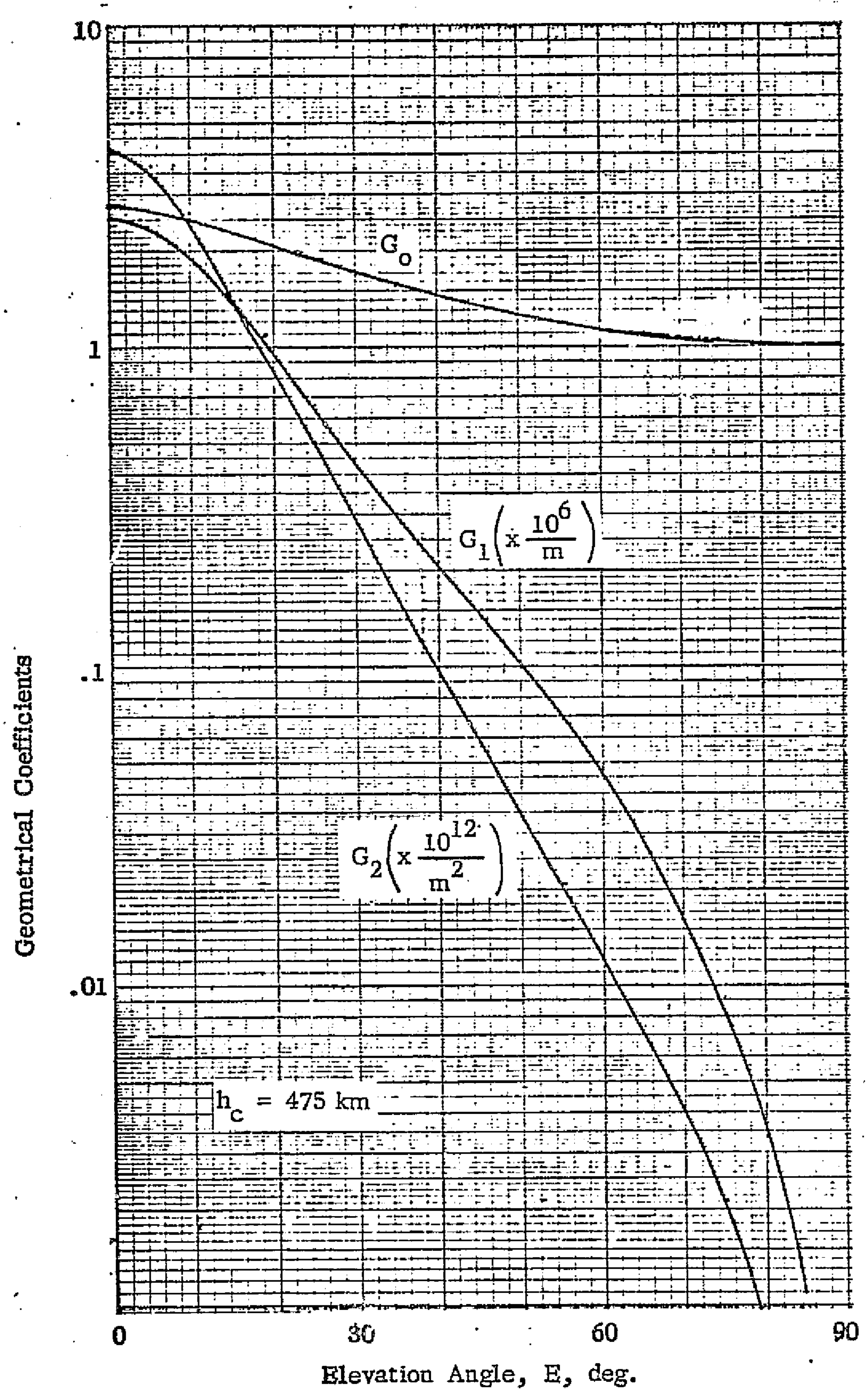

FIGURE 6.1
GEOMETRIC COEFFICIENTS OF THE MOMENT EXPANSION

TABLE 6.1

COMPARISON OF ESSA BOTTOMSIDE PROFILE EXTRAPOLATIONS AND JACKSON COMPOSITE PROFILES IN TERMS OF MOMENTS

f = 434 MHz

		ORDER OF MOMENT		
		n = 0 (meters)	1 (meters)^2	2 (meters)^3
$\overline{DD}_n$	= Mean	-1.79	8.62 E4	1.53 E10
σ_n	= Std. Dev	3.075	2.34 E5	3.97 E10
$\sqrt{\overline{DD}_n^2 + \sigma_n^2}$	= RMS	3.56	2.49 E5	4.25 E10

C-2

ORIGINAL PAGE IS
OF POOR QUALITY

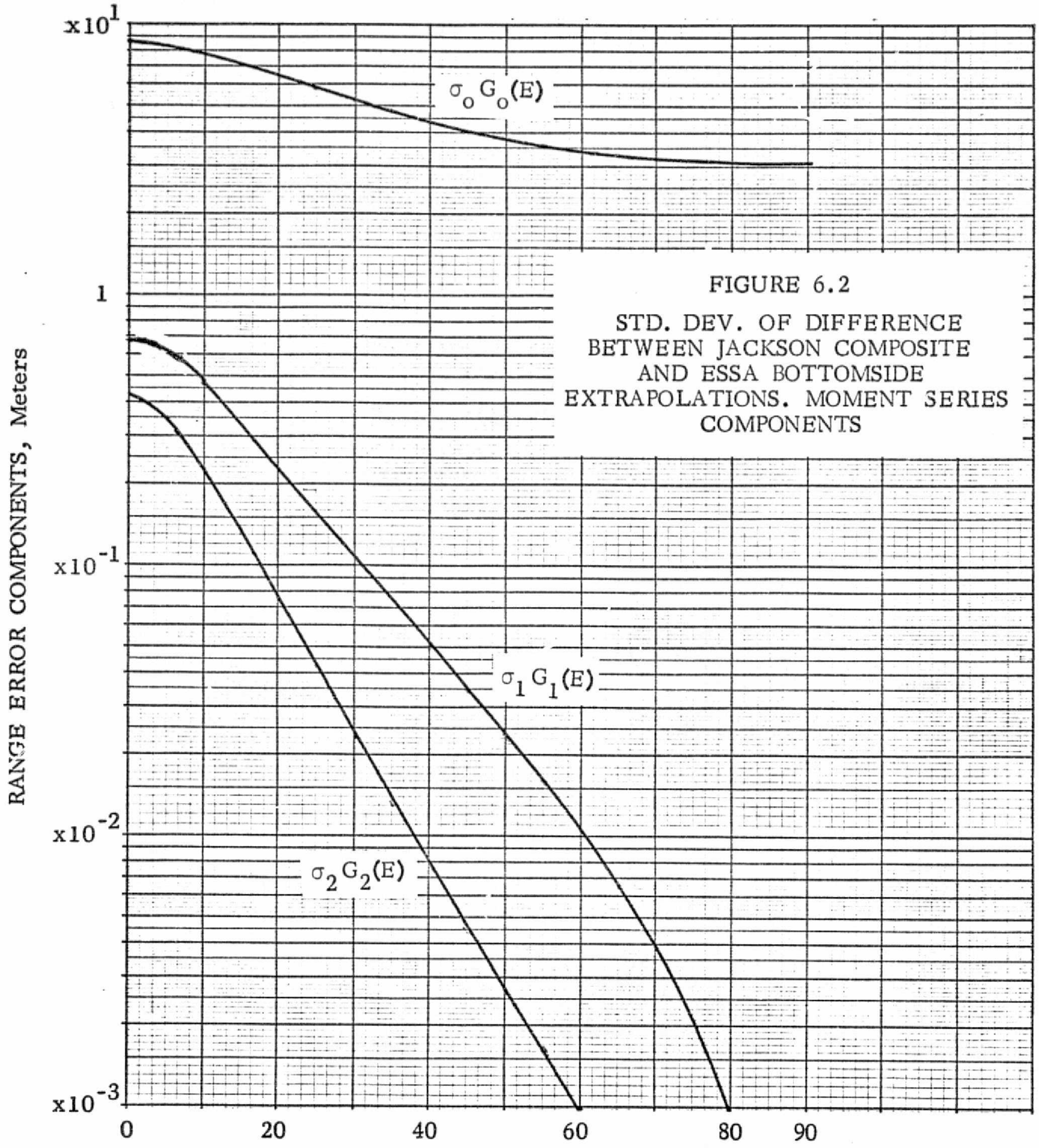

FIGURE 6.2

STD. DEV. OF DIFFERENCE BETWEEN JACKSON COMPOSITE AND ESSA BOTTOMSIDE EXTRAPOLATIONS. MOMENT SERIES COMPONENTS are multiplied with their corresponding coefficients and plotted as the terms

$$\sigma_0 G_0(E),\ \sigma_1 G_1(E),\ \sigma_2 G_2(E).$$

It is immediately evident from Figure 6.2 that the zero order term predominates by more than an order of magnitude and accounts for better than 99% of the total variance even in the worst case of low elevation angles and fully correlated moment discrepancies. The analysis of Ref. 28 considered the actual correlation effects between the various orders of moments by computing the full moment discrepancy covariance matrix and propagating the resulting covariance in the correct manner through the moment series summation to compute the total rance variance; the results reconfirm the above general conclusion as to the dominance of the zero order term.

The first and second order moments add significantly to the accuracy of the zero order term for actual data correction. For the purpose of profile accuracy comparisons, however, the above analysis indicates that essentially all the significant difference is in the zeroeth order term and further comparisons can be made most efficiently in terms of M_0 alone, independent of elevation angle.

This comparison is carried out in Table 6.2 for the 17 Alouette-GEOS coincidence passes, and for the four predictions discussed above. In addition, as a point of comparison, Table 6.2 includes the actual ionospheric total content measured by the SECOR two-frequency data at the point of GEOS closest approach and adjusted from measured slant path to vertical path by the geometrical coefficient $G_0(E)$ evaluated at the elevation angle corresponding to the point of closest approach (50 degrees or greater in all cases) and using, in this case, expansion center $h_c = 350$ km.

The rms differences of the various predictors (columns) in Table 6.2 a) are shown in Table 6.2 b). The rms discrepancies lie generally in the range 4 to 11 meters or roughly 15 to 35% of the total error. It is tempting to utilize the matrix of rms discrepancies as a basis of estimation of the absolute errors of each of the columns in a modified Grubbs variance analysis. This is probably not legitimate because of correlations between the errors of various predictors; for example, columns 2 and 4 (Freeman predictions based on different ionospheric radio predictions) should be expected to be highly correlated.

TABLE 6.2a)

COMPARISON OF IONOSPHERIC PROFILE PREDICTORS IN TERMS OF M_0 (TOTAL REFRACTIVITY INTEGRAL) (METERS) AT F = 434 MHz

GMT Mo. Day Hr. Min.	1 SECOR ICOR (Measurement)	2 Freeman Method Using 3 Mo. Predictions	3 Modified Jackson Composites	4 Freeman's Method Using CCIR Predictions For R = 112	5 ESSA Bottomside Profile Extrapolations
4 03 0143	49.14	32.51	43.30	35.80	47.49
4 05 0221	33.49	29.60	29.75	33.00	28.69
4 10 0207	36.12	30.21	33.21	33.60	31.61
4 12 0245	27.44	28.55	28.86	32.10	30.37
4 17 0231	35.27	29.16	32.31	32.60	38.69
4 22 1743	##.##	58.13	##.##	73.30	##.##
5 24 0320	51.40	26.95	46.58	29.20	47.22
5 25 0339	31.47	26.09	27.26	27.97	##.##
5 29 0306	42.08	##.##	33.11	30.11	##.##
5 30 0325	36.45	26.70	28.64	28.88	##.##
6 04 0312	34.06	26.12	27.60	27.90	##.##
6 05 0331	37.47	25.04	35.19	27.63	##.##
6 11 1715	29.03	##.##	26.78	33.83	##.##
6 13 1753	33.34	##.##	30.53	35.91	##.##
6 18 1739	##.##	##.##	42.15	35.15	##.##
6 21 0458	23.07	##.##	19.30	21.55	##.##
6 25 0425	33.09	##.##	28.73	24.76	##.##

TABLE 6.b)

RMS DIFFERENCE MATRIX (METERS)

PREDICTION #

	1	2	3	4	5
1	0	11.42	4.78	8.77	3.74
2	11.42	0	7.94	5.32	11.04
3	4.78	7.94	0	6.09	3.28
4	8.77	5.32	6.09	0	9.34
5	3.74	11.04	3.28	9.34	0

Probably a more meaningful interpretation is to take the SECOR as a reference standard on the basis that its error is believed to be well under the 3 or 4 meters rms discrepancy between SECOR and the best of the predictors. Interpreted in this way, rough upper limits on the absolute error of the various predictions are as follows

Profile Measurements	$\overline{\Delta m}$ meters	Δ_{rms} meters	Std. Dev. σ_Δ meters	RMS % of $\overline{m}$
Jackson Composite	−4.1	4.8	2.5	13
ESSA Bottomside Extrapolation (only 6 cases)	−1.5	3.7	3.4	10
Profile Predictions				
CCIR Report 340	−5.2	8.8	7.1	24
3 Mos. Advance Predictions	−9.1	11.4	6.9	32

The assessment of the ESSA bottomside profile extrapolations is of questionable validity as it only includes 6 cases. The Profile measurements clearly provide a better basis than the predictions with errors something less than 10-15%. The Freeman predictions based on the CCIR #340 radio predictions show about 24% residual error, remarkably consistent with the original claim of Freeman (Ref.26) of 25% but notably on a completely independent data set. It may be marginally significant that all the mean biases are of a negative sense.

6.6 Geographical Gradients

The visibility period of the GEOS satellite during WICE typically was such that the line-of-sight ray swept over some 20 degrees of latitude through the ionosphere. Naturally, the ionospheric changes over this distance are often significant, occasionally as much as 2:1 in terms of total electron content or M_o.

Considerable effort had been expended on defining the Jackson composite topside-bottomside ionospheric profiles at Wallops Island with considerable success when compared to SECOR measurements at the point-of-closest approach to Wallops as reported in the previous section. An investigation was then undertaken of various proposed methods of scaling the Wallops predicted profile for its geographic variation based on either predicted or observed (bottomside sounder) geographical variations.

Define

$N^j(W,h)$ = Jackson composite refractivity at Wallops at Height h, applicable at time of closest approach.

$p(e,h)$ = geographical position (lat,long) of height h along ray at elevation e.

$N^p(p,h)$ = predicted (Freeman-CRPL Radio predictions) refractivity at position p, height h.

$N^p_{max}(p)$ = predicted maximum refractivity at point p - proportional to $(f_oF_2)^2$.

$N^m_{max}(p)$ = measured max refractivity at p, proportional to $(f_oF_2)^2$.

h_o = reference height in the ionosphere, taken as 425 km.

Definition of scaling methods:

$$N_4(h) = N^j(W,h)\left[\frac{N^p(p(e,h),h)}{N^p(w,h)}\right]$$

(Scaling by predicted ratio of electron densities at height h)

$$N_5(h) = N^j(W,h)\left[\frac{N^p_{max}(p(e,h))}{N^p_{max}(w)}\right]$$

(Scaling by predicted ratio of $(f_oF_2)^2$ at $p(e,h)$)

$$N_7(h) = N^j(W,h)\left[\frac{N^p_{max}(p(e,h_o))}{N^p_{max}(w)}\right]$$

(Scaling by predicted ratio of $(f_oF_2)^2$ at $p(e,h_o)$)

$$N_8(h) = N^j(W,h)\left[1+\frac{(N^m_{max}(L_2)-N^m_{max}(L_1))}{N^m_{max}(L_w)}\;\frac{(L(p(e,h_o))-L_w)}{(L_2-L_1)}\right]$$

(Scaling by Latitudinal Interpolation between observed $(f_oF_2)^2$)

Note that in N_7 and N_8 the scaling factors are not functions of height so that the ray tracing can be done on $N^j(W,h)$ and the result scaled by the factors F_7 or F_8 in brackets. For #8, the scaling was based on linear Latitude interpolation in terms of refractivity (or f_o^2) between the Ottowa and Grand Bahama f_oF_2's.

Each of the corrections:

R_o = SECOR measurement

R_c = Ray trace on local composite profile - not scaled geographically

R_5 = Ray trace on N_5

R_7 = $R_c \times F_7$

R_8 = $R_c \times F_8$

were computed at the southerly and northerly points of 25^o elevation and point-of-closest approach, denoted by: EL = 25^o South, (25 S), Point of Closest approach to Wallops (W) and EL = 25^o North (25N). The corrections are given in Table 6.3 in this order.

The overall scaling factor including geographic and elevation angle dependence is defined by the ratios

$$G_i(S/W) = R_i(25S)/R_i(W)$$

and

$$G_i(W/N) = R_i(W)/R_i(25N)$$

$$G_i(S/N) = R_i(25S)/R_i(25N)$$

where $i = o, c, 4, 5, 7, 8.$

For the R_c data, which is based on the assumption of non-geographically scaled profile equal to the local composite, this ratio represents only the elevation angle scaling. This is then used as a basis to remove the first-order elevation angle dependence by forming the geographic scaling factors

$$F_i(S/W) = G_i(S/W)/G_c(S/W)$$

$$F_i(W/N) = G_i(W/N)/G_c(W/N)$$

$$F_i(S/N) = G_i(S/N(/G_c(S/N)$$

tabulated in Table 6.4.

Finally, using the actual measurements as given by the SECOR data, (F_o) the

TABLE 6.3

RANGE CORRECTIONS (METERS)

VARIOUS GEOGRAPHIC SCALINGS

Date	EL (deg)	RO	RC	F7	F8	R5	R7	R8
4 03	25.01 S	104.61	83.28	1.030	1.090	86.41	85.78	90.75
	67.80	52.86	46.90	0.978	1.000	45.83	45.87	46.90
	25.03 N	77.03	83.35	0.946	0.910	78.95	78.85	75.82
4 05	25.07 S	65.20	57.54	1.112	1.056	64.07	62.25	60.76
	69.49	36.69	32.41	1.013	1.000	32.85	32.73	32.41
	25.03 N	50.77	57.64	0.961	0.945	55.56	55.69	54.46
4 10	24.98 S	66.93	64.19	1.067	0.944	68.75	68.49	60.58
	82.53	37.26	33.73	0.995	1.000	33.55	33.56	33.73
	25.03 N	72.83	64.24	0.954	1.060	61.36	61.29	67.95
4 12	24.99 S	54.50	55.06	1.115	1.038	61.79	61.39	57.19
	56.19	32.24	34.12	1.011	1.000	34.52	34.49	34.12
	25.04 N	51.80	55.11	0.948	0.962	52.37	52.24	53.05
4 17	25.07 S	70.95	62.03	1.106	1.103	68.75	68.60	68.44
	81.74	35.59	32.90	1.003	1.000	33.10	33.09	32.99
	25.00 N	60.05	62.34	0.945	0.899	59.04	58.91	56.06
5 24	25.24 S	125.04	88.24	1.190	1.088	106.57	105.01	96.01
	84.28	51.44	48.69	0.977	1.000	47.45	47.57	48.69
	30.20 N	42.25	81.03	0.920	0.752	74.79	74.55	60.93
5 25	30.30 S	52.90	47.12	1.334	1.016	62.95	62.86	47.86
	76.49	31.31	28.42	1.105	1.000	31.66	31.40	28.42
	34.88 N	48.77	43.44	1.103	1.008	48.30	47.91	43.79
5 29	25.33 S	83.72	62.83	1.115	0.975	70.92	70.06	61.26
	62.18	46.67	37.42	0.960	1.000	35.40	35.92	37.42
	25.22 N	77.09	62.23	0.848	0.951	53.85	53.62	60.14
5 30	25.11 S	85.14	54.82	1.170	0.893	64.35	64.14	48.95
	79.51	37.62	29.81	0.948	1.000	28.25	28.26	29.81
	34.94 N	54.15	45.61	0.897	0.924	41.16	40.91	42.14
6 04	32.26 S	62.31	46.01	1.125	1.037	52.09	51.76	47.71
	59.61	39.50	32.01	0.938	1.000	30.20	30.03	32.01
	25.18 N	59.10	52.96	0.807	0.950	43.15	42.74	50.31
6 05	25.38 S	93.34	67.26	1.375	1.008	90.93	92.48	67.80
	75.16	39.40	36.88	0.974	1.000	35.96	35.92	36.88
	35.18 N	56.29	55.81	0.809	0.916	45.82	45.15	51.12
6 11	39.96 S	41.18	43.40	1.123	0.995	47.98	48.74	43.08
	68.99	31.35	31.87	1.061	1.000	33.60	33.81	31.87
	25.13 N	65.55	57.78	1.076	1.050	62.14	62.17	60.67
6 13	39.88 S	46.49	48.57	1.021	1.002	49.60	49.59	48.67
	77.97	32.74	34.25	0.979	1.000	33.57	33.53	34.25
	25.33 N	76.42	63.72	1.021	1.186	65.65	65.06	75.57
6 21	30.18 S	47.20	33.71	1.771	0.993	56.69	59.70	33.47
	49.68	30.82	24.71	1.117	1.000	27.23	27.60	24.71
	45.13 N	30.82	26.25	0.951	0.978	25.12	24.96	25.67
6 25	29.82 S	65.19	50.69	1.657	0.981	81.98	83.99	49.73
	83.98	33.84	29.52	1.020	1.000	29.95	30.11	29.52
	39.99 N	44.39	42.46	0.751	0.957	32.69	31.89	40.63

fractional error is taken as

$$e_i(X) = \frac{F_i(X) - F_o(X)}{F_o(X)}$$

$$X = \begin{cases} S/W \\ W/N \\ S/N \end{cases}$$

The mean and estimated standard deviation of these errors are given in Table 6.4.

Within the limitation of the small data sample here represented, the following conclusions emerge.

1) In all cases - even unscaled, the mean scaling factor errors are relatively small compared to the random part. There is no significant indication of bias.

2) Without any scaling at all the standard deviation of the error is of the order of 13% (S/W), 28% (W/N), 24% (S/N).

3) The 5, 7 corrections which are based on the predictions are no significant improvement over no geographic scaling at all.

4) The best scaling is #8 which is the linear scaling in latitude based on bottomside f_oF_2 measurement.

This conclusion should be further qualified by noting that these passes were all essentially South-North and represent only two times of day.

TABLE 6.4

GEOGRAPHIC SCALING FACTORS, F(X, Y)

	DATE - 1968															FRACTIONAL ERROR REFERENCE: SECOR	
	4-03	4-05	4-10	4-12	4-17	5-24	5-25	5-29	5-30	6-04	6-05	6-11	6-13	6-21	6-25	MEAN	STD. DEV.
								F(S/W)									
SECOR	1.114	1.000	0.943	1.047	1.055	1.341	1.019	1.068	1.231	1.097	1.299	1.153	1.255	1.123	1.122	0	0
RC	1.000	1.000	1.000	1.000	1.000	1.000	1.000	1.000	1.000	1.000	1.000	1.000	1.000	1.000	1.000	-0.102	0.133
R5	1.062	1.098	1.076	1.109	1.105	1.239	1.199	1.193	1.239	1.200	1.387	1.020	1.051	1.526	1.594	0.079	0.173
R7	1.053	1.071	1.076	1.102	1.103	1.218	1.207	1.162	1.234	1.199	1.412	1.014	1.043	1.586	1.624	0.079	0.185
R8	1.090	1.055	0.943	1.038	1.103	1.088	1.016	0.975	0.893	1.037	1.008	1.050	1.186	0.993	0.981	-0.076	0.120
								F(W/N)									
SECOR	1.222	1.284	0.974	1.005	1.120	0.494	1.019	0.978	0.941	0.904	0.944	0.965	1.001	0.941	0.912	0	0
RC	1.000	1.000	1.000	1.000	1.000	1.000	1.000	1.000	1.000	1.000	1.000	1.000	1.000	1.000	1.000	0.064	0.280
R5	1.031	1.051	1.041	1.064	1.059	0.947	0.998	0.900	0.952	0.864	0.842	1.049	1.042	0.868	0.759	0.020	0.255
R7	1.034	1.045	1.043	1.066	1.062	0.942	0.998	0.883	0.946	0.860	0.831	1.059	1.043	0.851	0.736	0.014	0.255
R8	1.099	1.058	0.945	1.038	1.112	0.752	1.008	0.951	0.924	0.950	0.915	0.995	1.002	0.978	0.957	0.022	0.147
								F(S/N)									
SECOR	1.359	1.286	0.919	1.053	1.187	2.718	1.000	1.093	1.308	1.214	1.376	1.196	1.253	1.193	1.230	0	0
RC	1.000	1.000	1.000	1.000	1.000	1.000	1.000	1.000	1.000	1.000	1.000	1.000	1.000	1.000	1.000	-0.182	0.238
R5	1.095	1.155	1.121	1.181	1.170	1.308	1.202	1.325	1.301	1.390	1.647	0.973	1.009	1.757	2.101	0.071	0.297
R7	1.089	1.119	1.118	1.176	1.170	1.293	1.210	1.315	1.304	1.394	1.700	0.958	1.000	1.863	2.206	0.081	0.325
R8	1.198	1.117	0.892	1.079	1.226	1.337	1.008	1.025	0.966	1.092	1.101	1.058	1.184	1.015	1.025	-0.119	0.172

7. MULTIPLE FREQUENCY IONOSPHERIC MEASUREMENTS COMPARISONS

Two of the systems used in the WICE made multiple frequency measurements of the ionosphere to provide their own corrections, but incidentally provided a valuable basis of intercomparison and reference for other external ionospheric corrections.

The SECOR system utilizes a pair of 2:1 coherently related carriers on the down-link at 224.5 and 449.0 MHz. Group range is measured on each and the difference provides an absolute measurement of the ionospheric error as explained in section 2.3.1.

The TRANET system transmits from the satellite pure CW frequencies of 162, 324 and 972 MHz in a coherent 1:2:6 relationship. Processing of the data as explained in 2.4.4 yields an estimate of the ionospheric doppler or phase rate error Δf_I.

The SECOR and TRANET measurements can be scaled to any reference frequency using the f^{-2} law; the standard frequency for these comparisons has been the SECOR equivalent frequency, i.e., the single frequency equivalent on which would be observed the same errors as are seen on the actual primary up and down link frequencies defined by

$$\frac{2}{f_{eq}^2} = \frac{1}{f_{up}^2} + \frac{1}{f_{down}^2} \tag{7.1}$$

or

$$f_{eq} = \frac{1}{\left[\frac{1}{2}\left(\frac{1}{f_{up}^2} + \frac{1}{f_{down}^2}\right)\right]^{1/2}} \tag{7.2}$$

$$= \frac{1}{\left[\frac{1}{2}\left(\frac{1}{(420.9)^2} + \frac{1}{(449.0)^2}\right)\right]^{1/2}} \tag{7.3}$$

$$= 434.26 \text{ MHz.} \tag{7.4}$$

The SECOR measurements are referred to f_{eq} by

$$\Delta R_{eq_{secor}} = \Delta R_2 \times \left(\frac{f_2}{f_{eq}}\right)^2 \qquad (7.5)$$

and the TRANET measurements are referred to f_{eq} by

$$\Delta \dot{R}_{eq_{tranet}} = \frac{c}{f_1}\left(\Delta f_{I_1}\right)\left(\frac{f_1}{f_{eq}}\right)^2 \qquad (7.6)$$

where ΔR_2 and Δf_{I_1} are as defined in sections 2.3.1 and 2.4.1.

The fundamental problem remains that the TRANET measurements are basically range-rate error while the SECOR measurements are in range. In principle the comparison could be made either in the rate domain by differentiating SECOR data or in the range domain by integrating TRANET, but with the complication of an undetermined constant of integration. Both have been tried and it has emerged that the range comparison is more instructive, and that the undetermined constant can be resolved by a suitable regression procedure.

The general approach to this regression may be described as follows and is described in more detail in Refs. 29 and 30.

The measured ionospheric error is modelled as

$$\boxed{\Delta R^*(t) = \Delta R^c(t) + B + \varepsilon} \qquad (7.7)$$

where ε is a random fitting error to be minimized

B is a bias term to be recovered

$\Delta R^c(t)$ is the computed range error at time t modelled as either

1) "Time Gradient" model

$$\Delta R^c(t) = \left[N_m + \dot{N}_m (t - t_o)\right] \Delta R_1(t) \qquad (7.8)$$

or

2) "Latitudinal Gradient" model

$$\Delta R^c(t) = \left[N_m + \hat{N}_m (L(t) - L(t_o))\right] \Delta R_1(t) \tag{7.9}$$

where N_m = maximum ionization density (e/m^3)

$\dot{N}_m$ = time gradient of max. ionization density, $(e/m^3/sec)$

$\hat{N}_m$ = latitudinal gradient of max. electron density $(e/m^3/deg)$

t_o = time of closest approach

L = latitude

$\Delta R_1(t)$ = per unit maximum density range error at time t

$$= \int_0^{R_{sat}} (n(h(s)) - 1)\, ds \tag{7.10}$$

where $h(s)$ is taken as the straight path

$$h(s) = \sqrt{a^2 + s^2 + 2as \sin E(t)} - a \tag{7.11}$$

a = radius of earth

$$n(h) - 1 = -40.25\, N_1(h)/f^2_{Hz} \tag{7.12}$$

$N_1(h)$ is the per unit maximum density ionospheric model taken in various cases as either "Chapman" or "empirical"

"Empirical" model defined by Figure 7.1

"Chapman" model defined by

$$N_1(h) = \exp(1 - z - e^{-z}) \quad (e/m^3) \tag{7.13}$$

$$z = \frac{h - h_m}{H_s} \tag{7.14}$$

$$h_m = 375 \text{ km} \qquad \text{(nominal)} \tag{7.15}$$

$$H_s = \frac{5}{3}[30 + 0.2(h_m - 200)] \qquad \text{(km)} \tag{7.16}$$

(or in some experiments

$$H_s = \frac{k_s}{3}[30 + 0.2(h_m - 200)] \quad \text{km)} \tag{7.17}$$

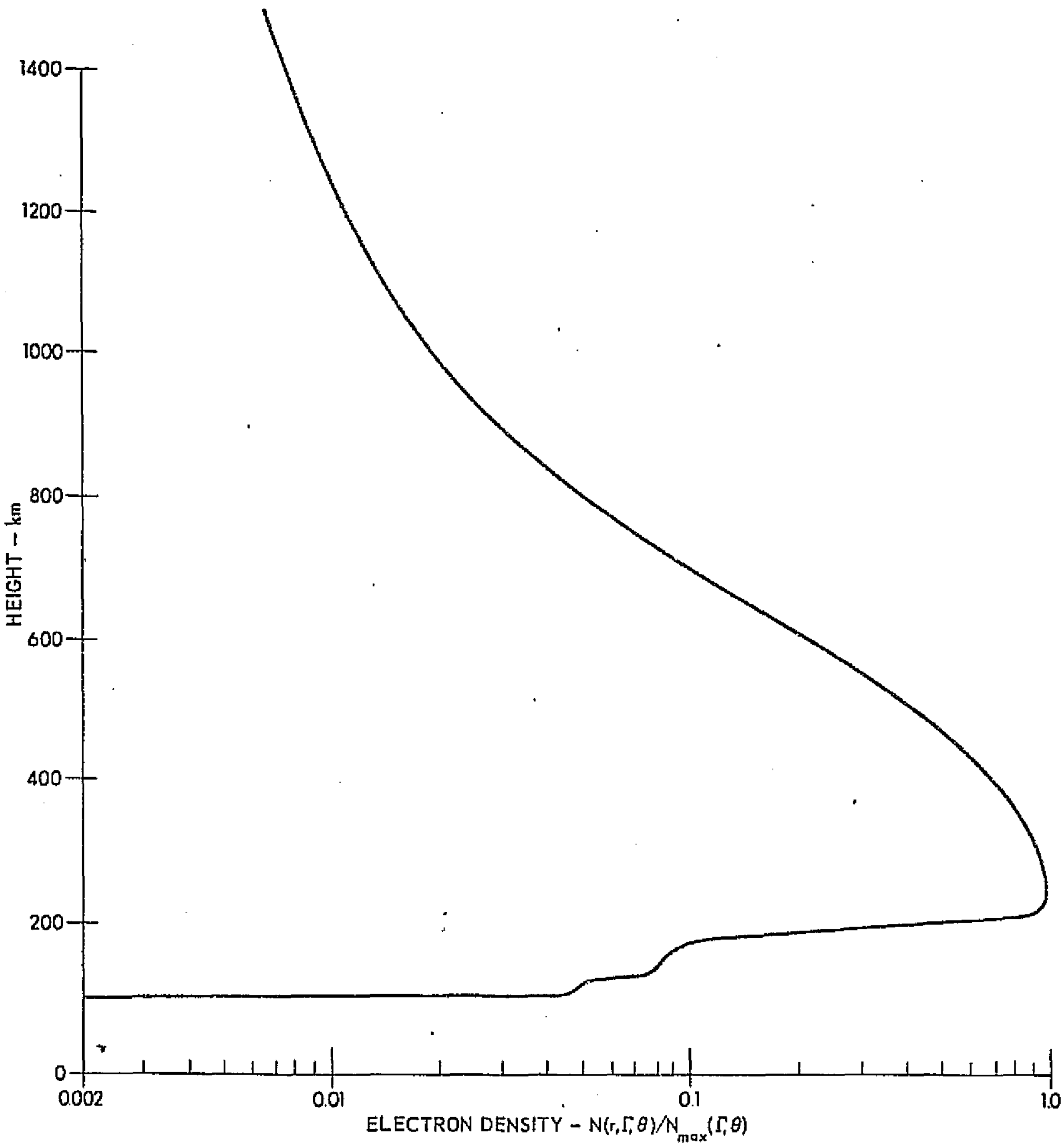

FIGURE 7.1

VERTICAL PROFILE
FOR ELECTRON DENSITY DISTRIBUTION

As a first test of this regression procedure it was excercised on the problem of determining bias if any in the SECOR two-frequency ionospheric data (ICOR) (Ref. 30).

Several preliminary runs with variations in the model by adding an $\ddot{N}$ term showed that the regression was badly unstable in this case (overmodelled). Similarly several runs eliminating the $\dot{N}$ term showed that the gradient term was necessary in general to avoid badly biased results. Essentially all the succeeding runs then were with the three unknown terms as described, B, N_m and $\dot{N}_m$ (or $\hat{N}_m$).

Next a series of runs were made to test the sensitivity of the results to the ionospheric modelling parameters, k_s and h_m (in eqs. 7.14 and 7.17). The results are shown in Table 7.1. In interpreting these results it would be hoped that the recovered bias, B, would be relatively insensitive to the modelling. In fact, it is found that over the reasonable range of variation of the ionospheric layer shape parameters, the recovered bias varies by as much as 3.4 meters but generally less than 1/2 meter. The recovered N_m and $\dot{N}_m$ on the other hand should be expected to vary directly with the modelling parameters in such a way as to tend to hold the total ionospheric content more or less fixed. From equations(7.13) to (7.17) the total layer refractivity content, M_o, which is just the range error on a vertical ray is given for the 434.26 MHz SECOR equivalent frequency by

$$
\begin{aligned}
M_o(k_s, h_m, N_m) &= \int_o^\infty (n-1)\, dh \\
&= -\frac{40.3}{f^2} H_s e N_m \\
&= -\frac{40.3\, e\, 200}{(434.26)^2\, 10^{12}\, 3} N_{m_{e/m}}\, k_s \left[h_{m_{km}} - 50\right] \\
&= 3.873 \cdot 10^{-8} N_{m_{e/cc}}\, k_s \left[h_{m_{km}} - 50\right] \quad \text{meters}
\end{aligned}
$$

Similarly

$$\dot{M}_o(k_s, h_m, N_m) = 3.873 \cdot 10^{-8} \dot{N}_{m_{e/cc/min}}\, k_s \left[h_{m_{km}} - 50\right] \text{ meters/min.}$$

TABLE 7.1

SECOR BIAS REGRESSIONS
TESTS OF SENSITIVITY TO LAYER SHAPE PARAMETERS

	FIXED LAYER SHAPE PARAMETERS		RECOVERED PARAMETERS			INFERRED MOMENTS (Should be Invariant to Model for Date)		SECOR (RAW) (Adj. to Vertical)
Date	k (scale ht factor) in eq. (7.17)	h_m Used	SECOR Bias, B (meters)	N_m(el/cc)	$\dot{N}_m$ (el/cc/min)	M_o (meters)	$\dot{M}_o$ (meters/min)	M_o (meters)
04/10/68	5.24	350	−2.3	0.6216×10^6	6574	37.79	.40	36.12
04/10/68	5.0	350	−2.1	0.6603	6858	38.31	.40	
04/12/68	5.24	350	−3.9	0.4998	− 3502	30.39	− .21	27.44
04/12/68	5.0	350	−3.8	0.5196	− 3640	30.15	− .21	
04/17/68	5.24	350	−2.1	0.5990	−12919	36.42	− .79	35.27
04/17/68	5.0	350	−2.0	0.6194	−13450	35.94	− .78	
04/05/68	5.24	350	+3.9	0.4892	−12980	29.74	− .79	33.49
05/24/68	5.24	375	+8.3	0.6415	−72301	42.26	−4.76	51.40
05/24/68	5.24	350	+9.7	0.6720	−77546	40.86	−4.71	
05/24/68	5.24	400	+6.3	0.6222	−67813	44.14	−4.81	
05/25/68	5.24	400	−2.0	0.4618	− 3135	32.76	− .22	31.47
05/25/68	5.24	375	−1.3	0.4869	− 3307	32.07	− .22	
05/25/68	5.24	350	−0.5	0.5163	− 3507	31.39	− .21	
05/25/68	5.0	350	−0.4	0.5368	− 3664	31.14	− .21	
05/30/68	5.24	350	−4.3	0.6280	−12539	38.18	− .76	36.45
05/30/68	5.0	350	−4.2	0.6575	−13145	38.15	− .76	
04/03/68	5.24	350	+2.4	0.7813	−26620	47.51	−1.62	49.14
04/03/68	5.0	350	+2.7	0.8138	−27821	47.21	−1.61	

The results of these calculations are given under the columns "inferred moments". Note that except for the anomolous date of 5/24/68 where extremely large gradients were observed, the results of the M_o and $\dot{M}_o$ calculations are indeed reasonably invariant (< 5%) to the assumed layer shape parameter variations. Finally in the last column are listed the SECOR (ICOR) measurements of M_o, adjusted to the vertical as in Table 6.2. These can be compared to the inferred M_o and the inferred ICOR bias.

Table 7.2 shows the results of a corresponding adjustment of the integrated TRANET data in column (B), and the comparison to the SECOR data in terms of the quantity

$$\epsilon_4 = \Delta R_{secor} - \frac{f^2_{tranet}}{f^2_{secor}} \times \Delta R_{tranet}$$

in column (C). This can be compared to the SECOR bias adjustment defined from (7.7) as

$$B = \Delta R_{secor} - \Delta R^c - \epsilon$$

where ΔR^c is the computed, modelled range error.

Five cases in the two sets of data overlapped and these are listed in column (D). While there may be some hint of a constant bias difference of several meters between ϵ_4 and B the small data sample precludes ascribing too much significance to it.

Column (E) lists the standard deviation of the difference between $\Delta R(t)_{secor}$ and $\Delta R_{tranet} \times \frac{f^2_{tranet}}{f^2_{secor}}$ over the duration of the common track after removing the mean difference. The differences run in the area of 1/2 to 1 meter and when plotted appear to show no consistent systematic trends.

The nature of these differences is further indicated in Figures 7.2 - 7.11 which show the variation over the observed pass of the difference between the SECOR and the TRANET observed ionospheric range error, referred to SECOR equi-

TABLE 7.2

LEAST-SQUARES SOLUTION USING TRANET DATA

DATE M/D	A SECOR(2) $\Delta R(t_o)$ Meter	B TRANET(1) $\Delta R(t_o)$ Meter	C SECOR(3)-TRANET $\epsilon_4(t_o)$ Meter	D SECOR(4) BIAS B Meter	E $\sigma_{\epsilon_4}^{(3)}$ Meter
4/05	35.1	28.4	6.7	3.9	.60
4/10	35.7	35.6	.1	−2.3	.61
4/11	24.7	28.6	−3.9		.55
4/12	32.5	32.8	− .3	−3.9	.43
4/16	45.6	43.5	2.1		.43
4/17	35.0	33.4	1.6	−2.1	1.02
4/18	29.5	31.4	−1.9		.43
4/21	40.0	39.2	.8		.50
4/23	42.3	34.4	7.9		.85
4/26	63.7	68.0	−4.3		.70
4/29	34.6	31.1	3.5		.40
4/30	29.4	27.7	1.7		.53
5/01	29.0	26.8	2.2		.40
5/02	44.1	47.9	−3.8		.59
5/03	37.2	41.9	−4.7		.36
5/04	36.2	36.3	− .1		.37
5/07	44.8	45.1	− .3		.36
5/08	20.0	27.2	−7.2		1.12
5/25	31.0	26.7	4.3	−0.5	.93

$\overline{\epsilon}_4 = 0.232\text{ m}$

$\sigma_{\epsilon_4} = 3.93\text{ m}$

(1) TRANET Data is self adjusted for Bias, N_m, $\dot{N}_m$ and scaled to f_{secor}

(2) SECOR Unadjusted, at f_{secor}

(3) $\epsilon_4 = \Delta R(t_o)_{secor} - \Delta R(t_o)_{tranet}$, all adjusted to f_{secor}

(4) From Table 7.1, using $k_s = 5.24$, $h_m = 350$ km

(5) t_o = time of closest approach

valent frequency and adjusted for the mean difference. For the purpose of this comparison it was found necessary to smooth the SECOR Ionospheric data rather heavily, by two successive passes through a 36-second span filter, with rejection of all points more than 1.5σ off the curve, between passes. There do not appear to be any consistent systematic trends in these differences.

It is of interest to compare the results of these SECOR-TRANET Comparisons with the SECOR vs Profile-Ray-Trace results in Table 6.2a), which indicate comparable RMS differences of the order of 3-4m. It is significant then that the TRANET data can be integrated with the integration constant resolved internally by absolute ionospheric error estimates to at least the same order of accuracy as the best profile determinations.

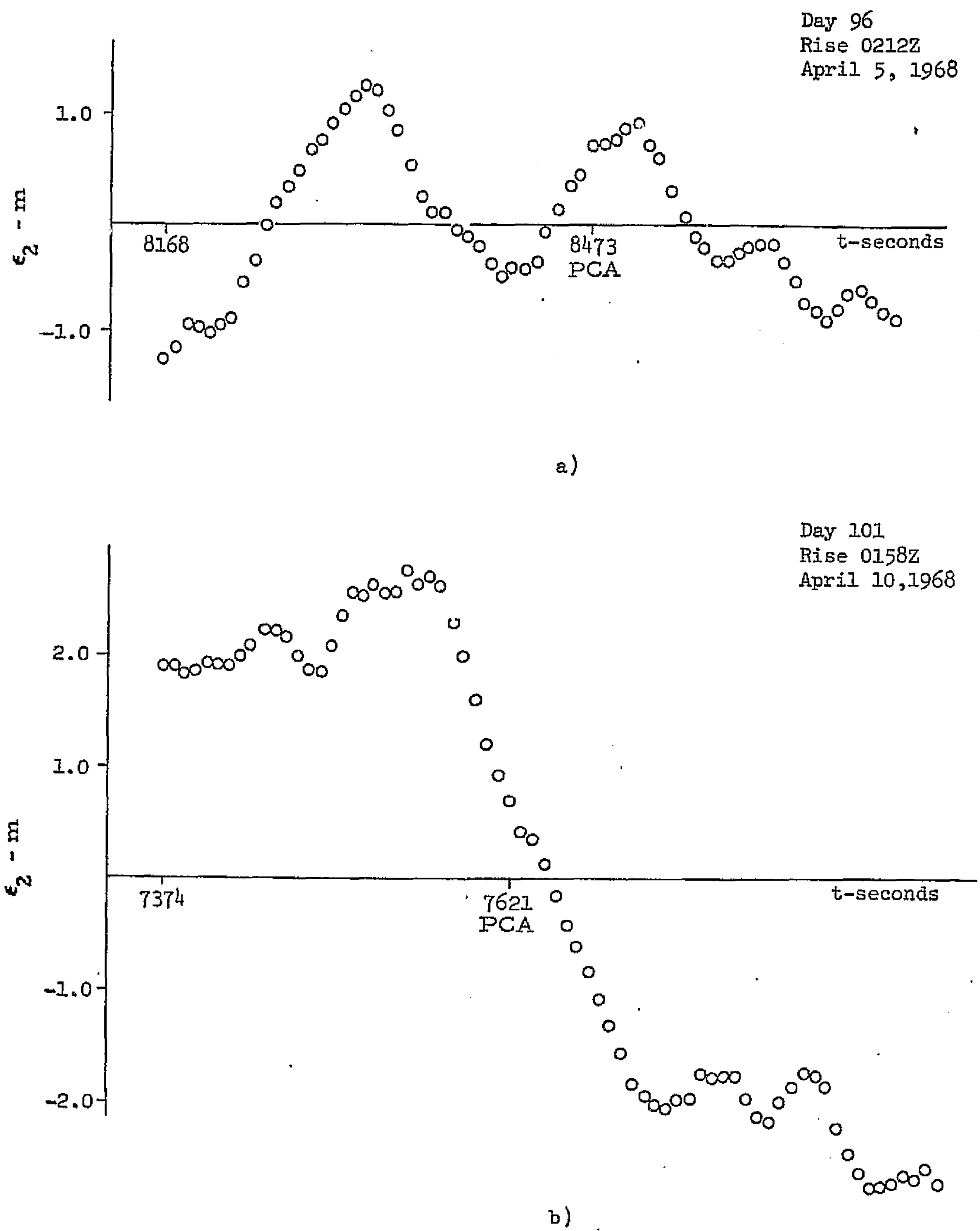

FIGURE 7.2

VARIATIONS IN THE DIFFERENCE BETWEEN SECOR AND INTEGRATED TRANET IONOSPHERIC RANGE ERROR MEASUREMENTS

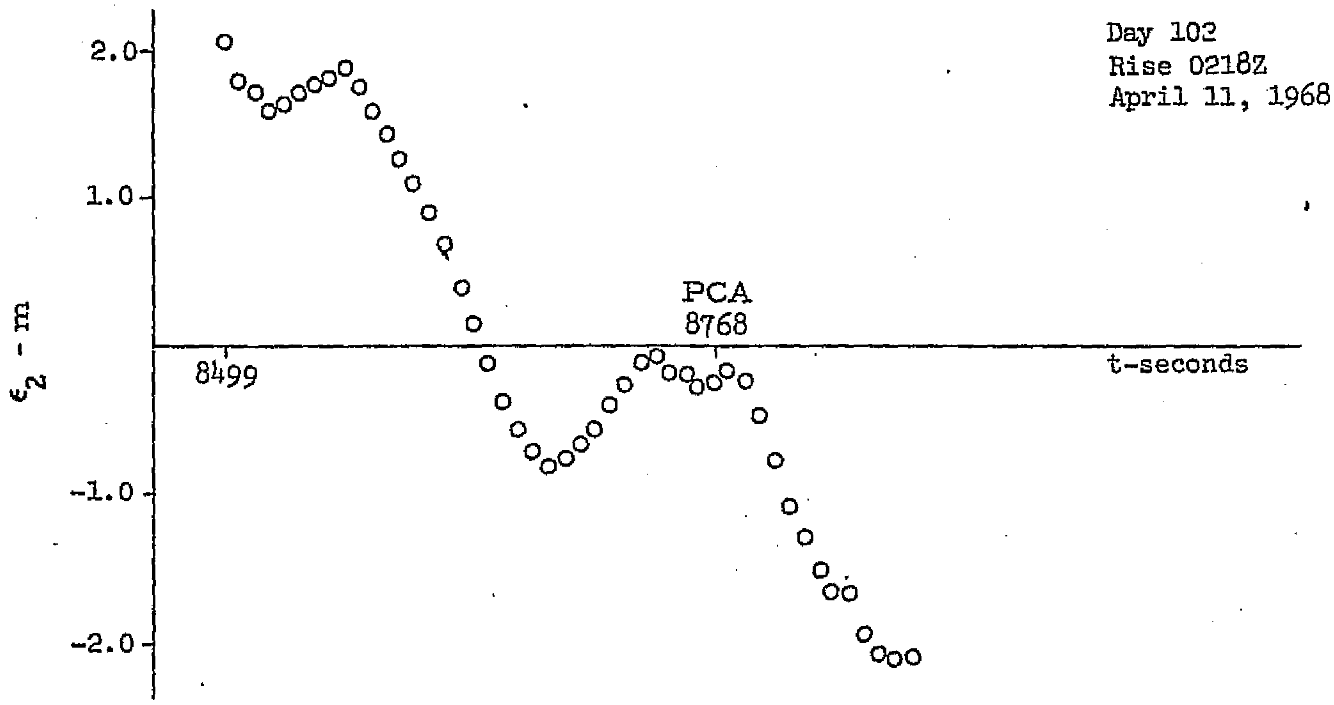

a)

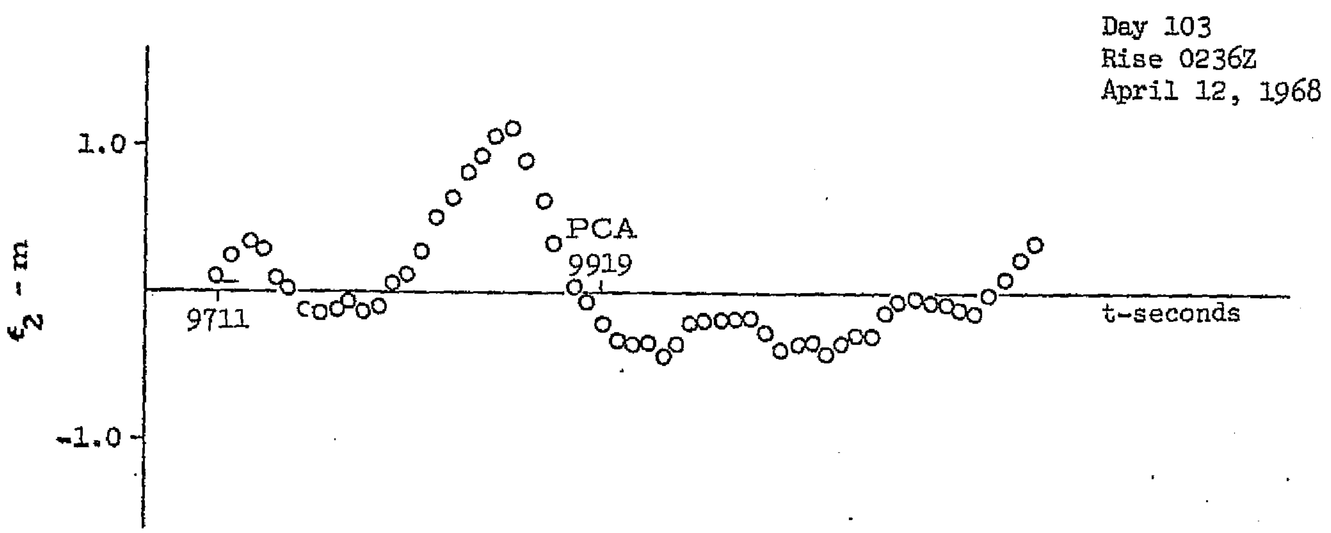

b)

FIGURE 7.3

DIFFERENCE IN VARIATIONS AS OBSERVED IN SECOR DATA AND INTEGRATED TRANET DATA

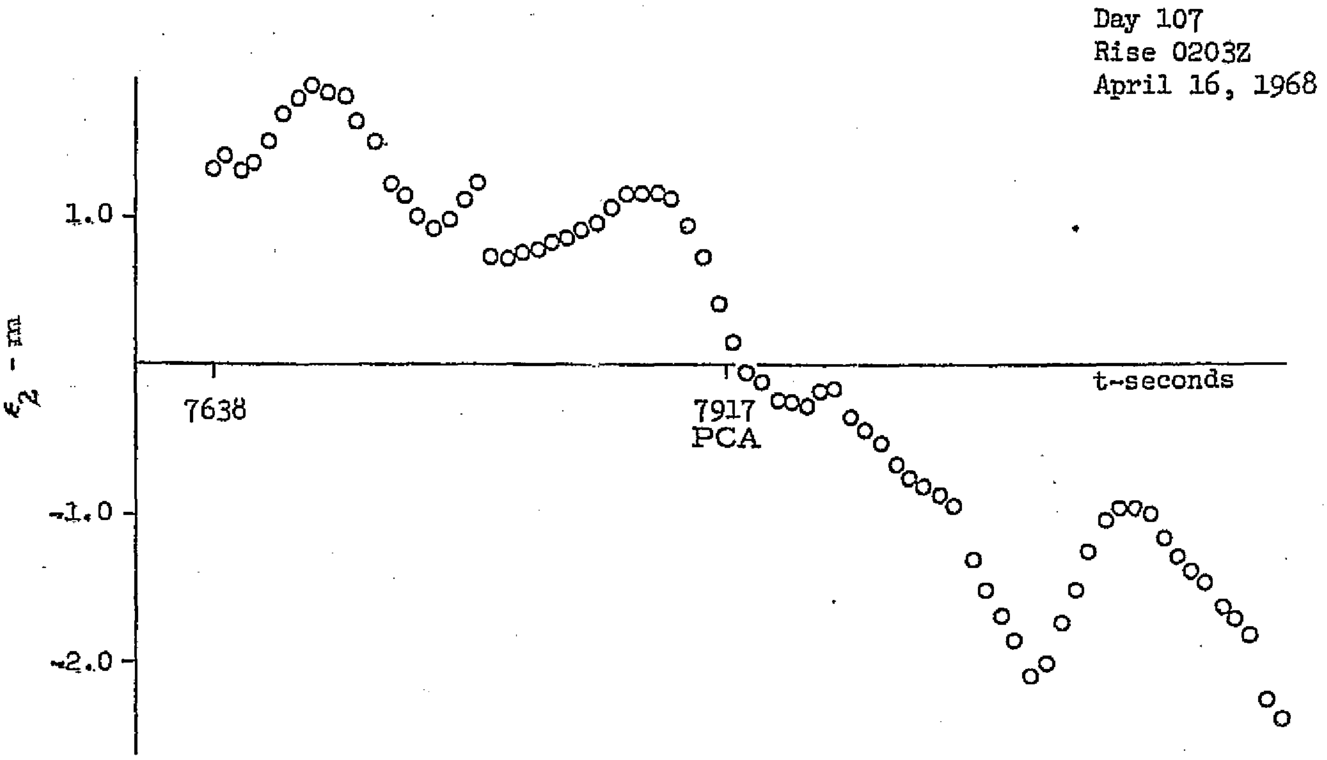

a)

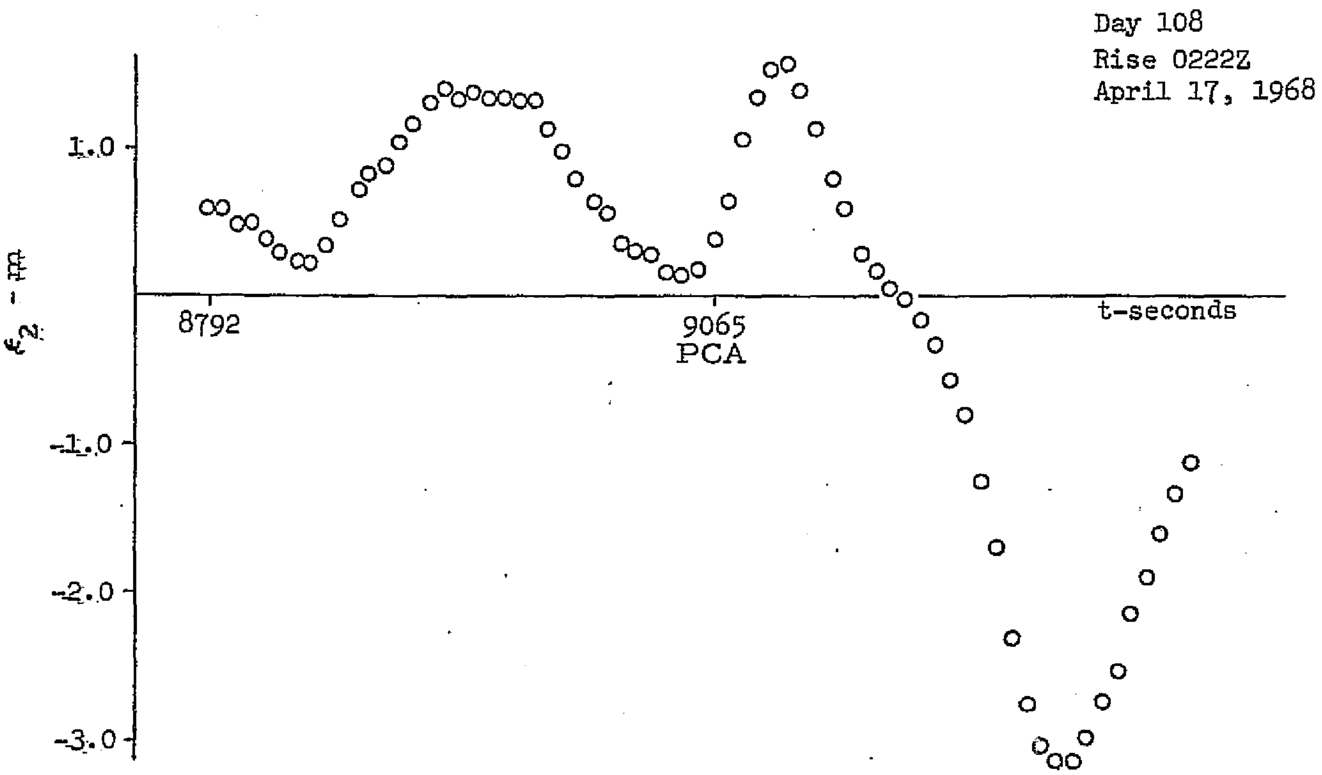

b)

FIGURE 7.4

DIFFERENCE IN VARIATIONS AS OBSERVED IN SECOR DATA AND INTEGRATED TRANET DATA

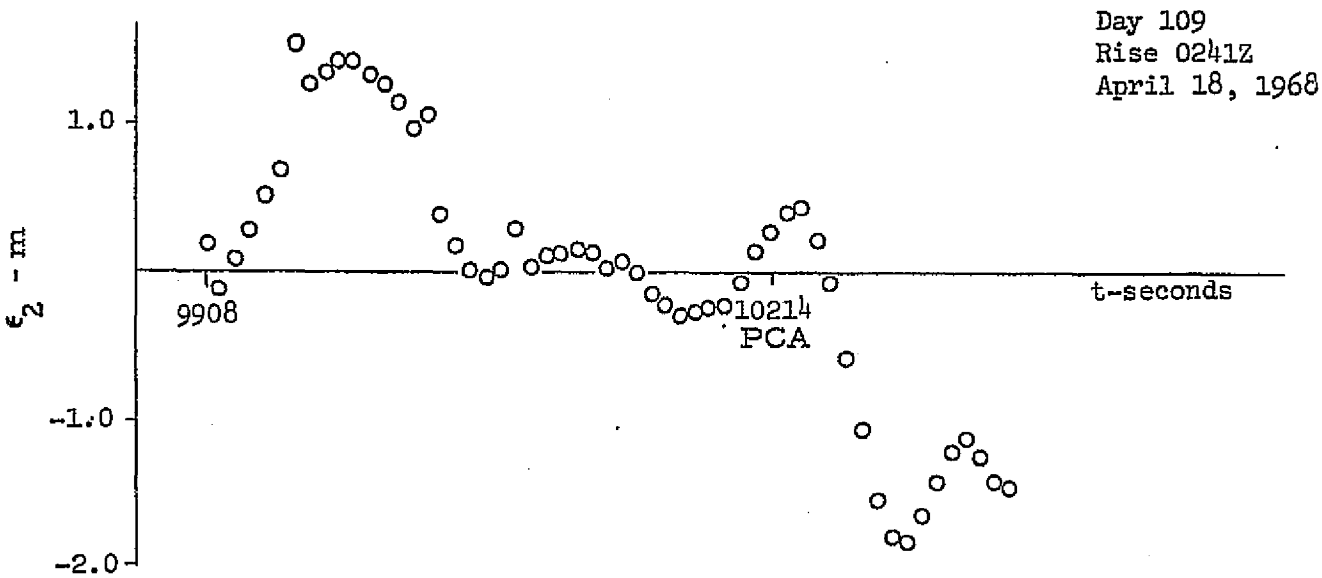

a)

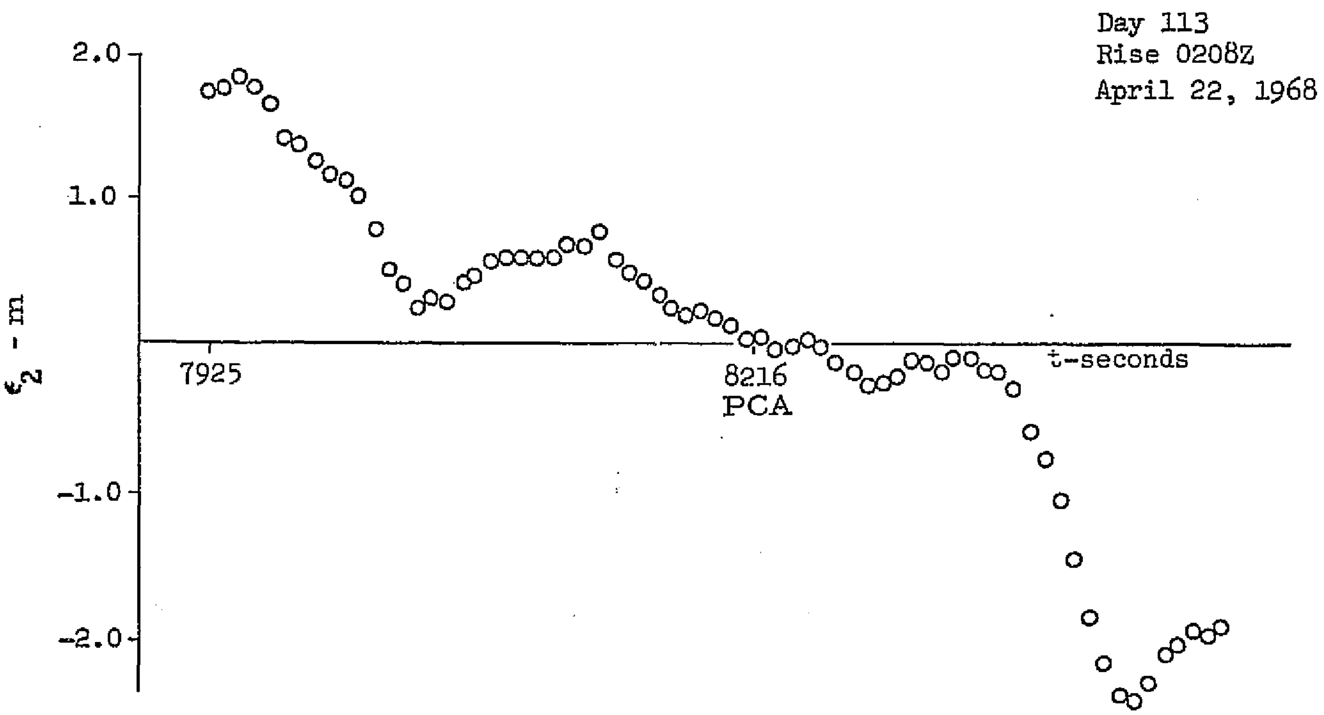

b)

FIGURE 7.5

DIFFERENCE IN VARIATIONS AS OBSERVED IN SECOR DATA AND INTEGRATED TRANET DATA

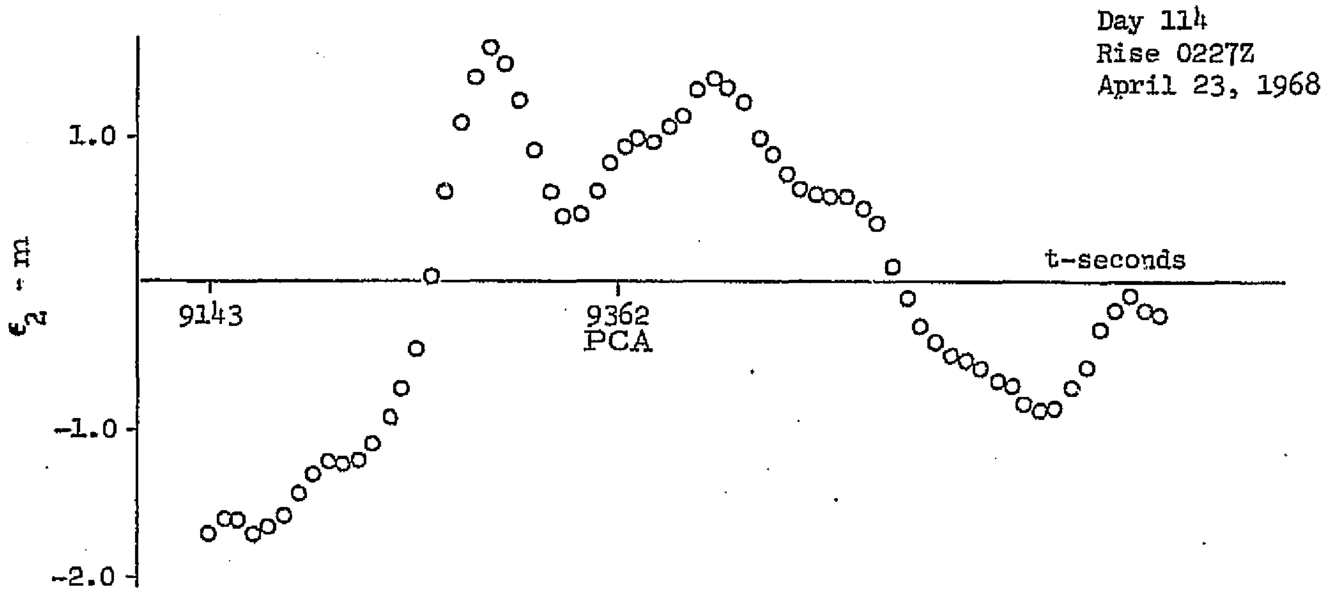

a)

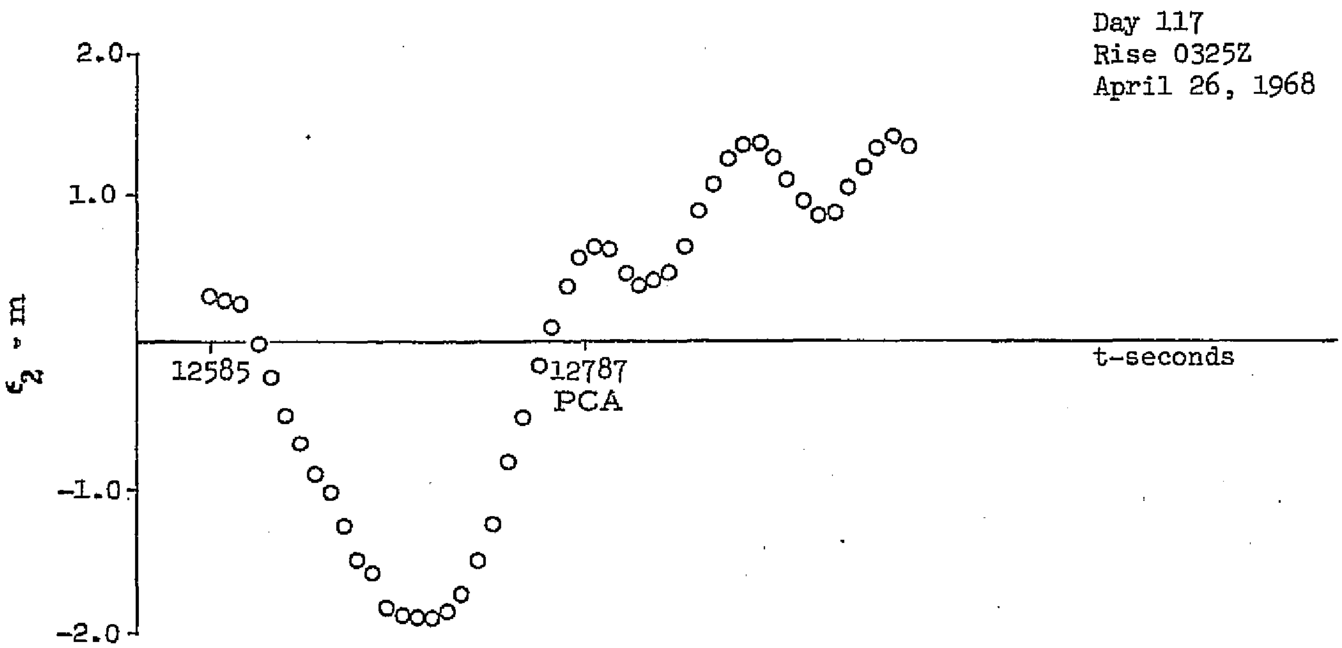

b)

FIGURE 7.6

DIFFERENCE IN VARIATIONS AS
OBSERVED IN SECOR DATA AND INTEGRATED
TRANET DATA

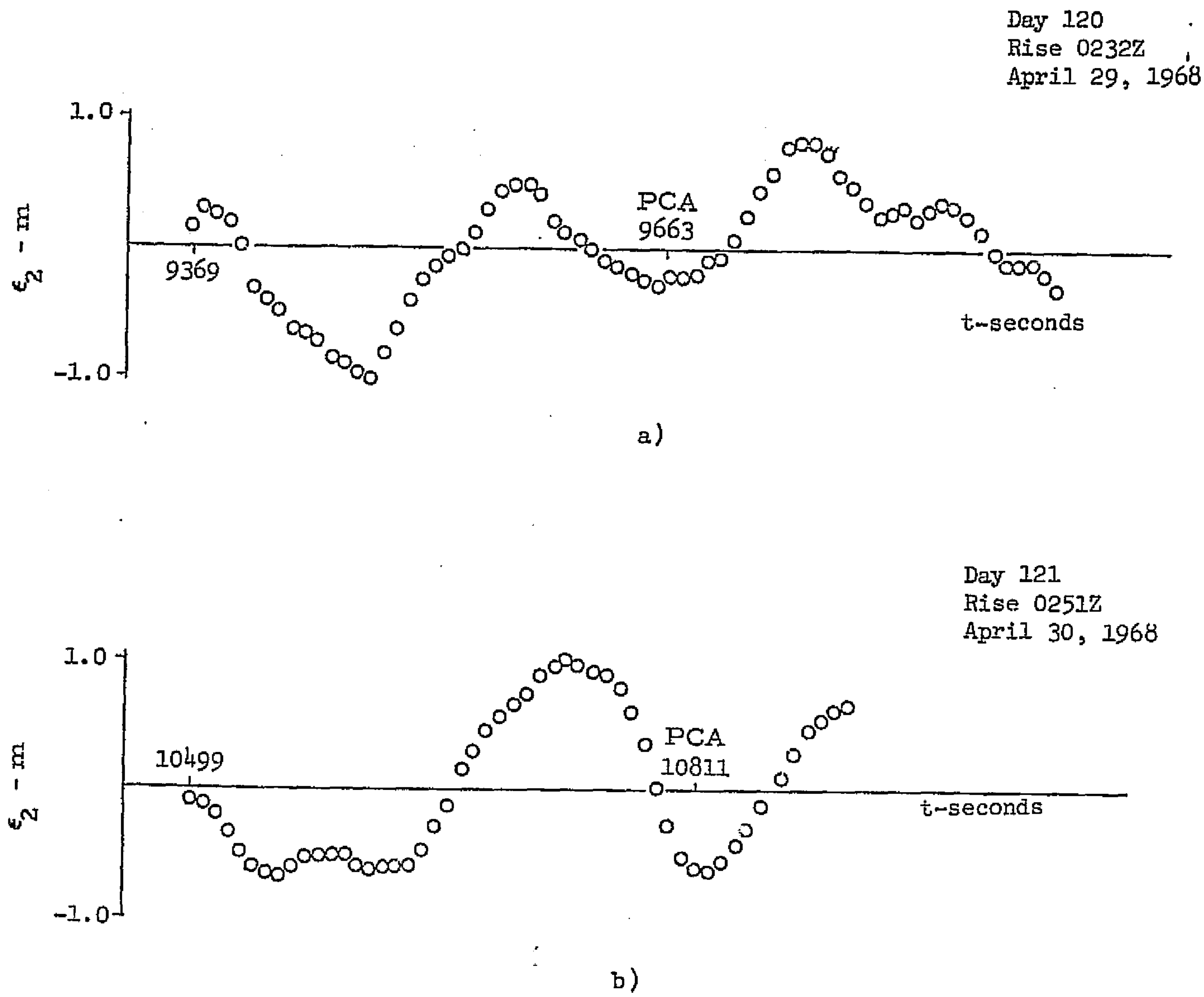

FIGURE 7.7

DIFFERENCE IN VARIATIONS AS OBSERVED IN SECOR DATA AND INTEGRATED TRANET DATA

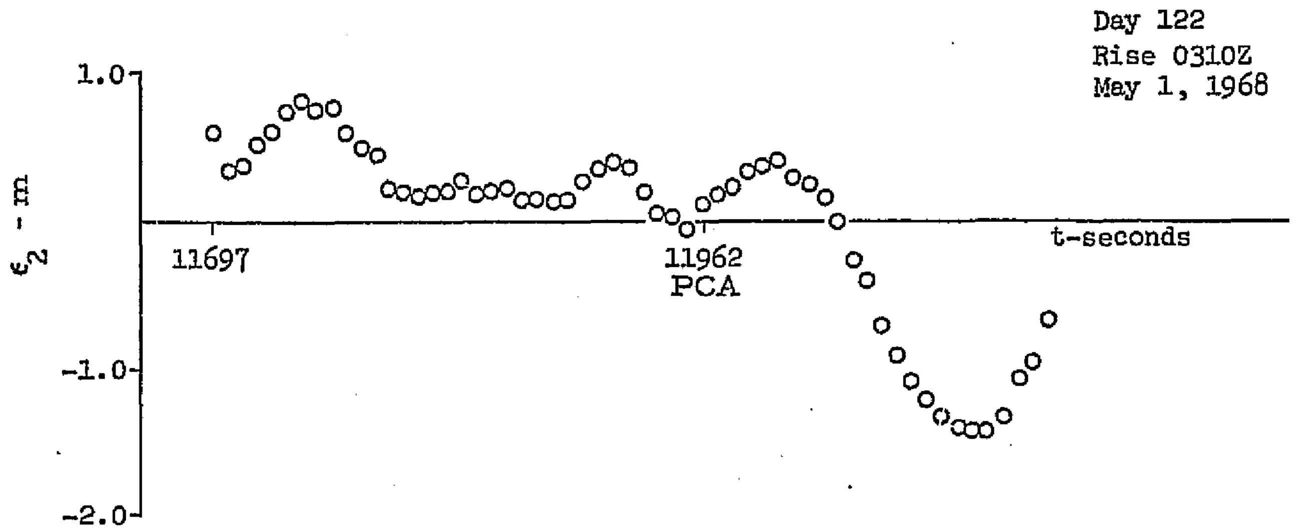

a)

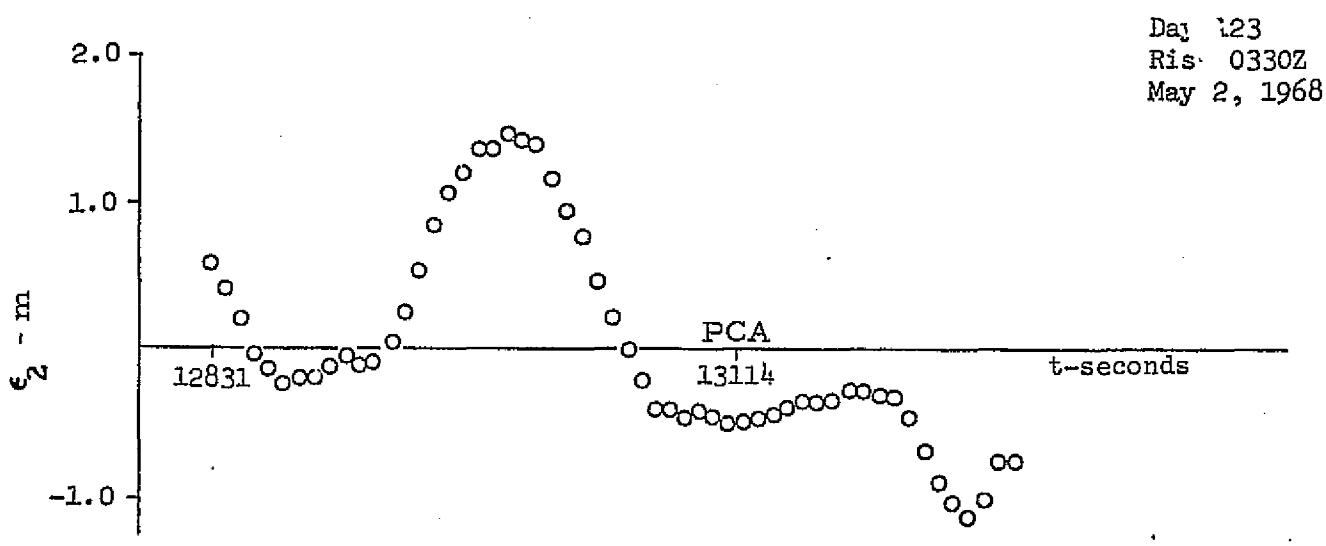

b)

FIGURE 7.8

DIFFERENCE IN VARIATIONS AS OBSERVED IN SECOR DATA AND INTEGRATED TRANET DATA

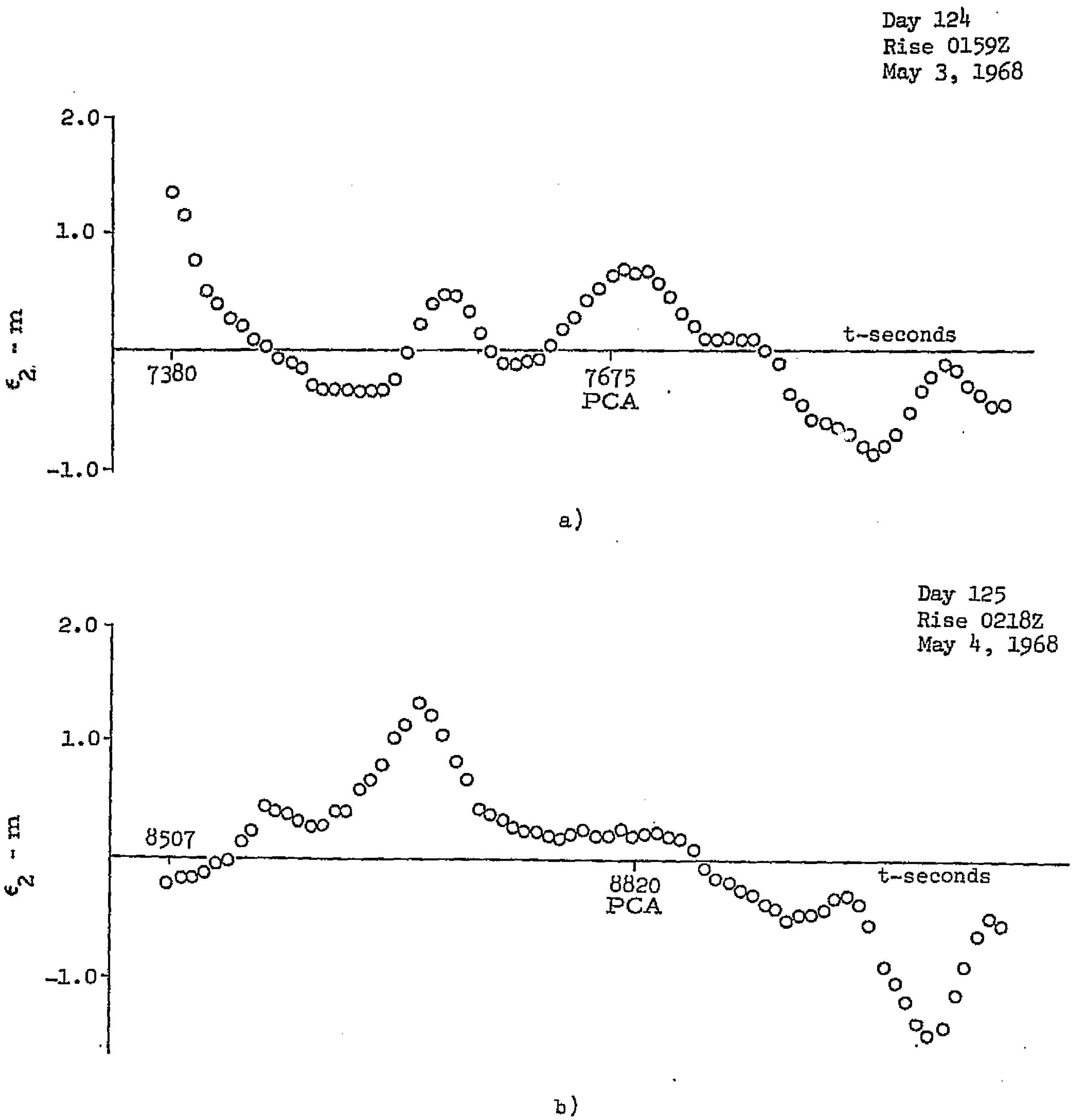

FIGURE 7.9

DIFFERENCE IN VARIATIONS AS OBSERVED IN SECOR DATA AND INTEGRATED TRANET DATA

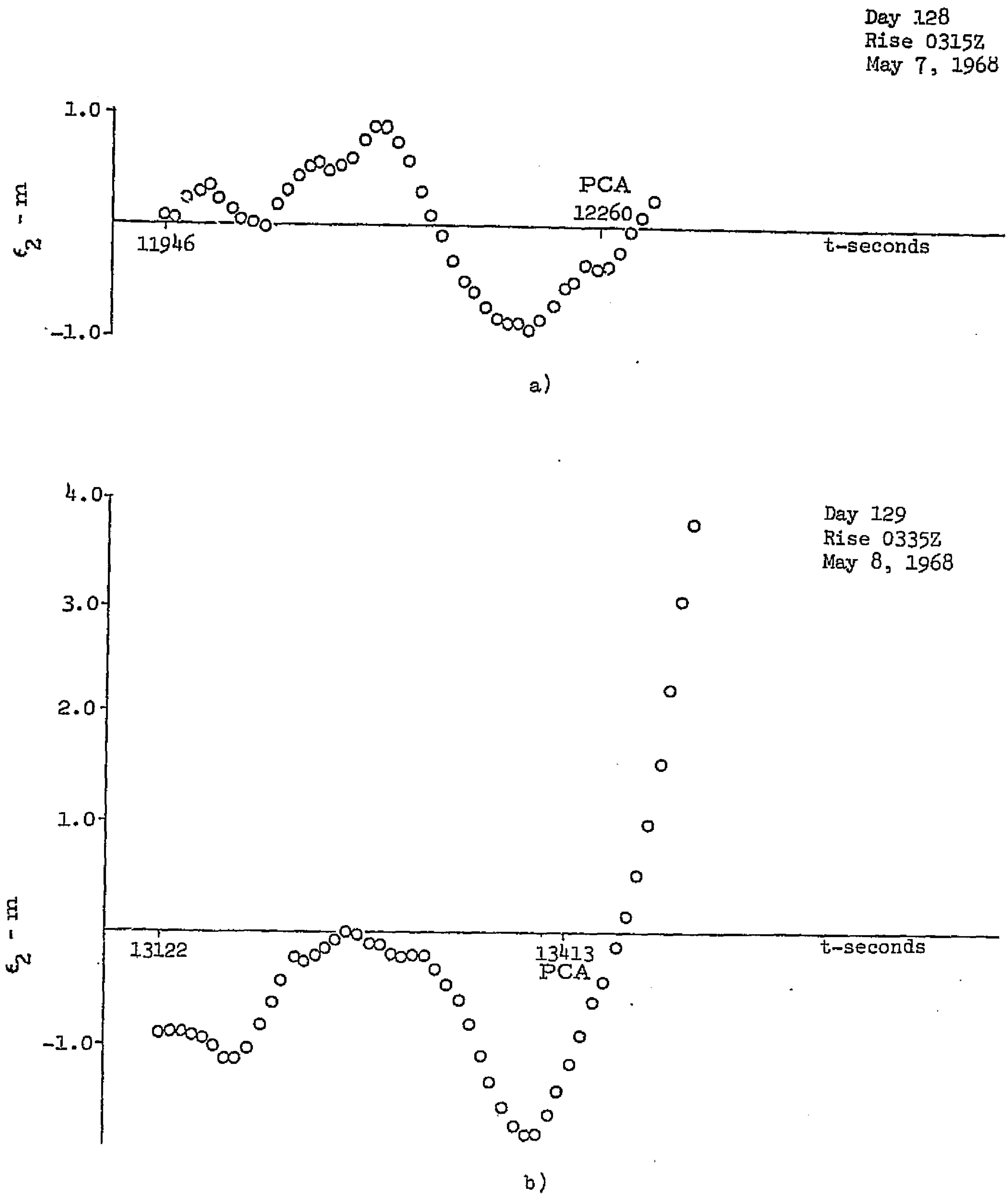

FIGURE 7.10

DIFFERENCE IN VARIATIONS AS
OBSERVED IN SECOR DATA AND
INTEGRATED TRANET DATA

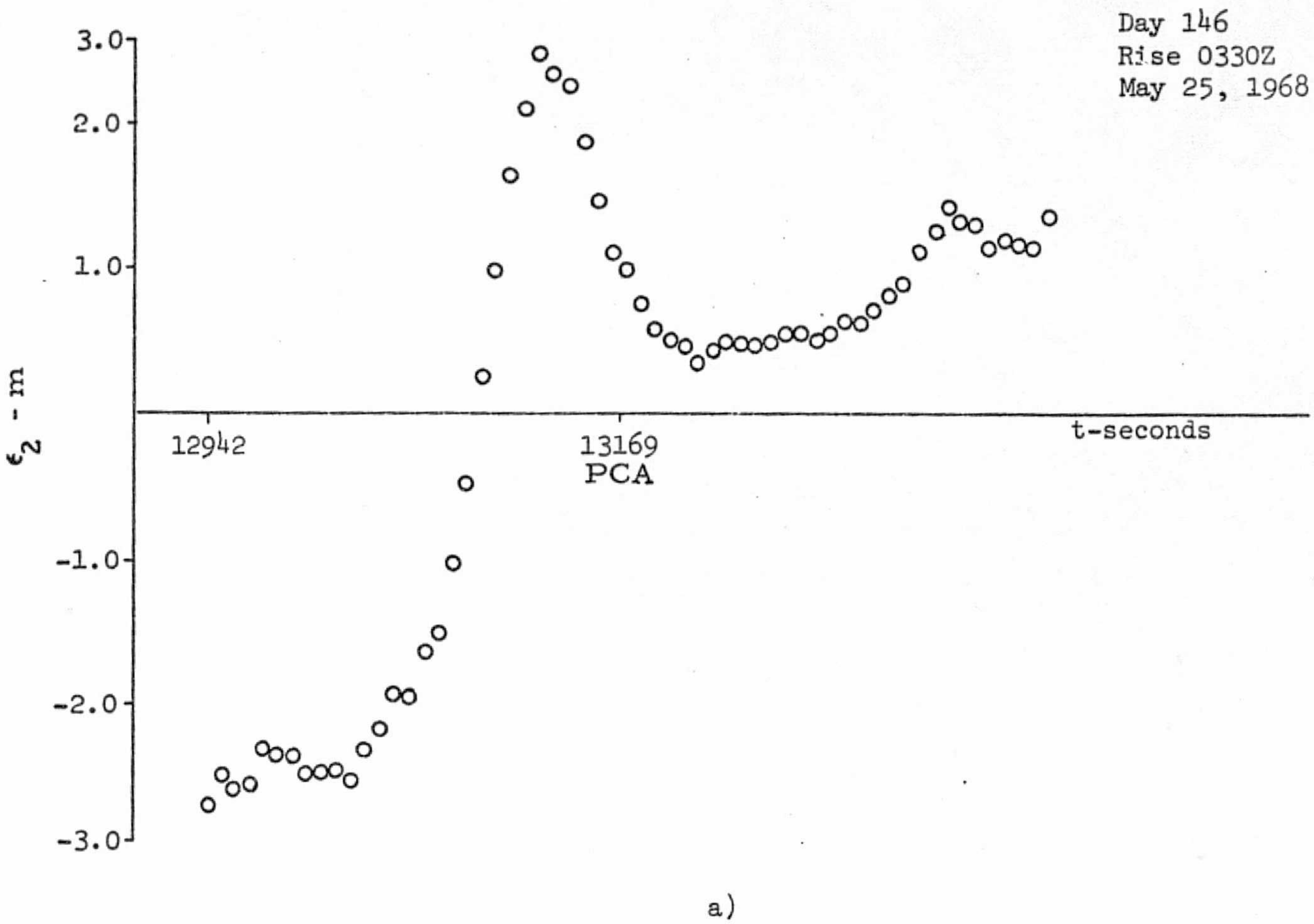

FIGURE 7.11

DIFFERENCE IN VARIATIONS AS OBSERVED IN SECOR DATA AND INTEGRATED TRANET DATA

8. SECOR-ORBIT COMPARISONS

Reference orbits were available for the 17 ionospheric test case passes. These reference orbits were derived from short arc orbital fits to observed Laser, C-Band Radar, and optics data. Over the Wallops observation span the orbital data is believed to be accurate to roughly ± 1 meter in the range component and ± 1 arcsecond in the angular components.

The SECOR Data, corrected for Tropospheric errors as described in section 2 and for Ionospheric errors by its own two-frequency determination was compared to the orbital data. The residual data was further adjusted for SECOR range bias and time bias to best fit the orbital data. The adjusted residuals are plotted in Figures 8.1 - 8.15, and the adjustment noted.

On the same plots for each day and to the same scale are plotted for comparison the ionospheric error corrections as determined by

a) SECOR itself, 2 frequency unadjusted

b) Raytracing of the local (Wallops) WICE composite ionospheric profile

c) Raytracing of the geographically-scaled composite profile, using the type 8 gradient scaling discussed in section 6.6, i.e., scaling proportional to f_oF_2 measured at the latitudes of Grand Bahama, Wallops, and Ottowa, with linear interpolation for intermediate latitudes.

Comparing the geographically scaled versus the unscaled composite raytrace computations to the SECOR ionospheric measurement confirms the general conclusion of section 6.6, namely that the best of the predicted latitudinal gradient modifications is not very good, in fact, hardly worth while.

Comparing the measured ionospheric correction with the orbital residuals after correction, plotted to the same scale, indicates the high degree of correction achieved for the SECOR data.

The recovered biases in range and time for the various passes are listed together in Table 8.1. While the overall bias trends are clearly persistent and statistically significant, it cannot necessarily be inferred that the discrepancies noted are in fact correctly attributed to SECOR range error or timing error. The recovered timing biases are in fact one or two orders of magnitude larger than should be considered reasonable and can probably be ascribed to aliasing of second-order (i.e., non-linear) latitudinal variations into recovered time bias.

TABLE 8.1

BIAS ADJUSTMENTS; SECOR-ORBIT FITS

Date	Recovered Bias Adjustments: Range Bias (Meters)	Recovered Bias Adjustments: Time Bias (Milli-Seconds)	RMS Adjusted Fit Error (Meters)
4/03	-11.12	-1.06	1.85
4/05	-16.15	-1.16	2.41
4/10	-10.19	-0.82	2.05
4/12	-14.30	-0.41	2.00
4/17	-13.21	-0.92	1.81
5/24	-20.8	-2.31	1.81
5/25	-13.5	-1.76	1.79
5/29			
5/30	-15.1	-1.16	1.67
6/04	-19.4	-0.87	1.50
6/05	-17.7	-0.44	1.85
6/11	-19.4	-0.87	2.16
6/13	-19.1	-0.96	1.58
6/21	-22.7	-1.39	
6/25	-10.1	-1.37	
Mean	-15.91	-1.11	
RMS	4.05	.50	

FOLDOUT FRAME

ORIGINAL PAGE IS
OF POOR QUALITY

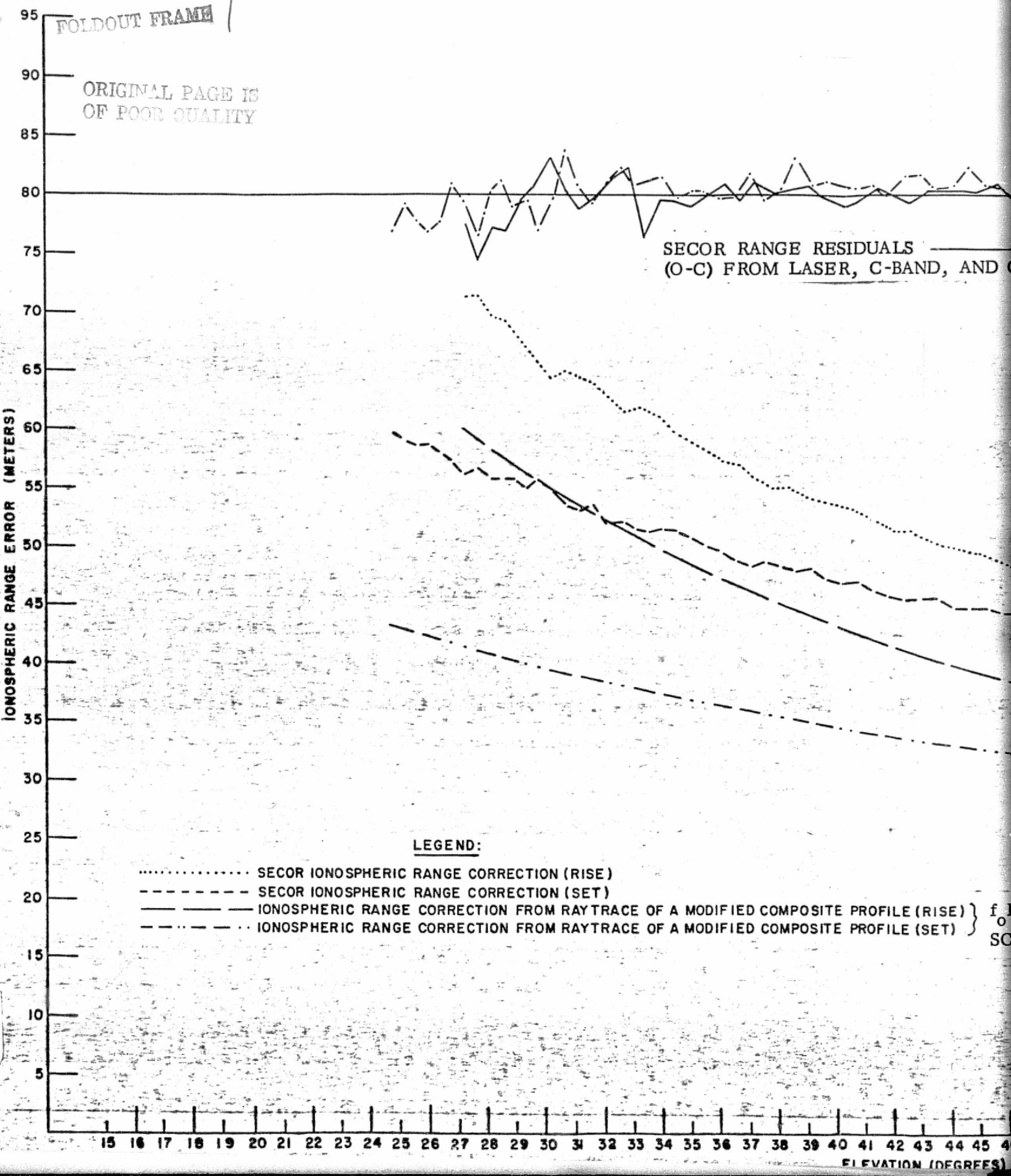

FOLDOUT FRAME 2

ORIGINAL PAGE IS OF POOR QUALITY

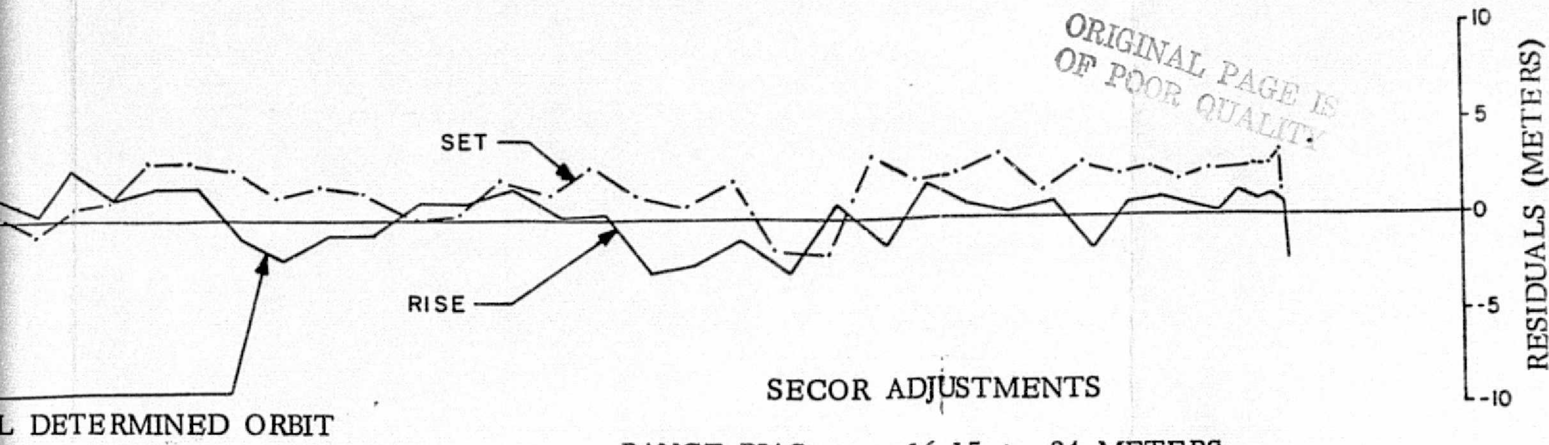

SECOR ADJUSTMENTS

RANGE BIAS = −16.15 ± .34 METERS

TIME BIAS = −1.16 ± .07 MILLISEC

RMS RESIDUAL = 2.41 METERS

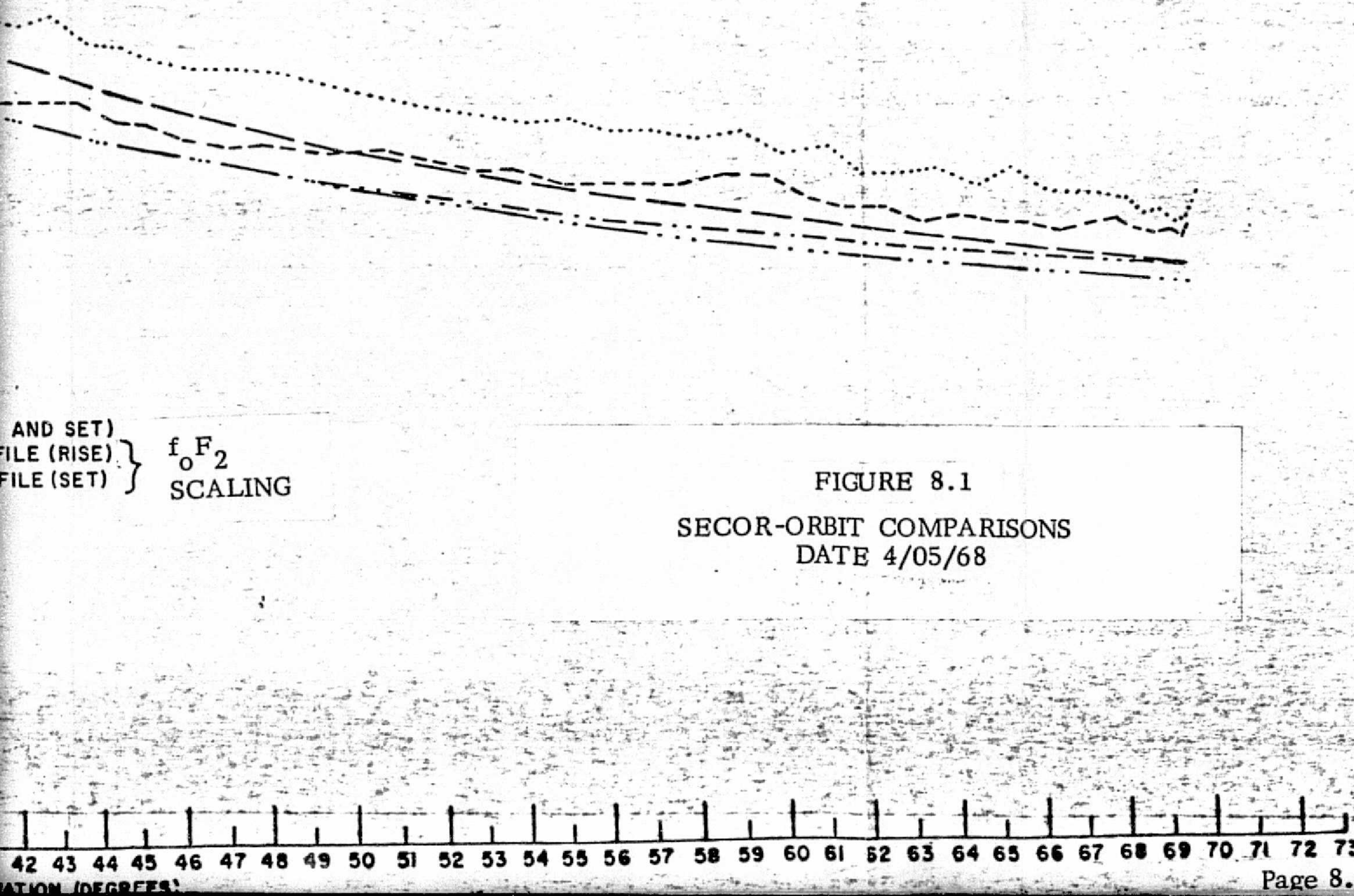

FIGURE 8.1

SECOR-ORBIT COMPARISONS
DATE 4/05/68

FOLDOUT FRAME 1

ORIGINAL PAGE IS
OF POOR QUALITY

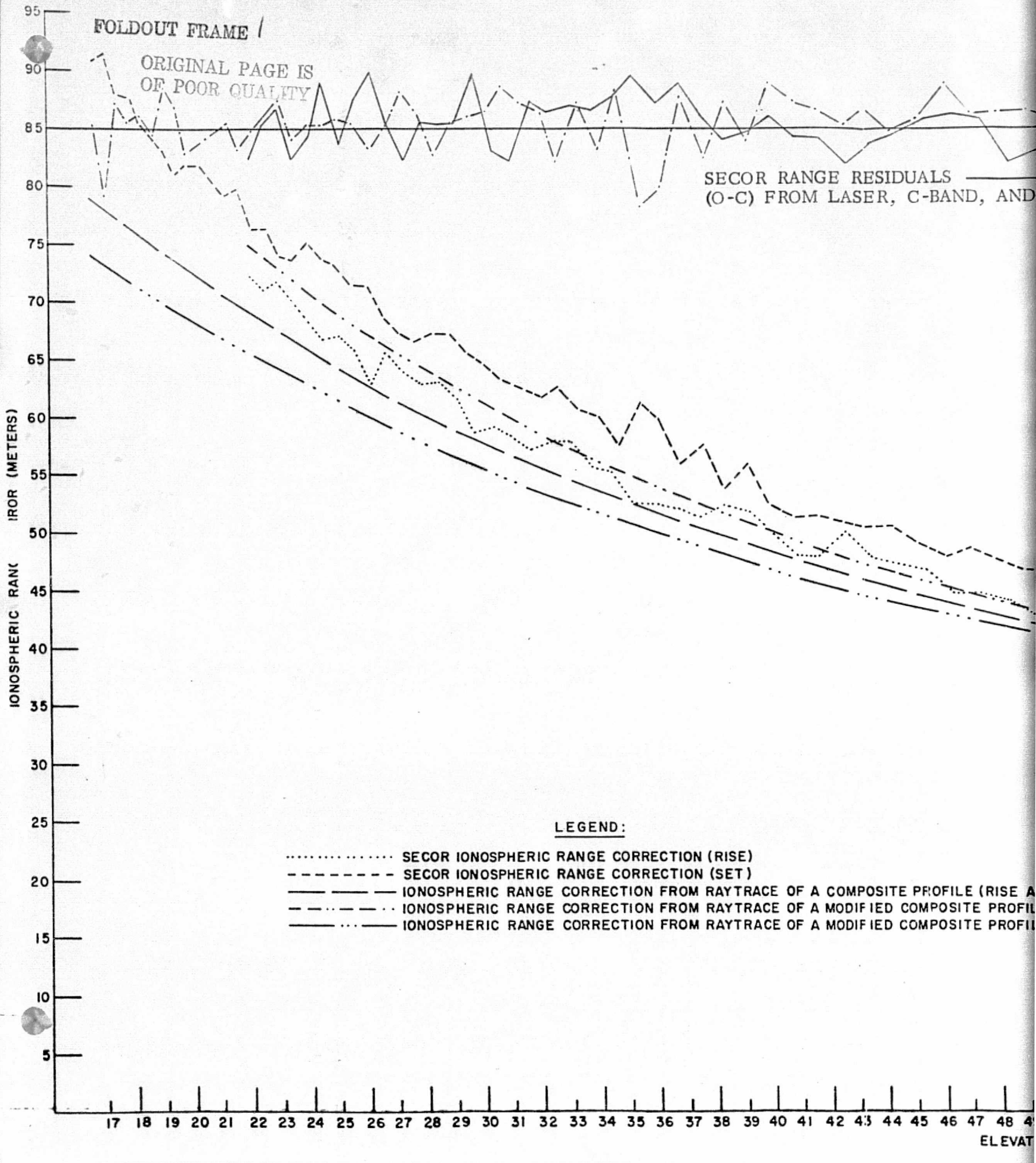

FOLDOUT FRAME 2

ORIGINAL PAGE IS
OF POOR QUALITY

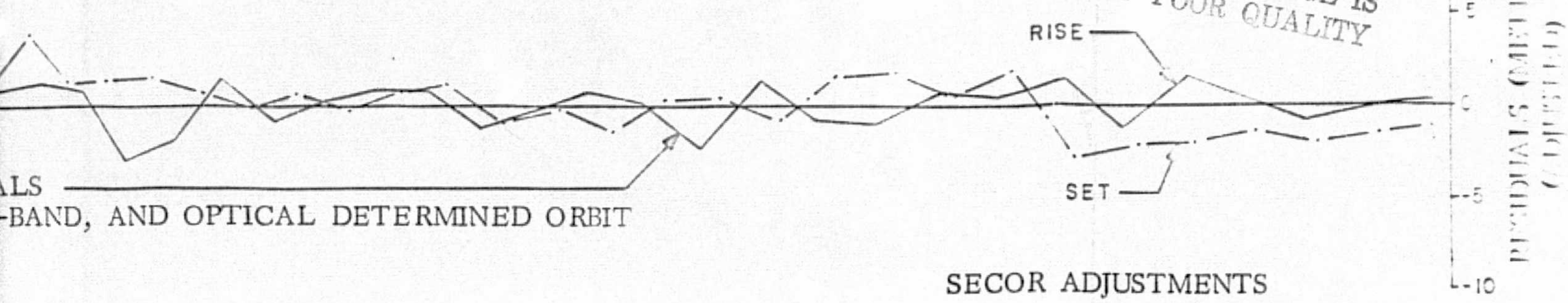

SECOR ADJUSTMENTS

RANGE BIAS = -10.19 ± .03 METERS

TIME BIAS = -.82 ± .07 MILLISEC

RMS RESIDUAL = 2.05 METERS

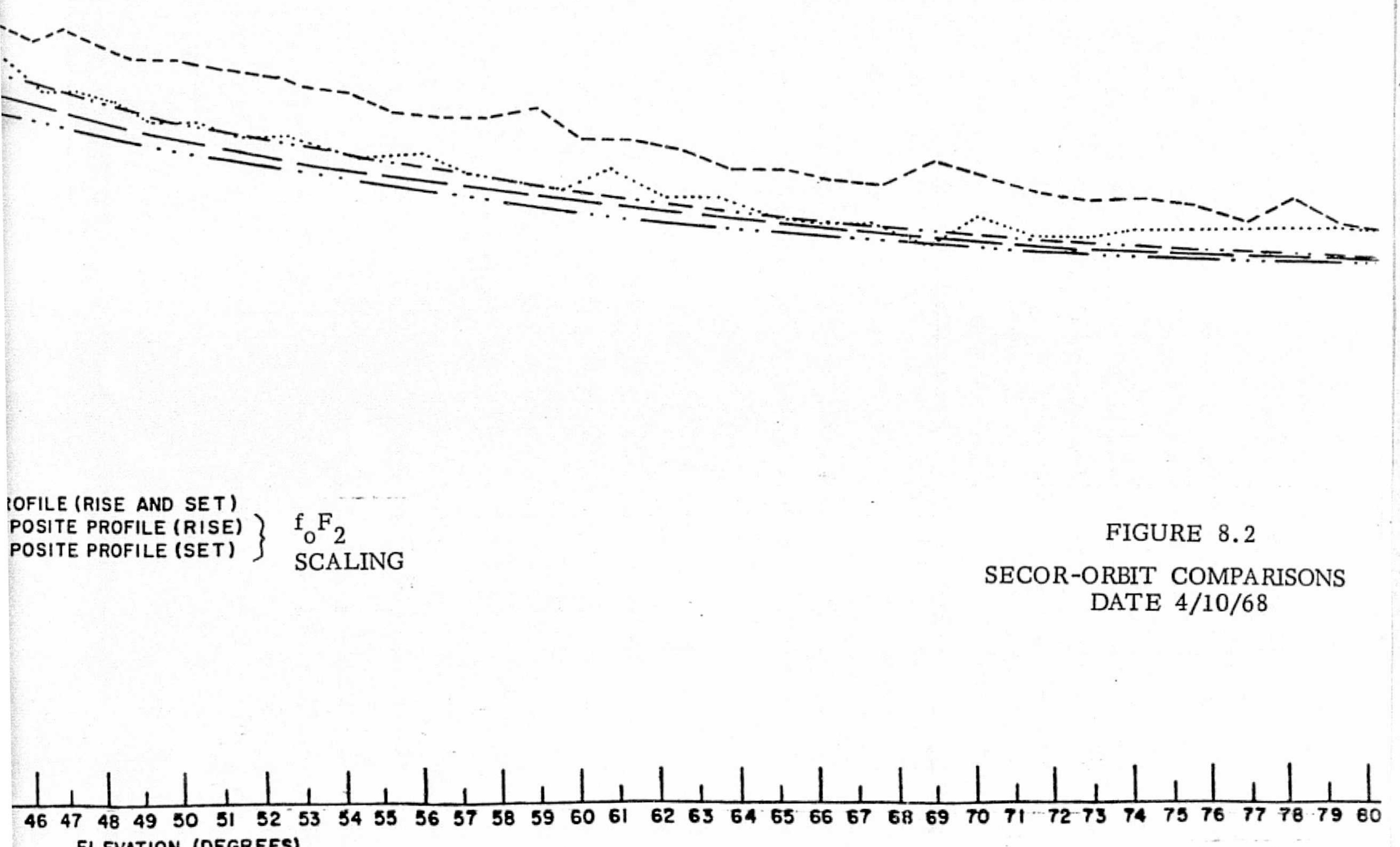

FIGURE 8.2

SECOR-ORBIT COMPARISONS
DATE 4/10/68

FOLDOUT FRAME

ORIGINAL PAGE IS
OF POOR QUALITY

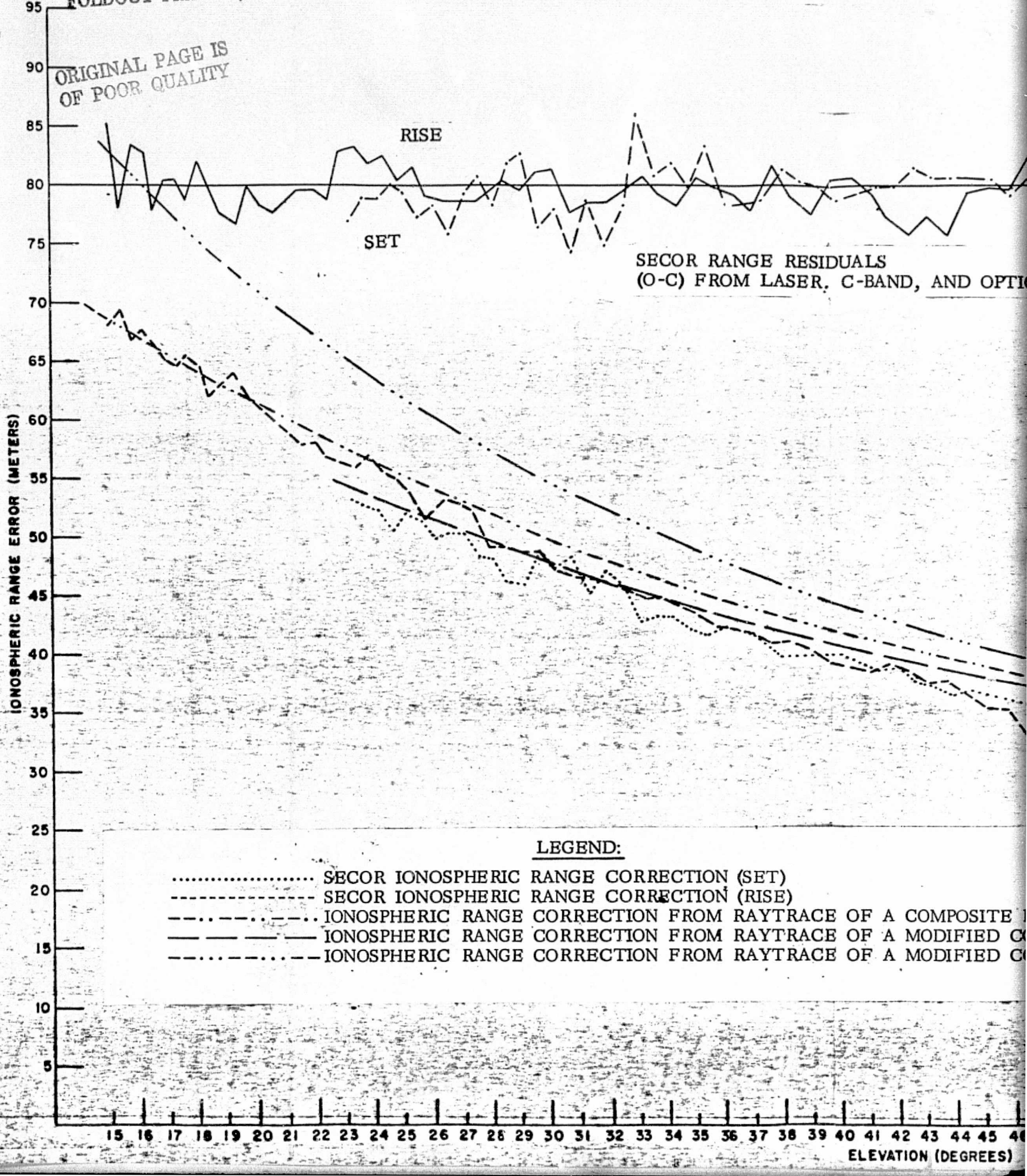

FOLDOUT FRAME 2

ORIGINAL PAGE IS
OF POOR QUALITY

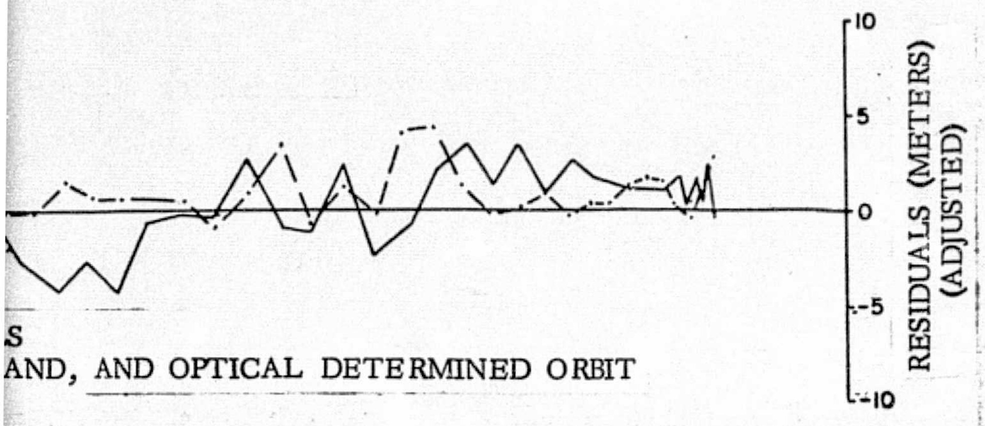

S
AND, AND OPTICAL DETERMINED ORBIT

SECOR ADJUSTMENTS

RANGE BIAS = −14.30 ± .33 METERS
TIME BIAS = −0.41 ± .08 MILLISEC

RMS RESIDUAL = 2 METERS

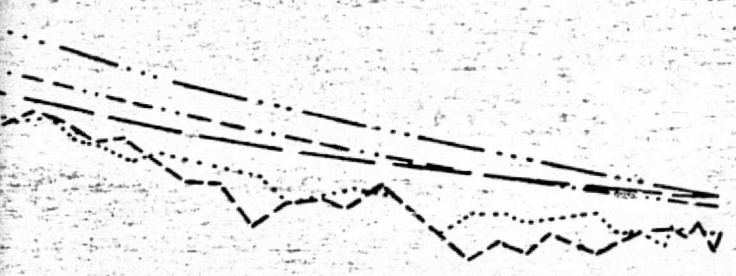

F A COMPOSITE PROFILE (RISE AND SET)
F A MODIFIED COMPOSITE PROFILE (SET) } f_oF_2
F A MODIFIED COMPOSITE PROFILE (RISE) } SCALING

FIGURE 8.3

SECOR-ORBIT COMPARISONS
DATE 4/12/68

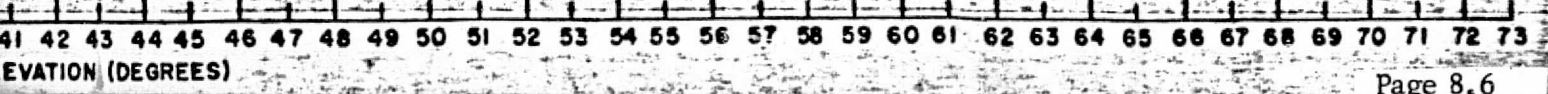

Communications Research Laboratories

FOLDOUT FRAME /

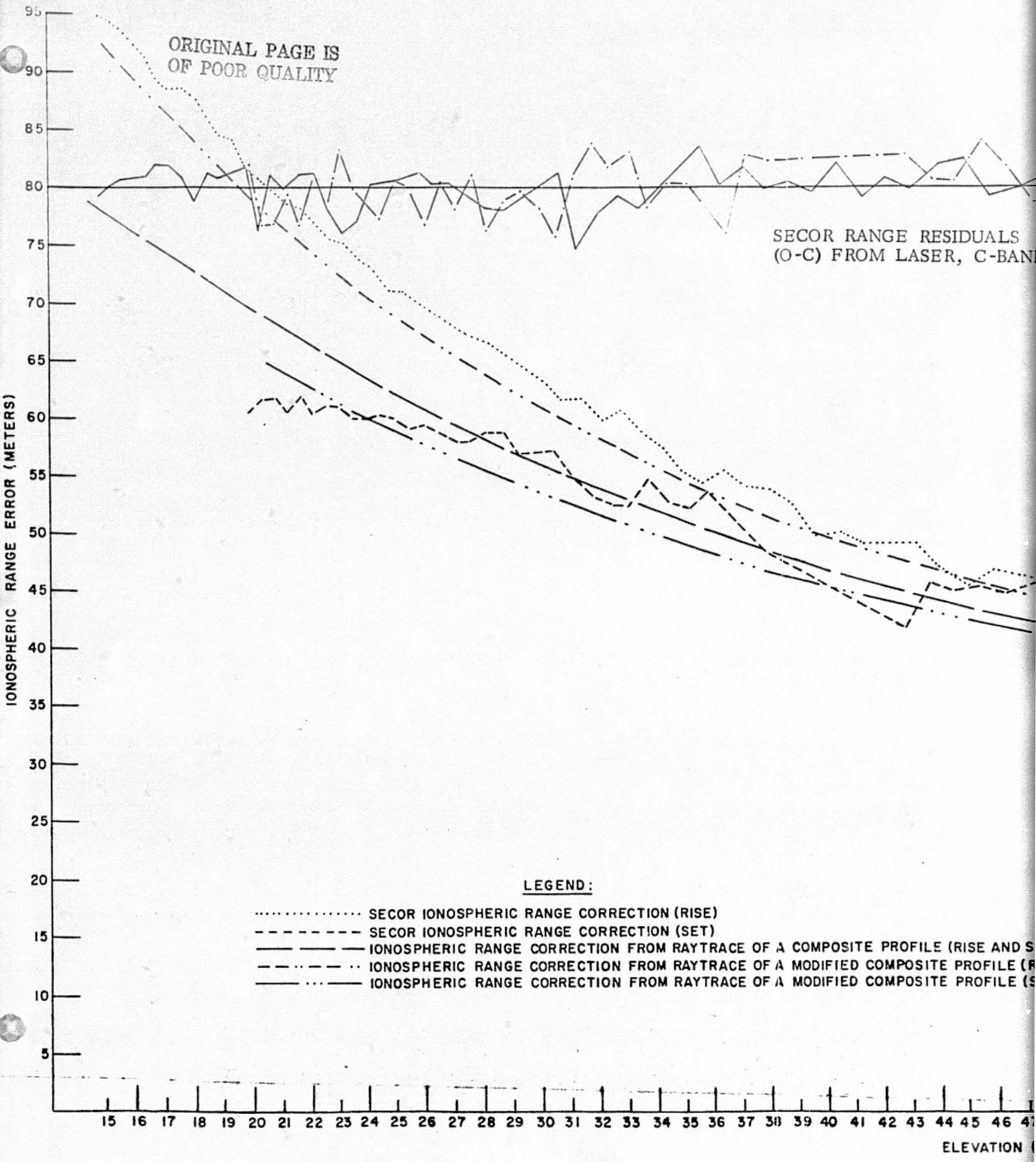

FOLDOUT FRAME 2

ORIGINAL PAGE IS
OF POOR QUALITY

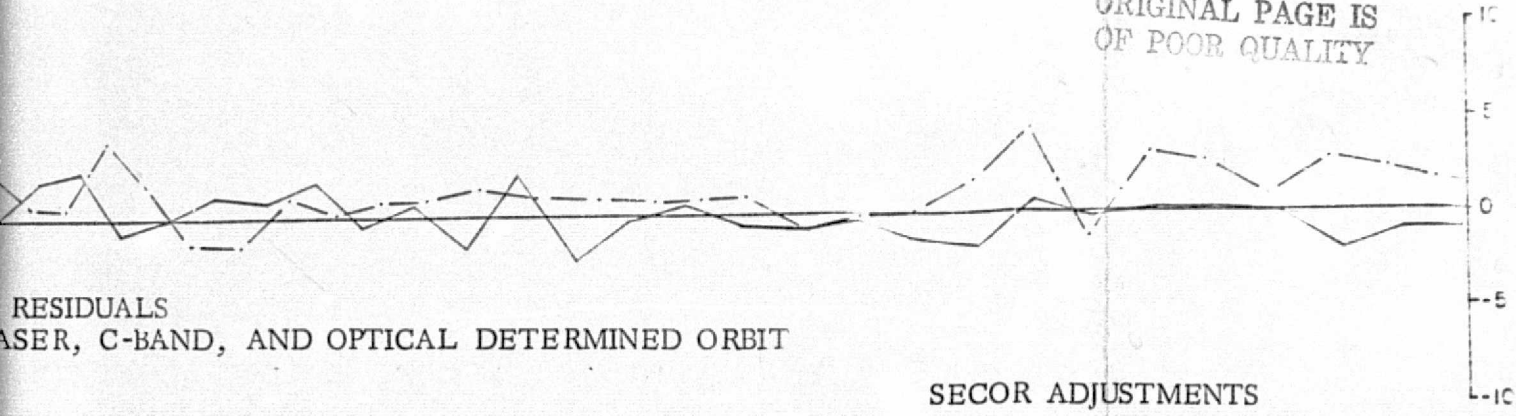

RESIDUALS
ASER, C-BAND, AND OPTICAL DETERMINED ORBIT

SECOR ADJUSTMENTS

RANGE BIAS = -13.21 ± .32 METERS

TIME BIAS = -0.91 ± .07 MILLISEC

RMS RESIDUAL = 1.81 METERS

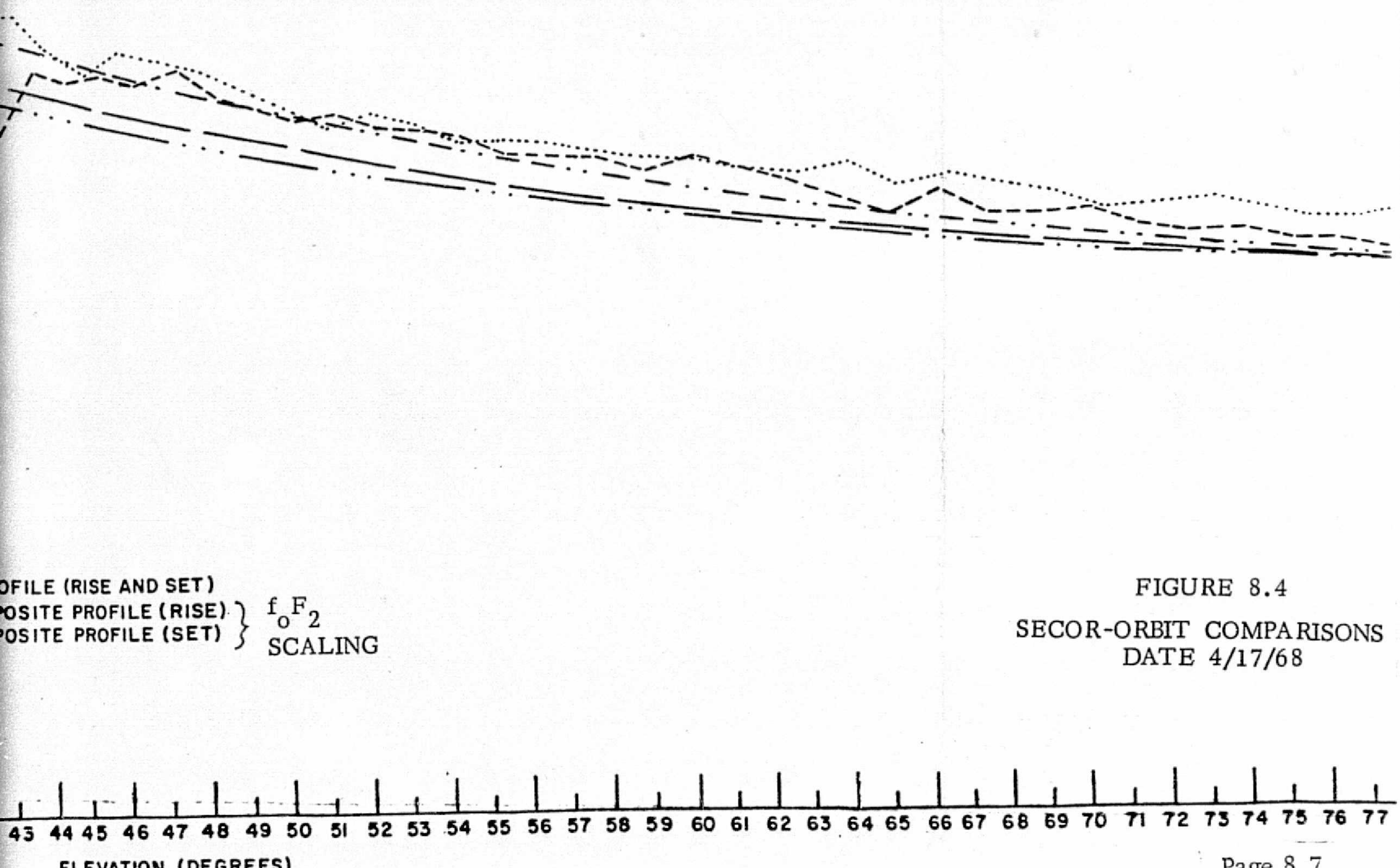

FIGURE 8.4

SECOR-ORBIT COMPARISONS
DATE 4/17/68

FOLDOUT FRAME

ORIGINAL PAGE IS
OF POOR QUALITY

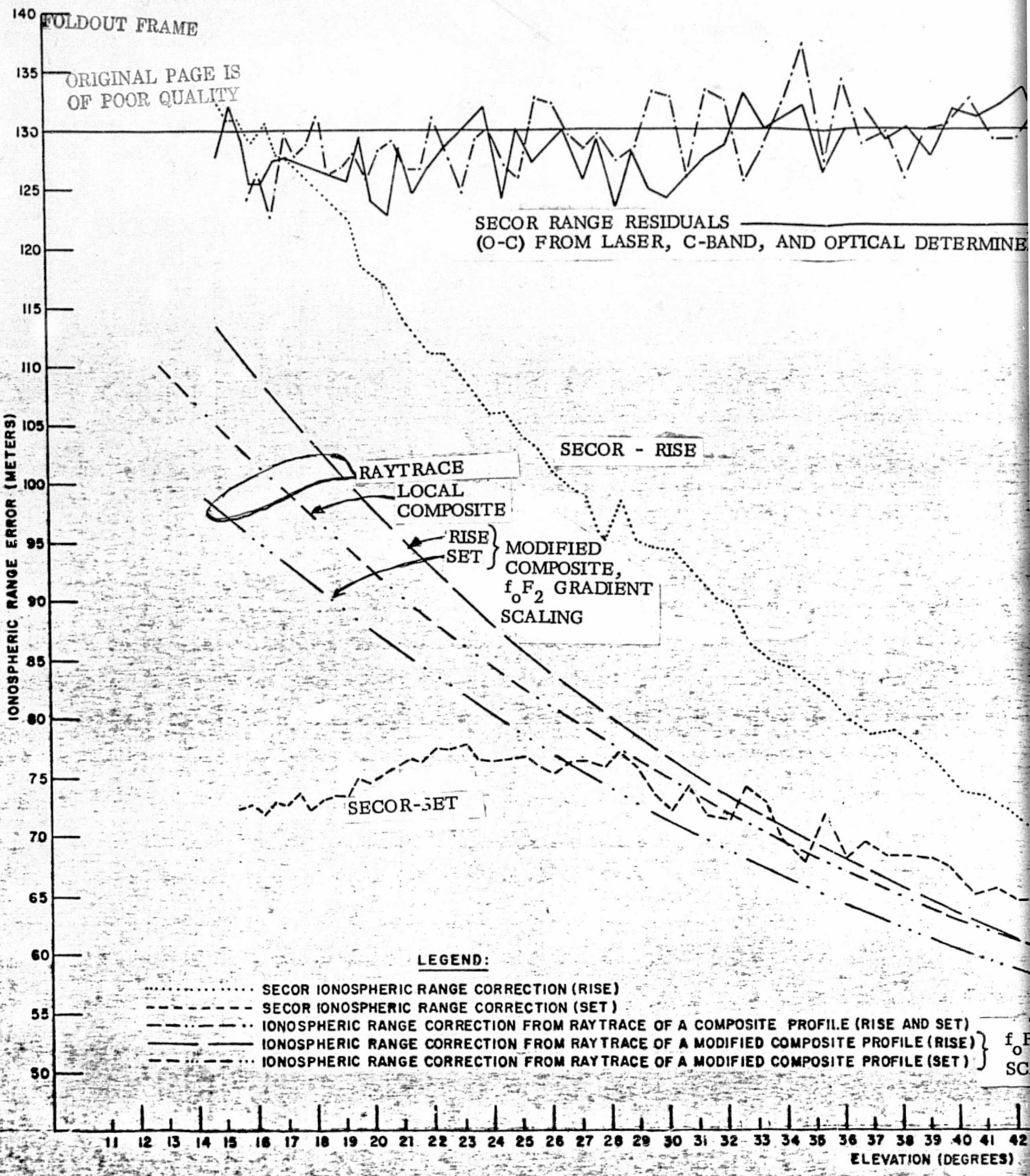

FOLDOUT FRAME

ORIGINAL PAGE IS
OF POOR QUALITY

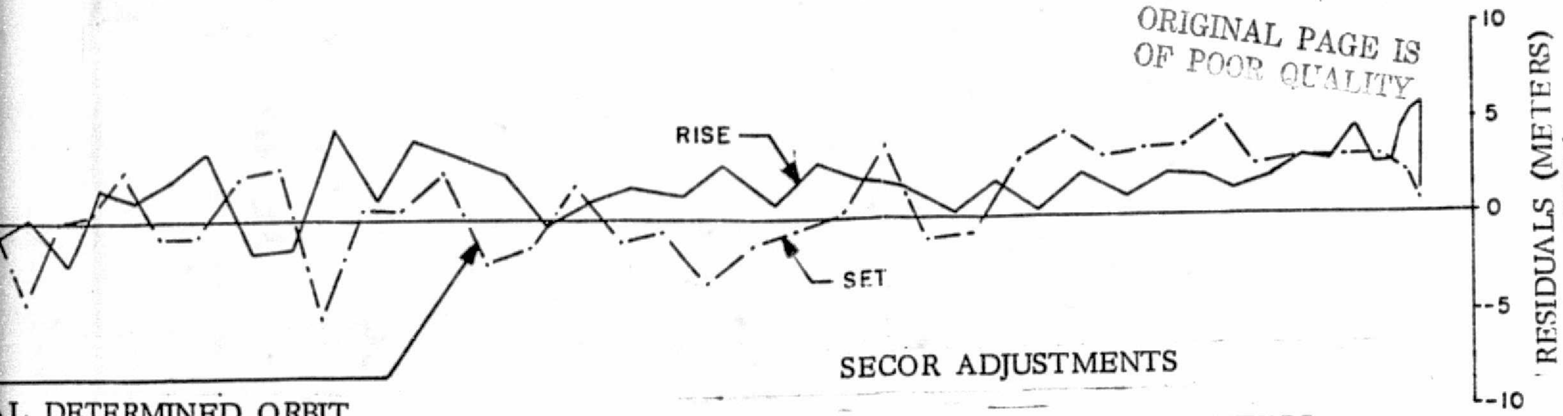

SECOR ADJUSTMENTS

RANGE BIAS = −11.12 ± .32 METERS
TIME BIAS = −1.07 ± .07 MILLISEC

RMS RESIDUAL = 1.85 METERS

FIGURE 8.5

SECOR-ORBIT COMPARISONS
DATE 4/30/68

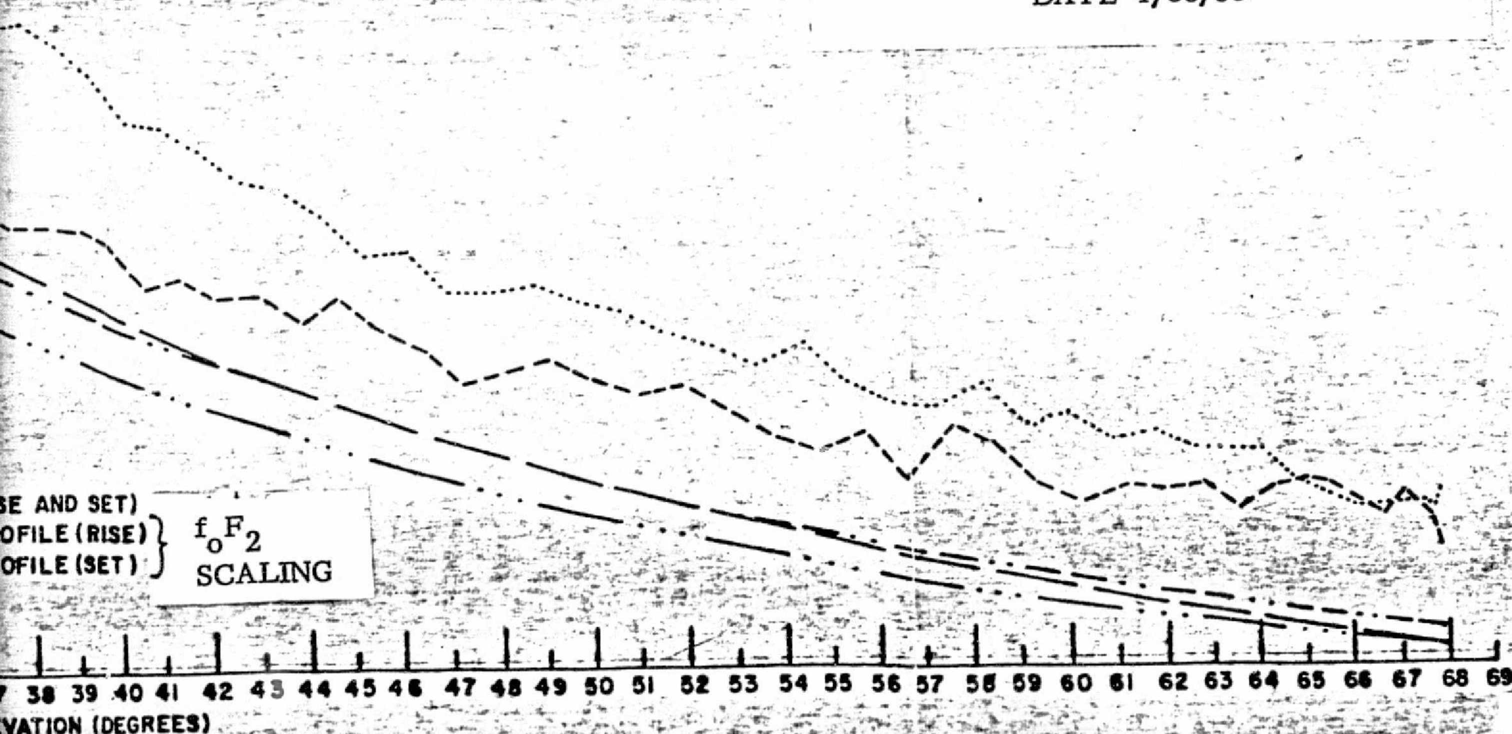

Communications Research Laboratories

FOLDOUT FRAME

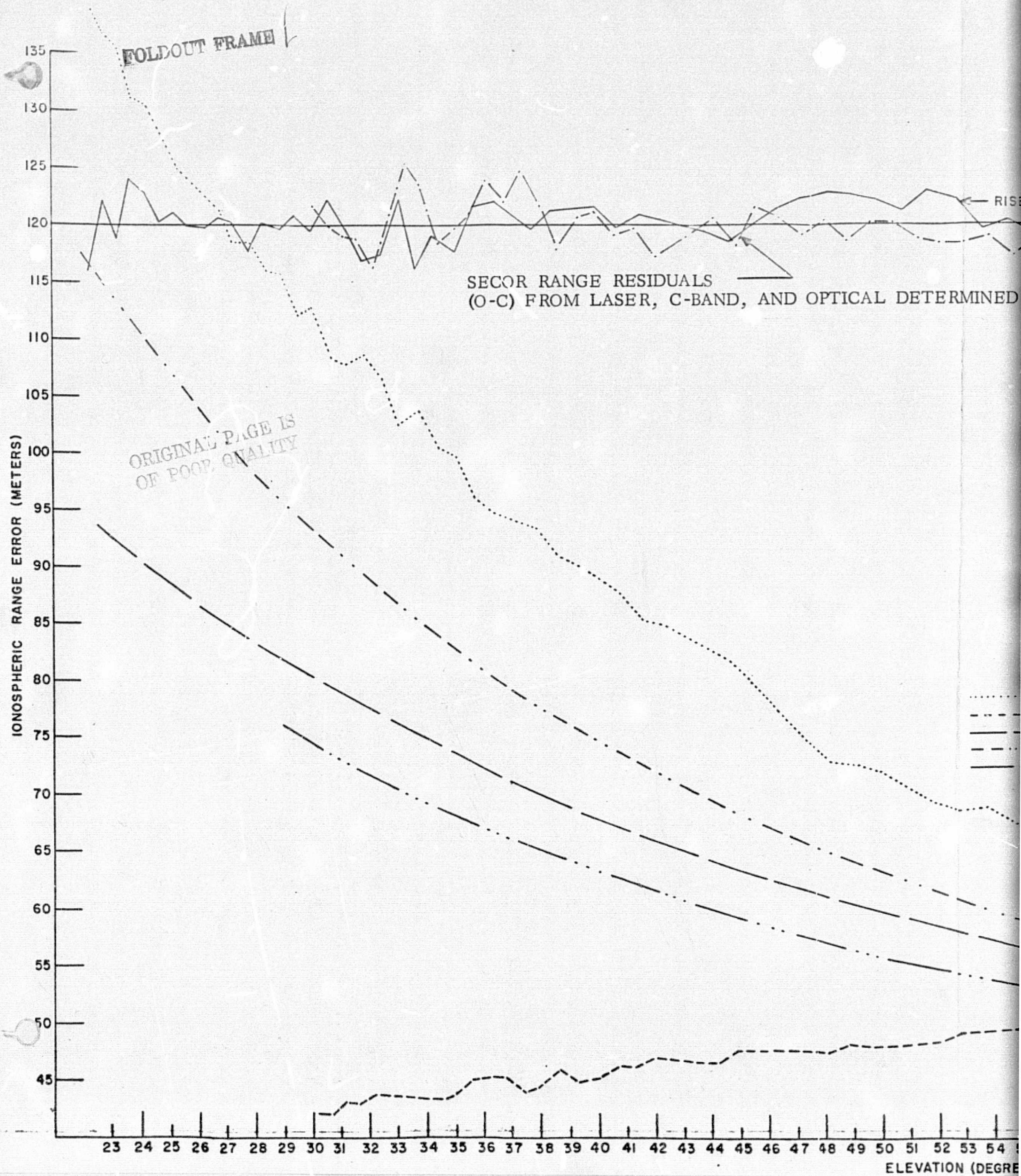

ORIGINAL PAGE IS
OF POOR QUALITY

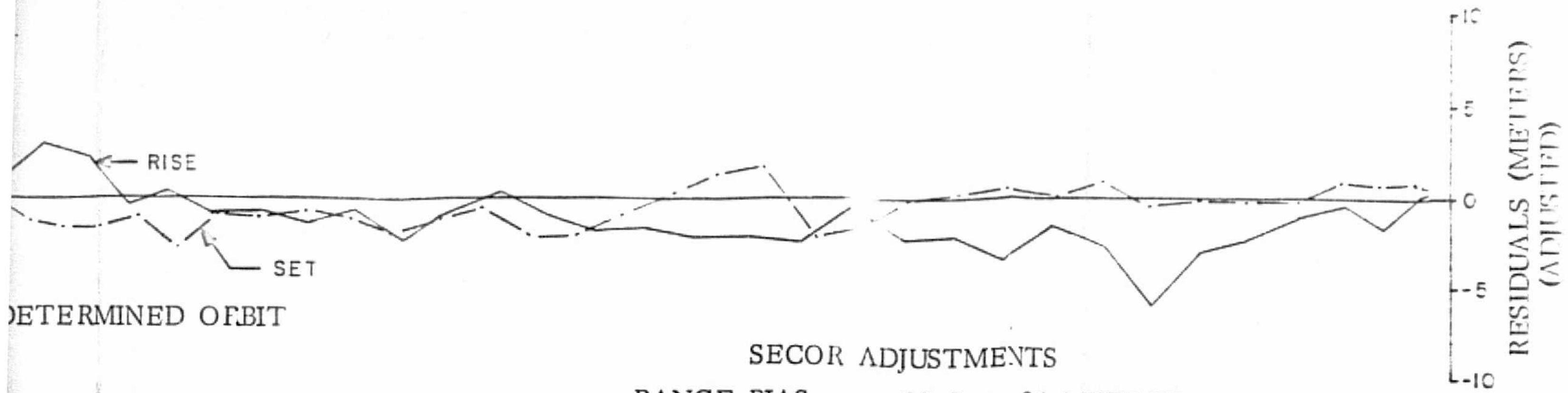

SECOR ADJUSTMENTS

RANGE BIAS = -20.8 ± .34 METERS
TIME BIAS = -2.31 ± .08 MILLISEC

RMS RESIDUAL = 1.81 METERS

ORIGINAL PAGE IS
OF POOR QUALITY

LEGEND:

- .... SECOR IONOSPHERIC RANGE CORRECTION (RISE)
- – – – – – – – SECOR IONOSPHERIC RANGE CORRECTION (SET)
- ——— ——— ——— IONOSPHERIC RANGE CORRECTION FROM RAYTRACE OF A COMPOSITE PROFILE (RISE AND SET)
- — — · — — · IONOSPHERIC RANGE CORRECTION FROM RAYTRACE OF A MODIFIED COMPOSITE PROFILE (RISE)
- ——— · · · ——— IONOSPHERIC RANGE CORRECTION FROM RAYTRACE OF A MODIFIED COMPOSITE PROFILE (SET)

$\left.\right\}$ f_oF_2 SCALING

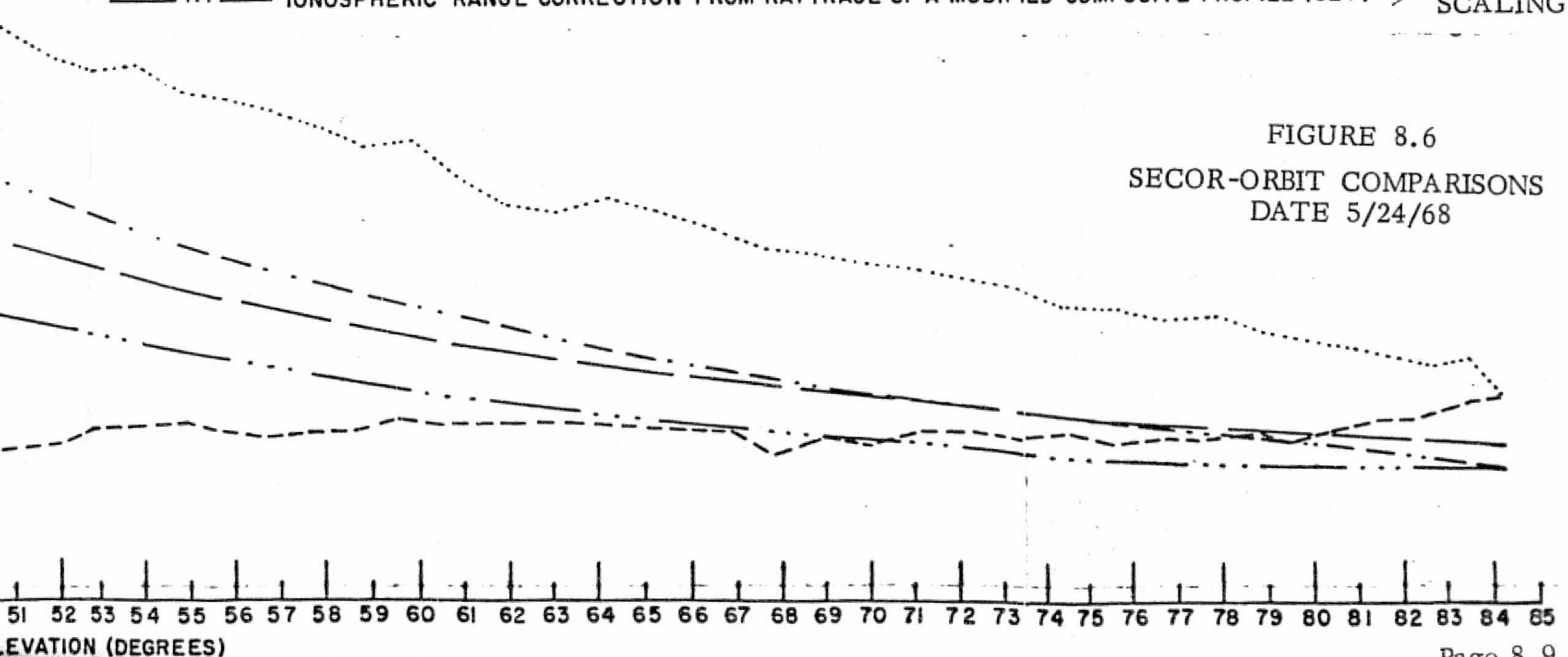

FIGURE 8.6
SECOR-ORBIT COMPARISONS
DATE 5/24/68

FOLDOUT FRAME

ORIGINAL PAGE IS
OF POOR QUALITY

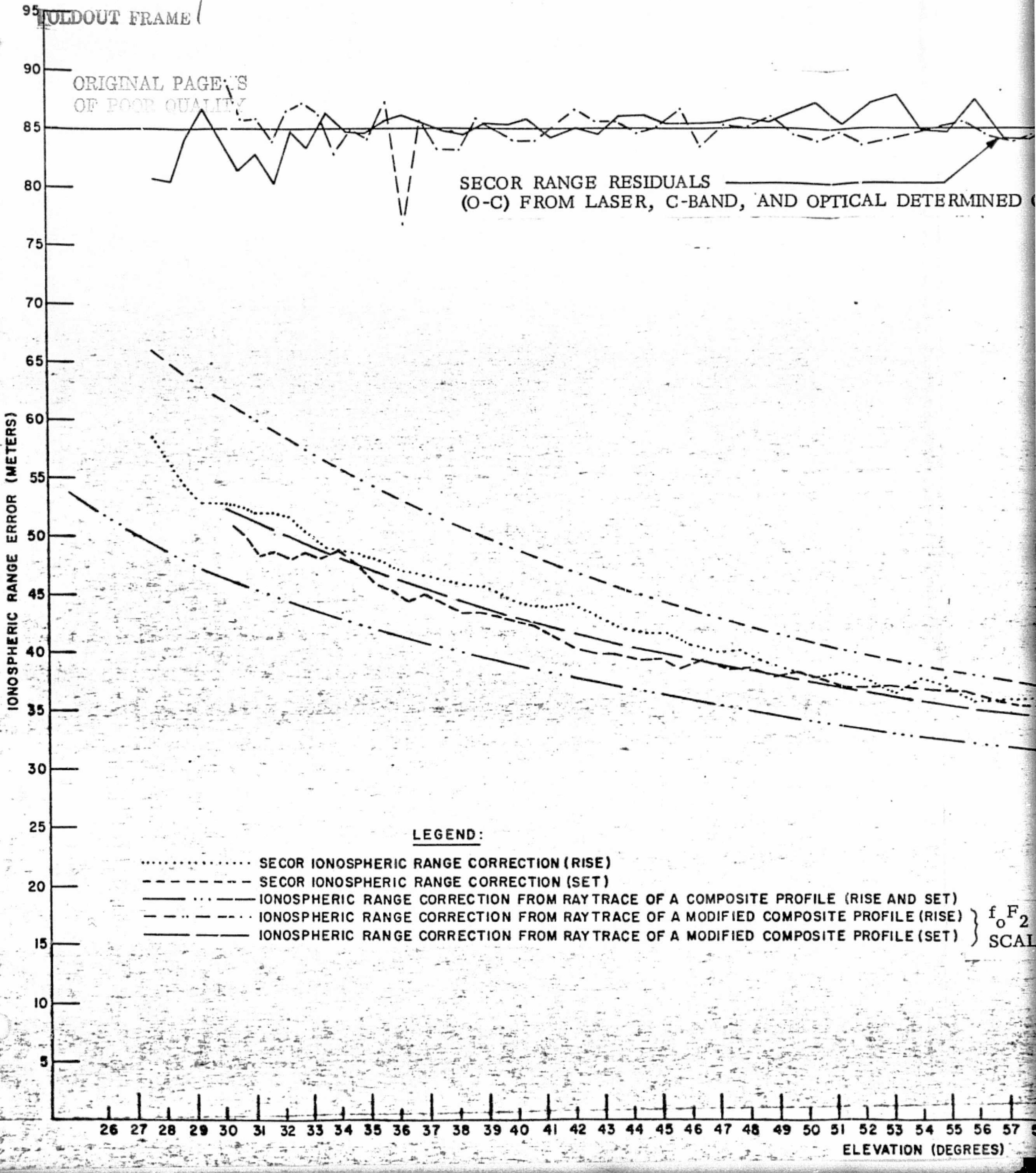

FOLDOUT FRAME 2

ORIGINAL PAGE IS
OF POOR QUALITY

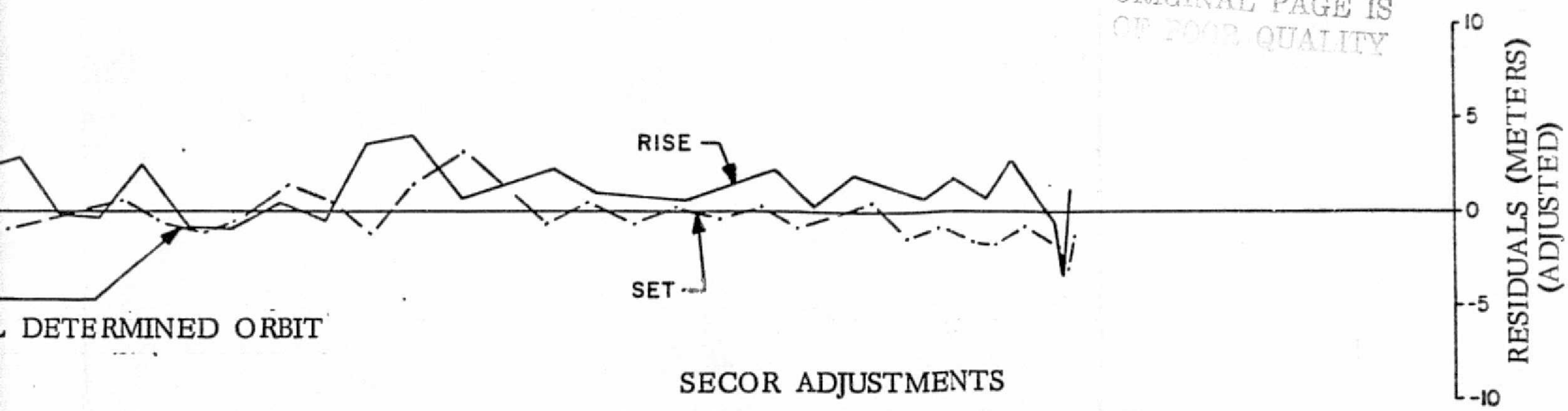

SECOR ADJUSTMENTS

RANGE BIAS = −13.51 ± .36 METERS

TIME BIAS = −1.76 ± .10 MILLISEC

RMS RESIDUAL = 1.79 METERS

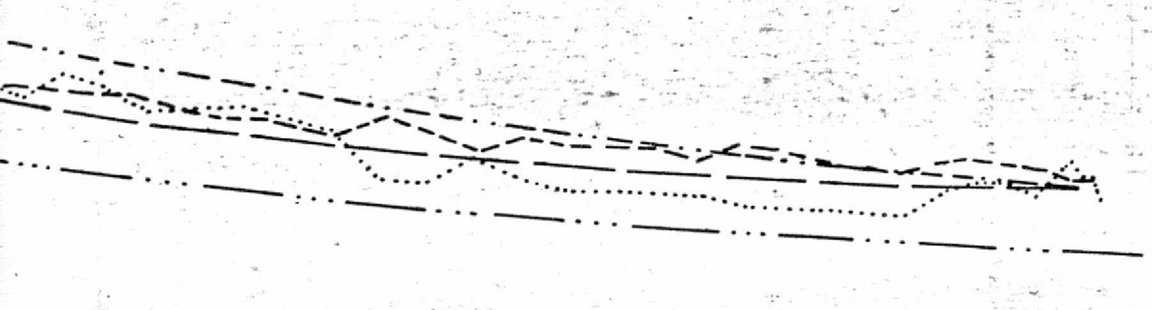

AND SET)
FILE (RISE) } f_oF_2
FILE (SET) } SCALING

FIGURE 8.7

SECOR-ORBIT COMPARISONS
DATE 5/25/68

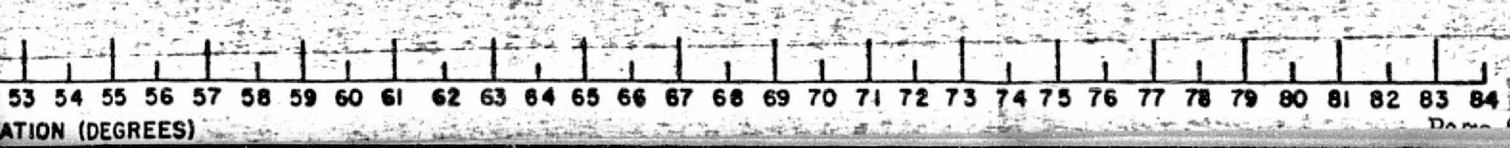

Communications Research Laboratories

FOLDOUT FRAME

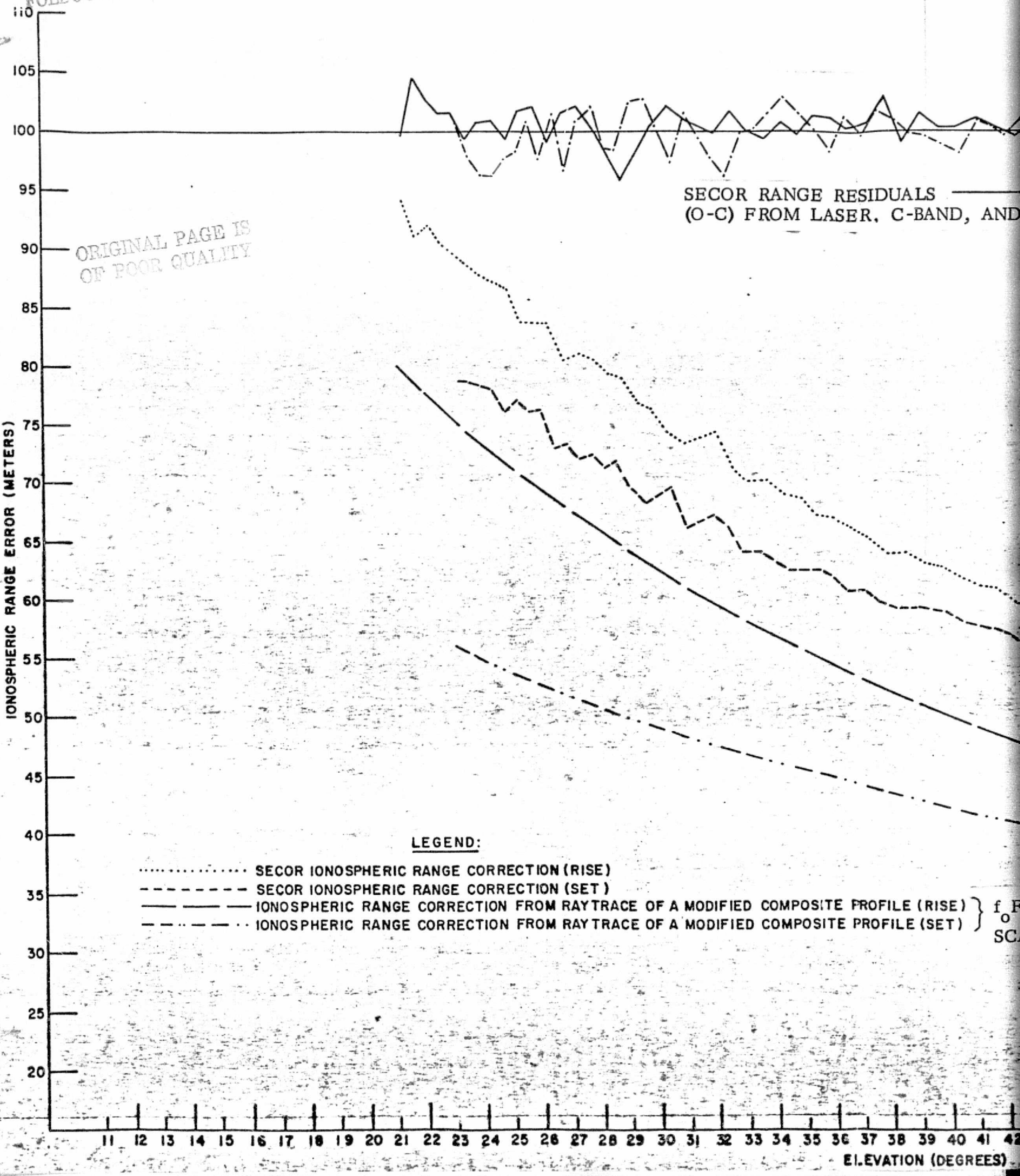

ORIGINAL PAGE IS
OF POOR QUALITY

FOLDOUT FRAME 2

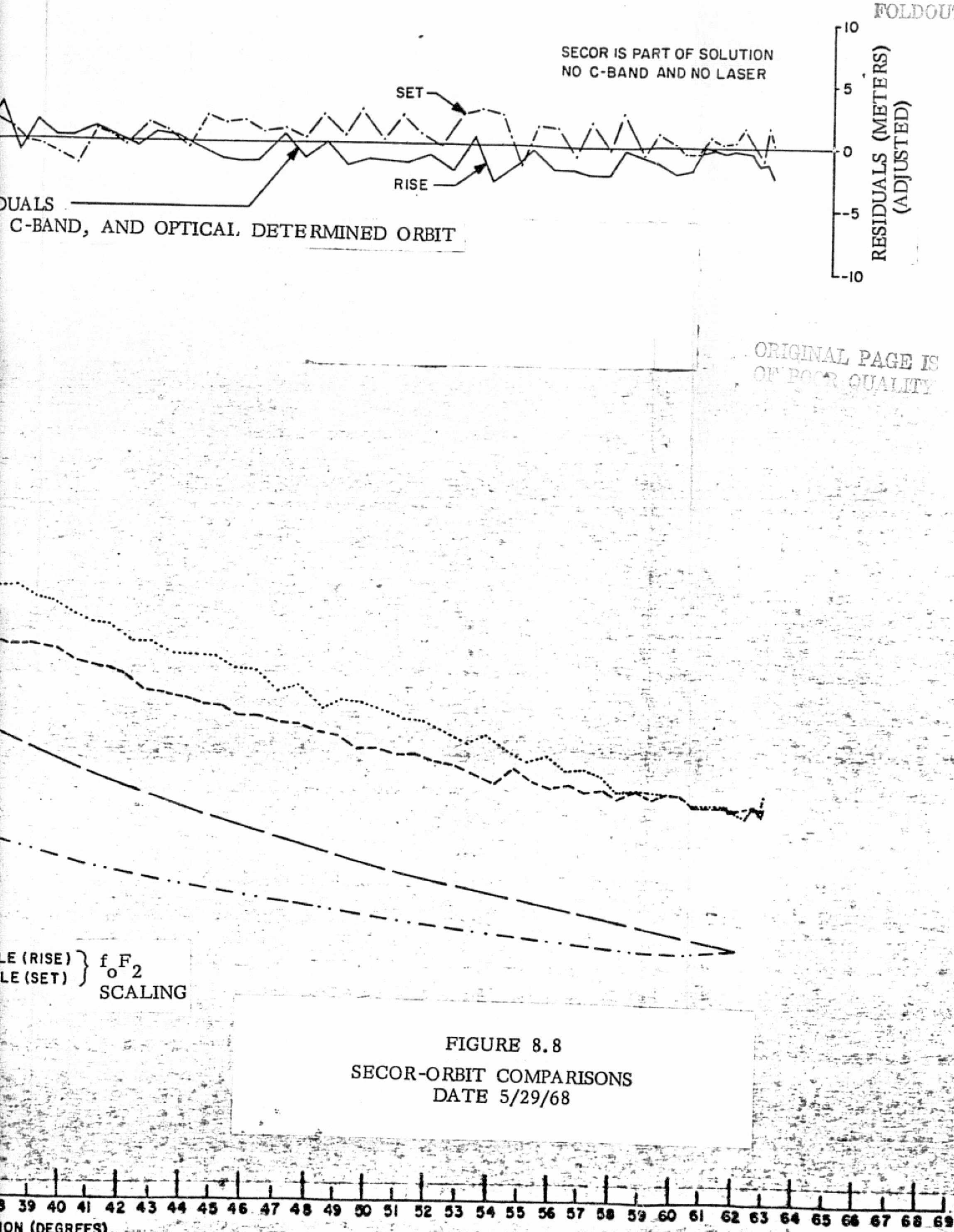

ORIGINAL PAGE IS
OF POOR QUALITY

FIGURE 8.8

SECOR-ORBIT COMPARISONS
DATE 5/29/68

Communications Research Laboratories

FOLDOUT FRAME

ORIGINAL PAGE IS
OF POOR QUALITY

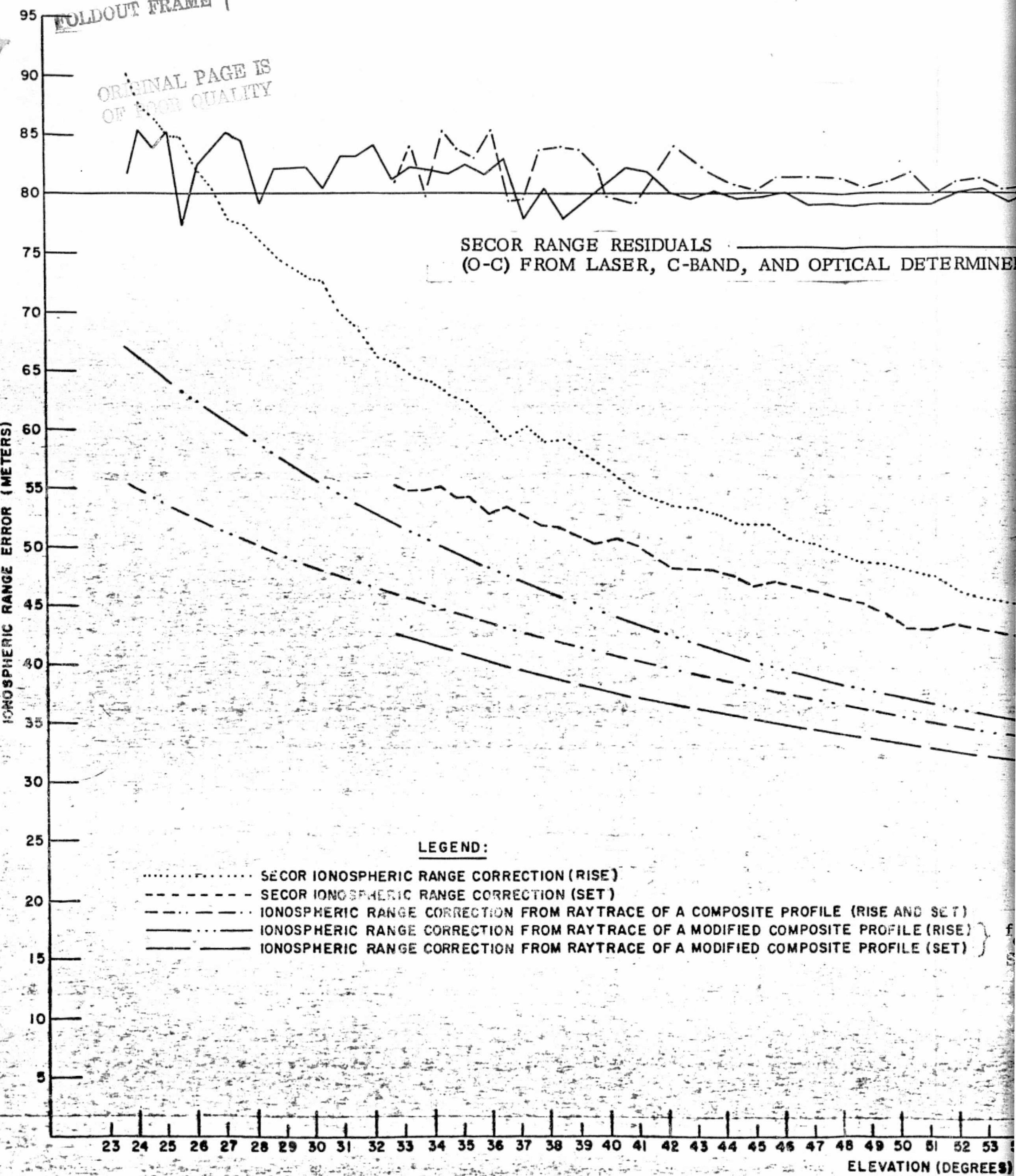

FOLDOUT FRAME

ORIGINAL PAGE IS
OF POOR QUALITY

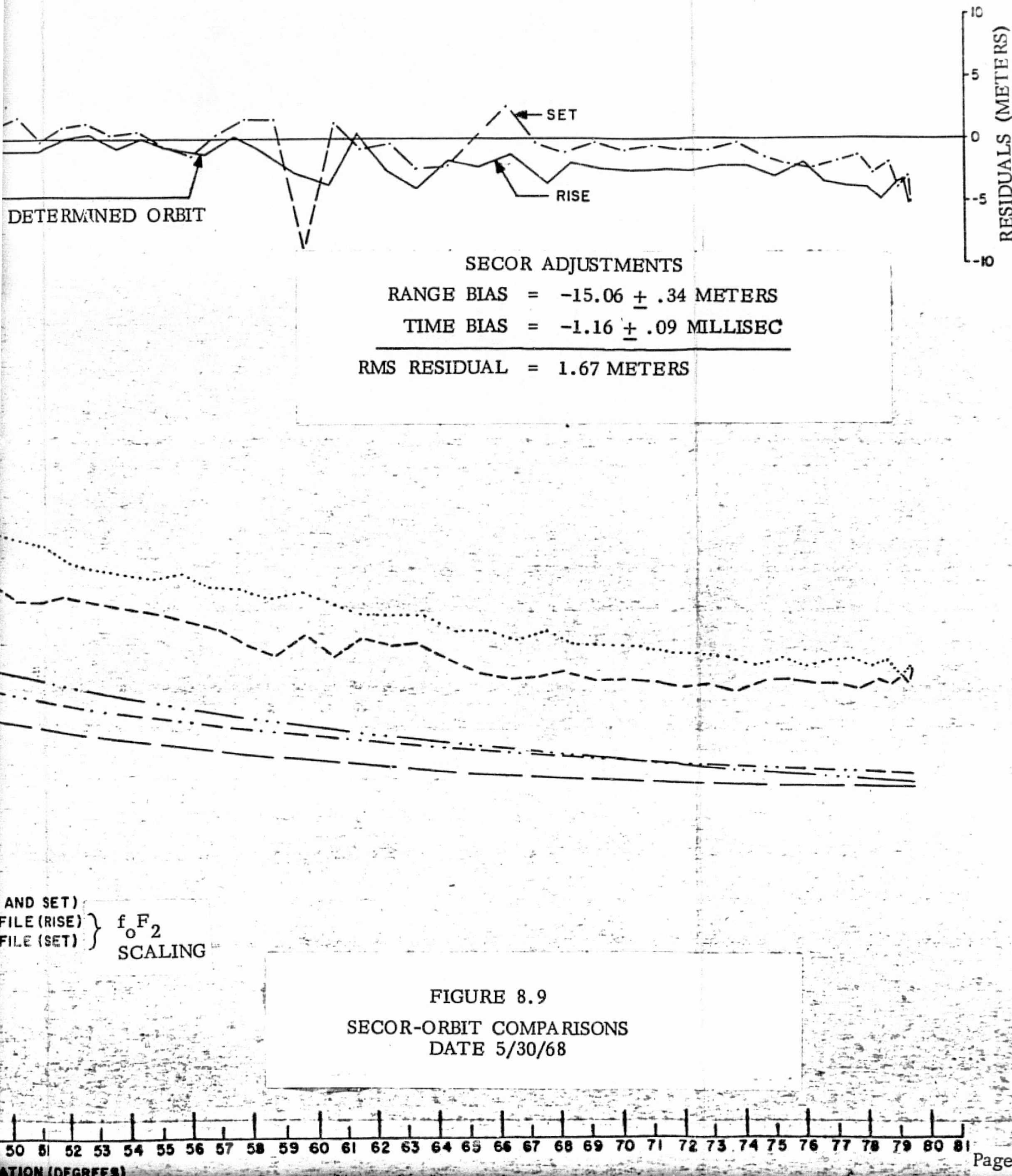

FIGURE 8.9

SECOR-ORBIT COMPARISONS
DATE 5/30/68

FOLDOUT FRAME

ORIGINAL PAGE IS
OF POOR QUALITY

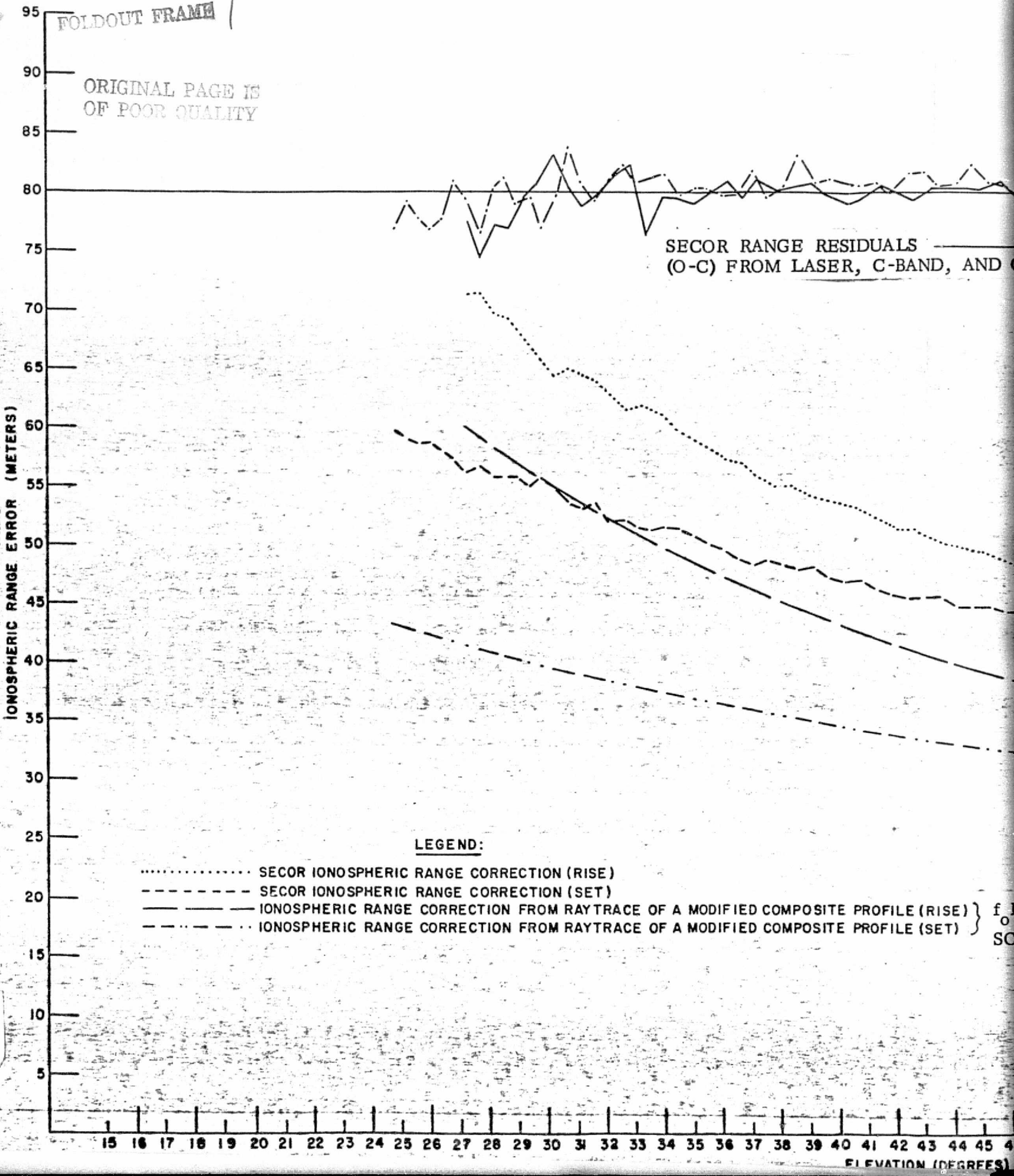

FOLDOUT FRAME

ORIGINAL PAGE IS
OF POOR QUALITY

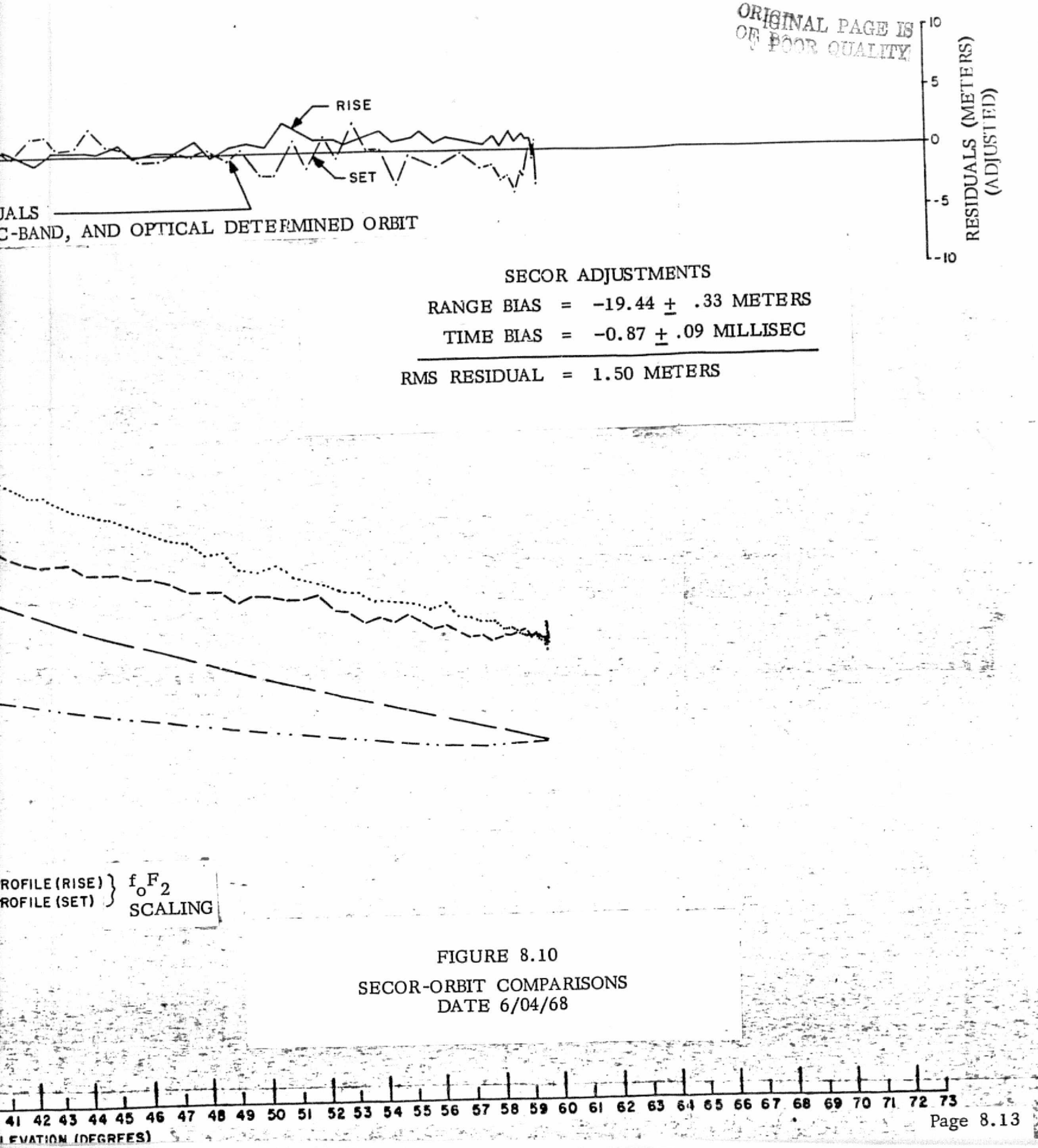

FIGURE 8.10

SECOR-ORBIT COMPARISONS
DATE 6/04/68

ORIGINAL PAGE IS
OF POOR QUALITY

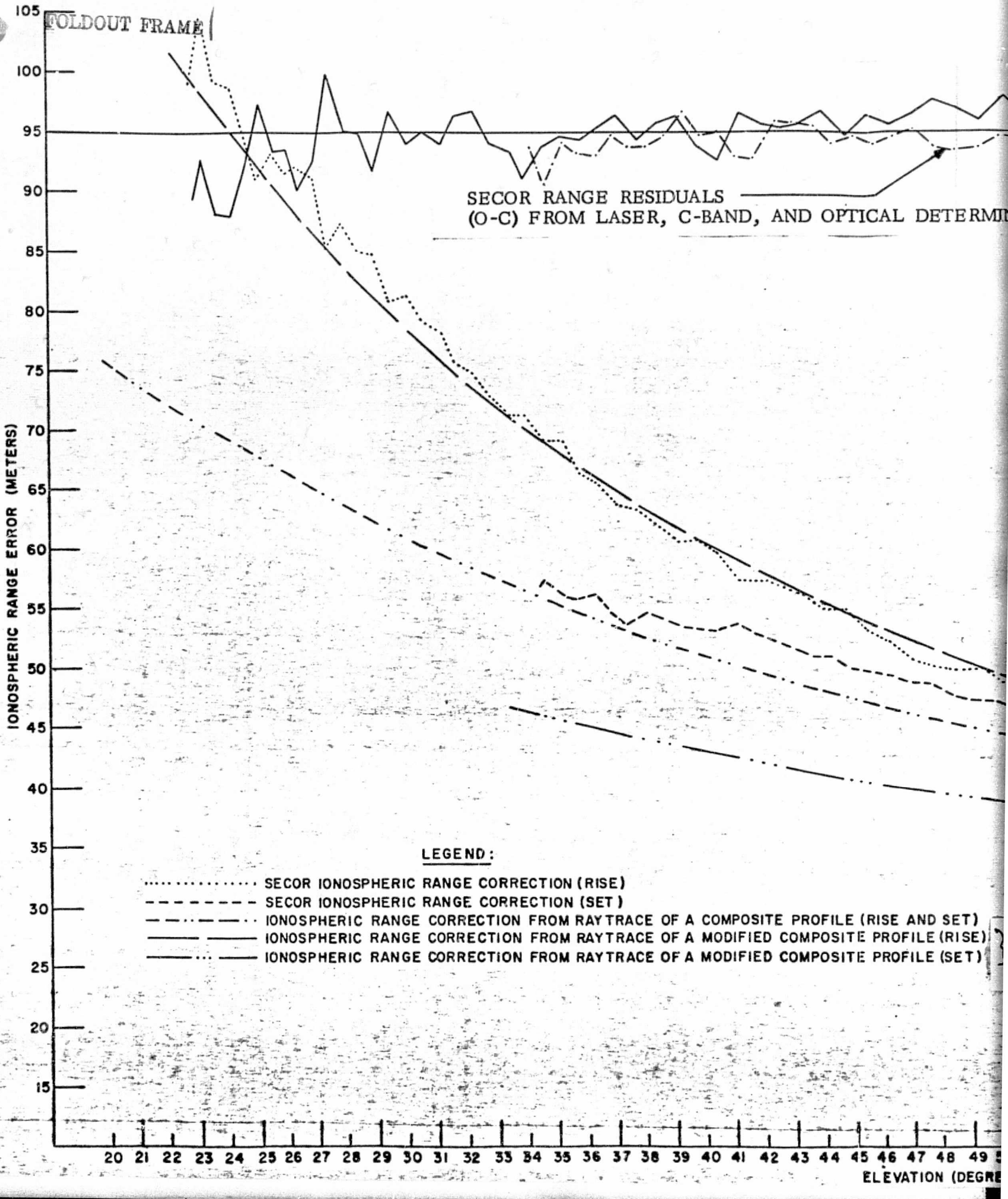

FOLDOUT FRAME 2

ORIGINAL PAGE IS
OF POOR QUALITY

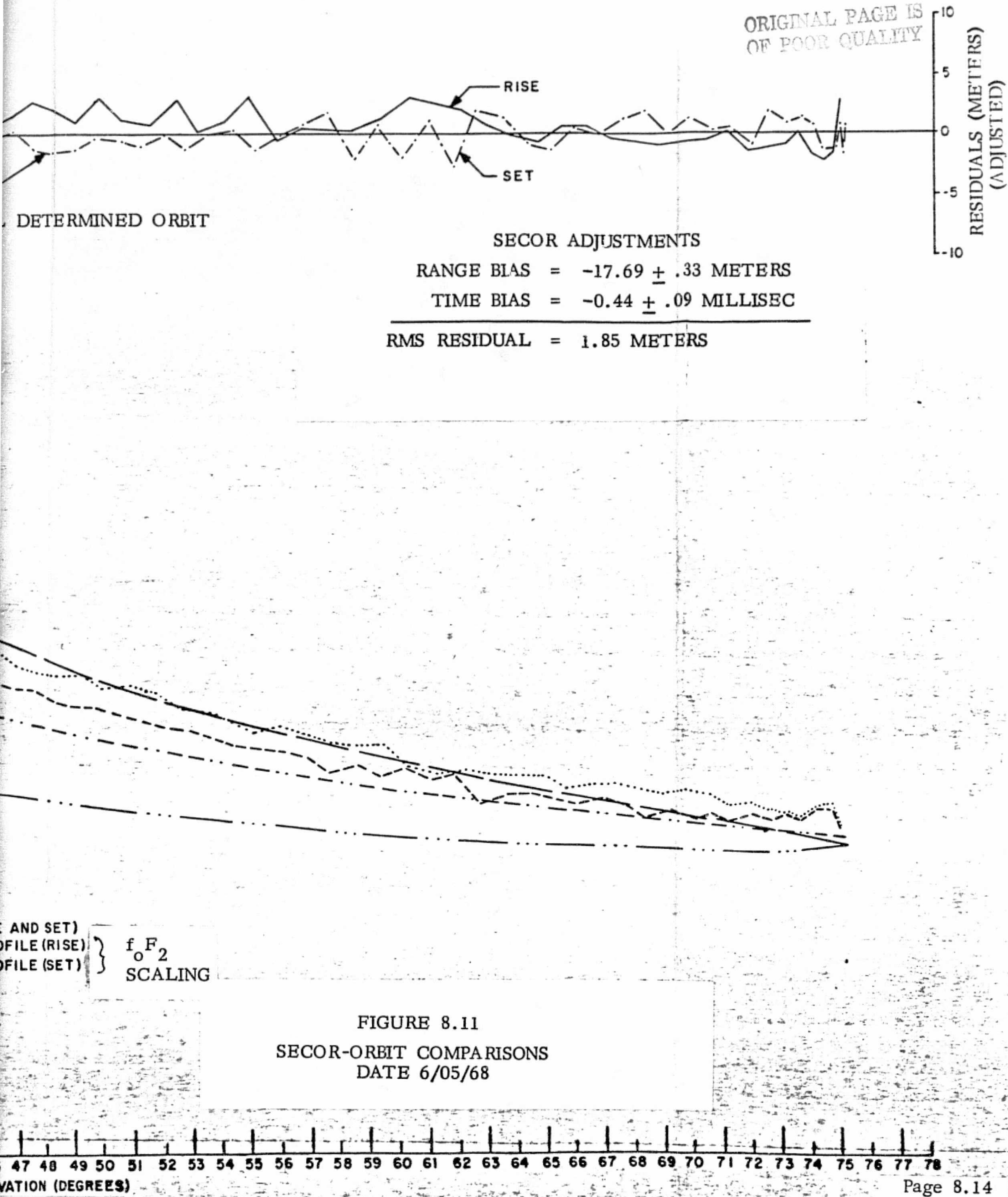

FIGURE 8.11

SECOR-ORBIT COMPARISONS
DATE 6/05/68

FOLDOUT FRAME (
ORIGINAL PAGE IS
OF POOR QUALITY

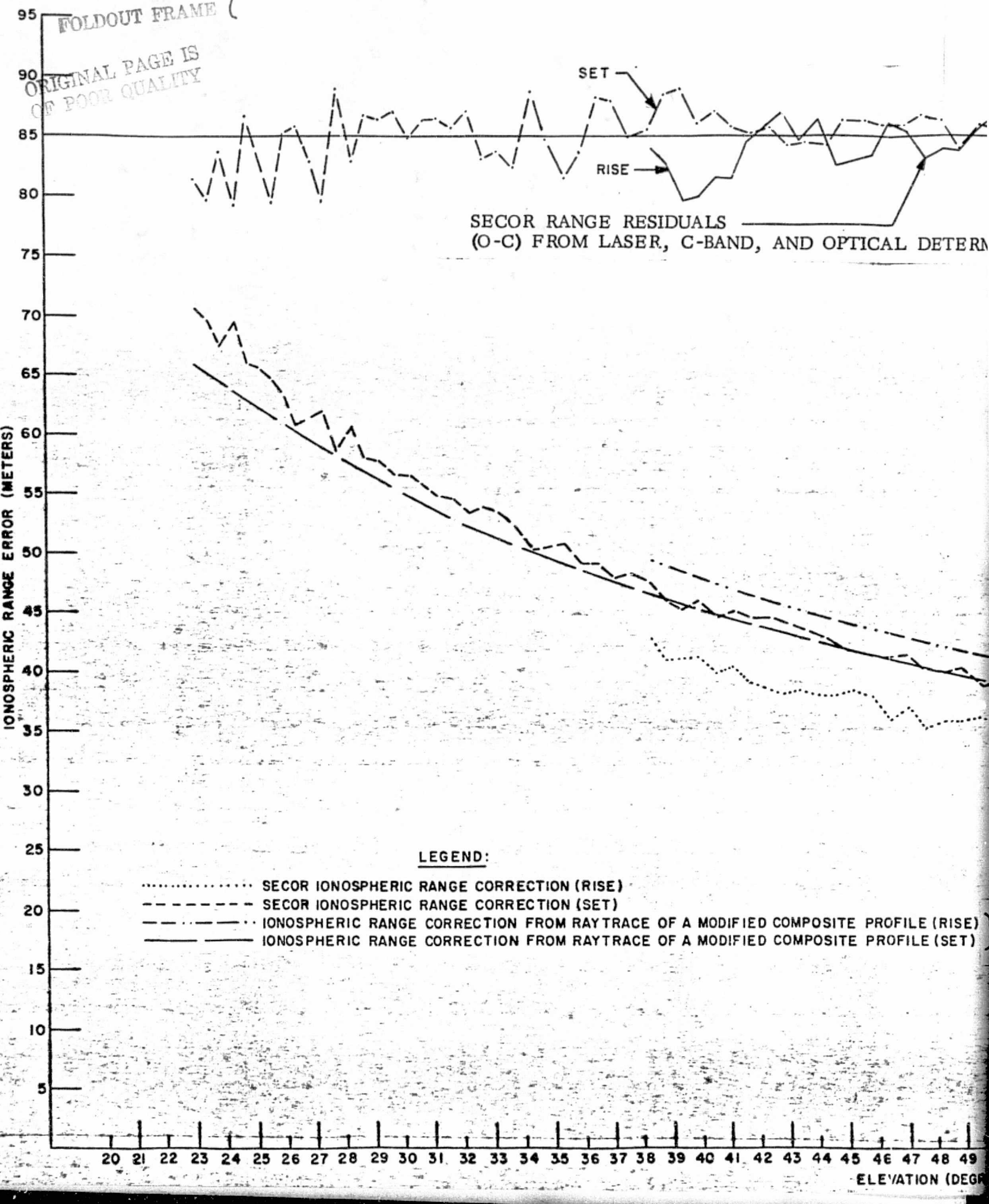

FOLDOUT FRAME 2

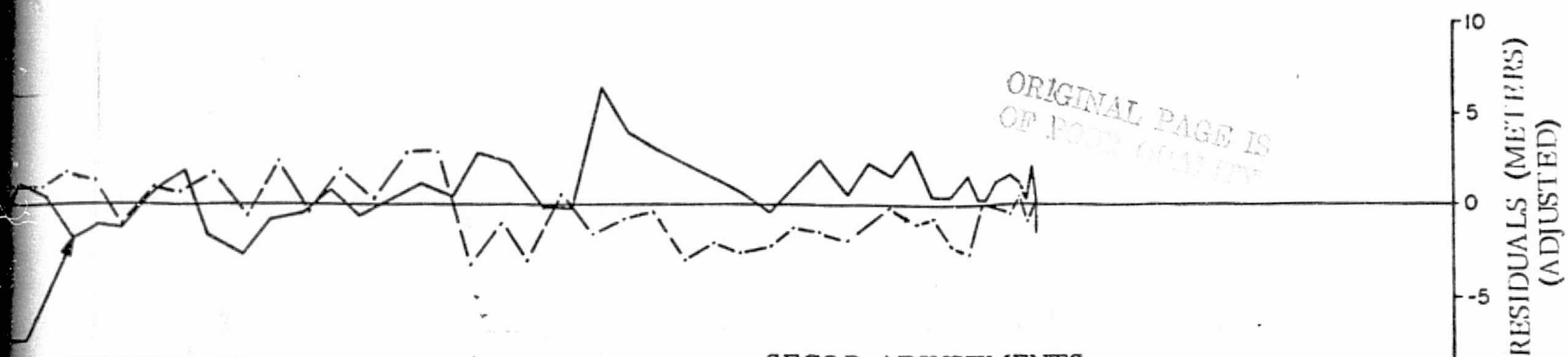

ORIGINAL PAGE IS
OF POOR QUALITY

SECOR ADJUSTMENTS

RANGE BIAS = −19.40 ± .34 METERS

TIME BIAS = −0.87 ± .10 MILLISEC

RMS RESIDUAL = 2.16 METERS

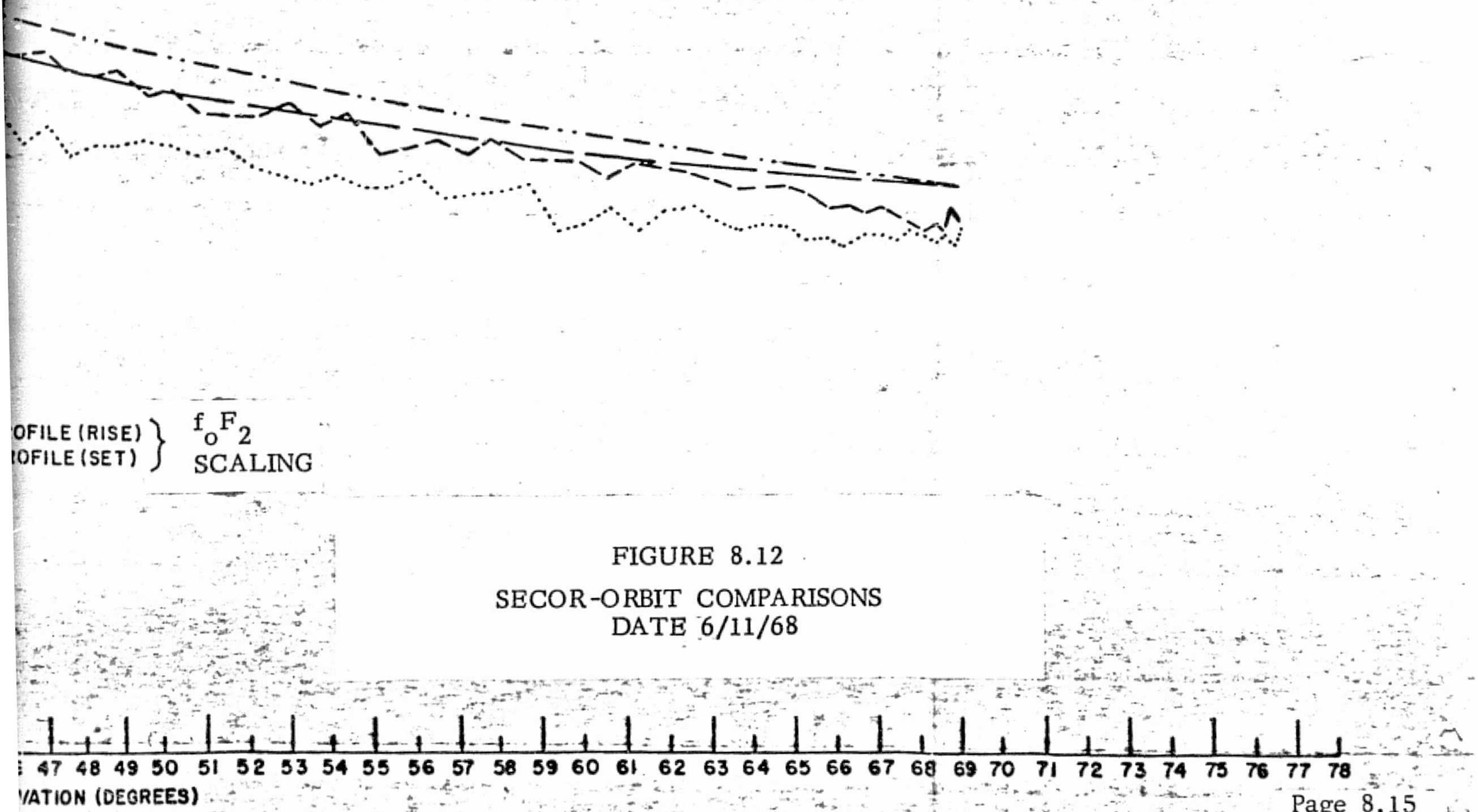

FIGURE 8.12

SECOR-ORBIT COMPARISONS
DATE 6/11/68

FOLDOUT FRAME

ORIGINAL PAGE IS
OF POOR QUALITY

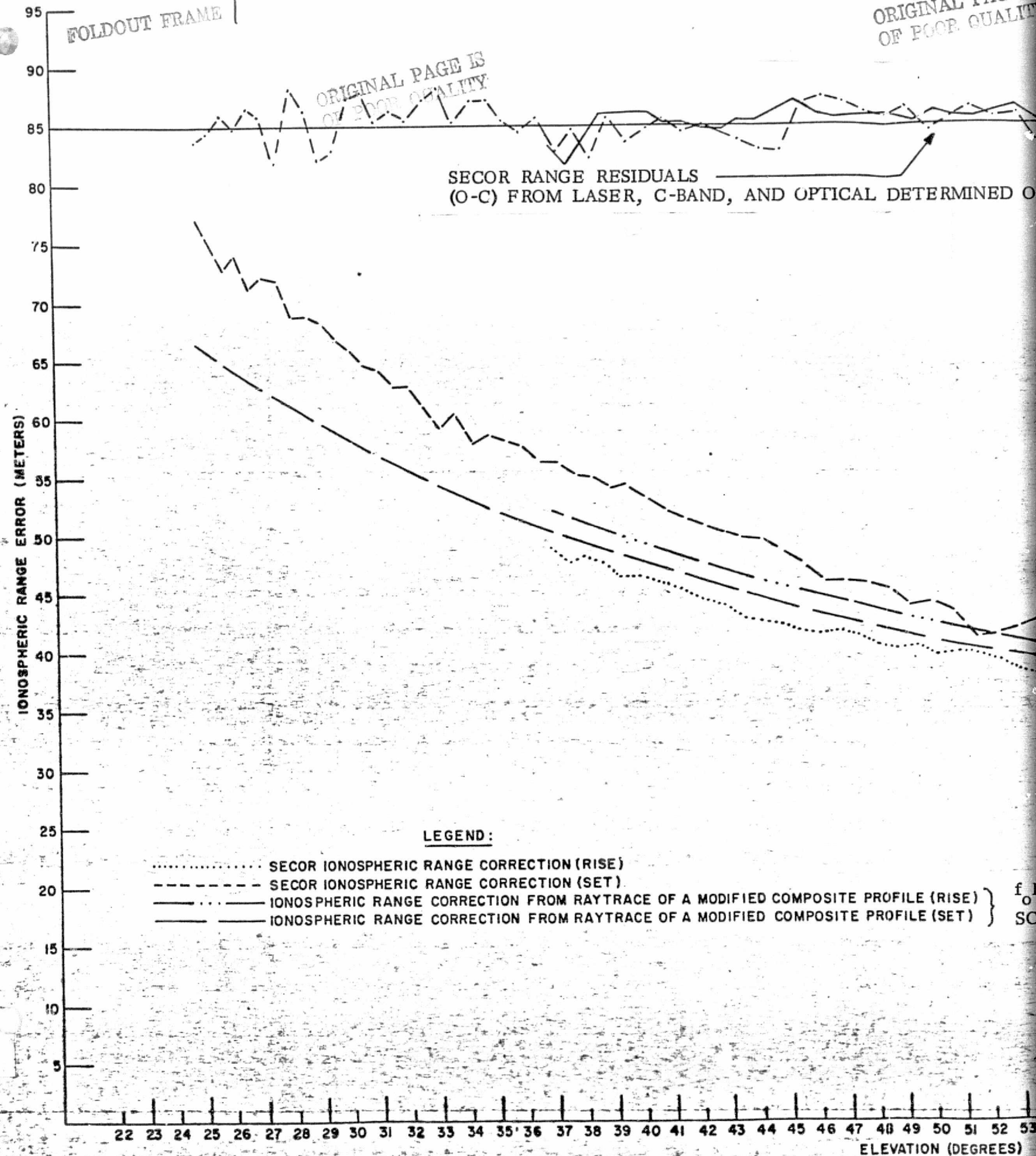

FOLDOUT FRAME 2

RIGINAL PAGE IS
)F POOR QUALITY

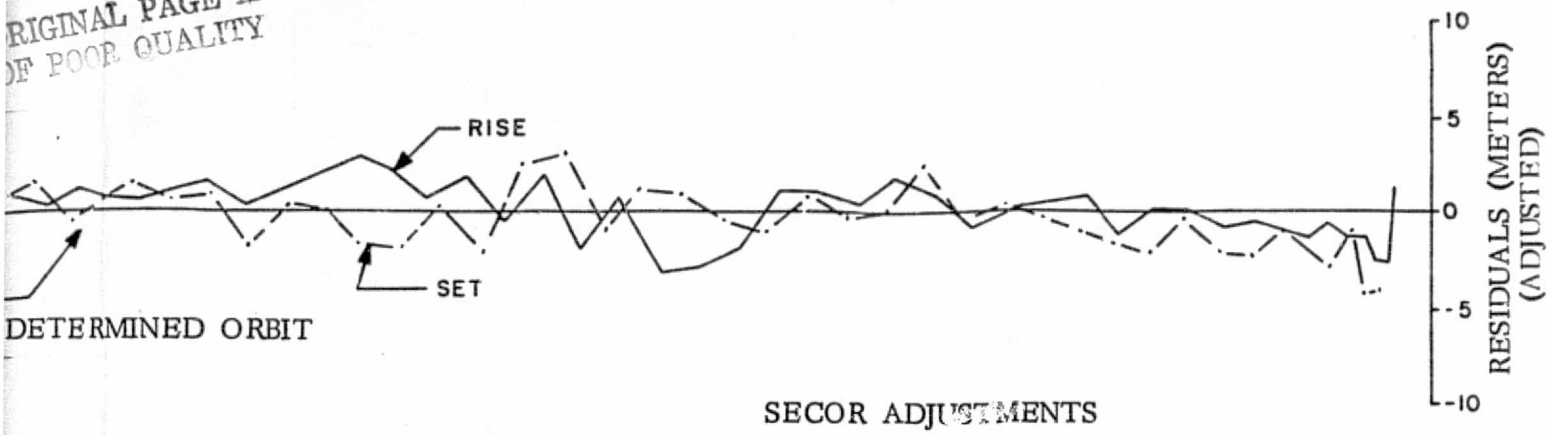

SECOR ADJUSTMENTS

RANGE BIAS = −19.13 ± .33 METERS

TIME BIAS = −0.96 ± .09 MILLISEC

RMS RESIDUAL = 1.58 METERS

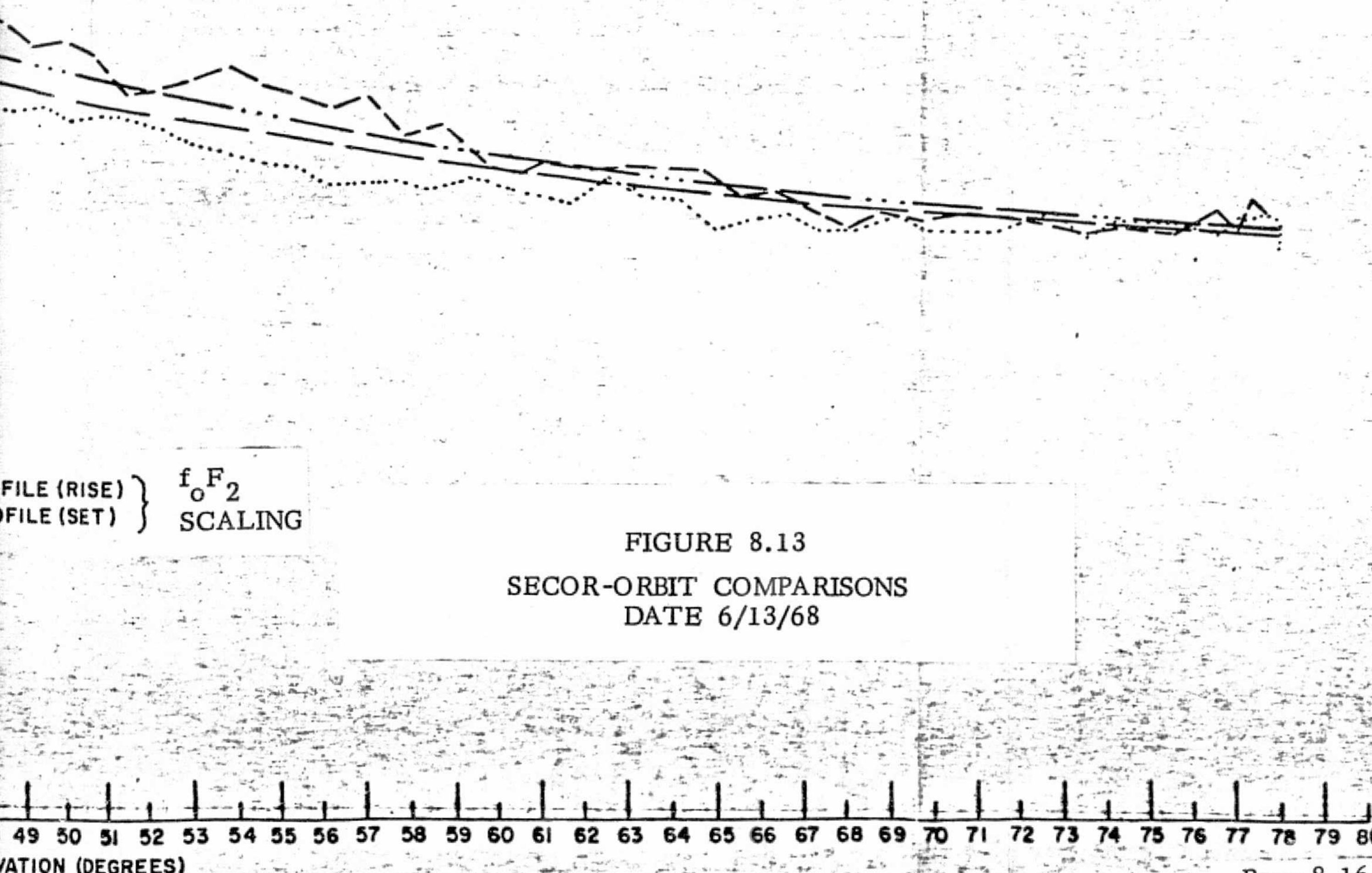

FIGURE 8.13

SECOR-ORBIT COMPARISONS
DATE 6/13/68

FOLDOUT FRAME

ORIGINAL PAGE IS
OF POOR QUALITY

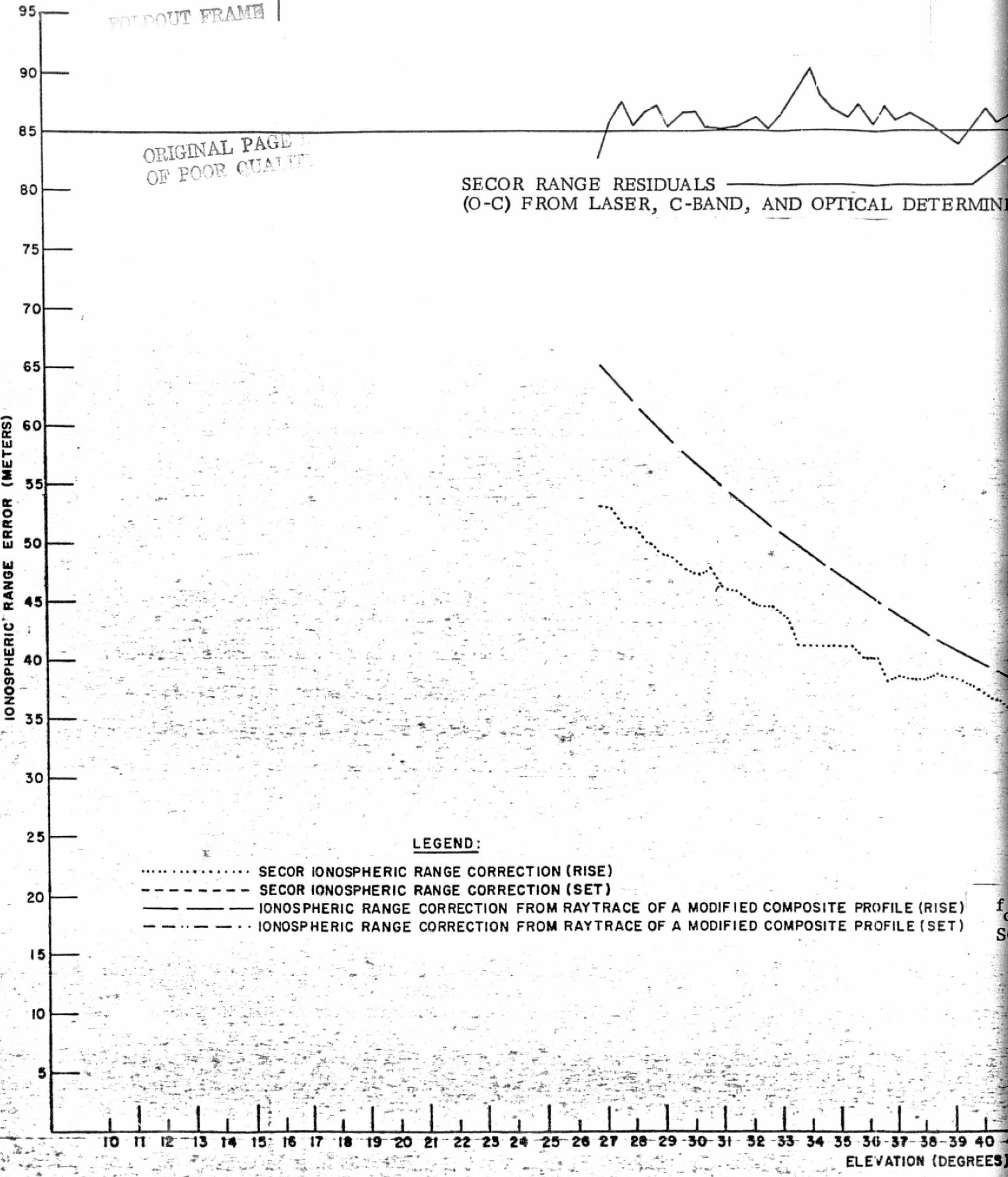

FOLDOUT FRAME 2

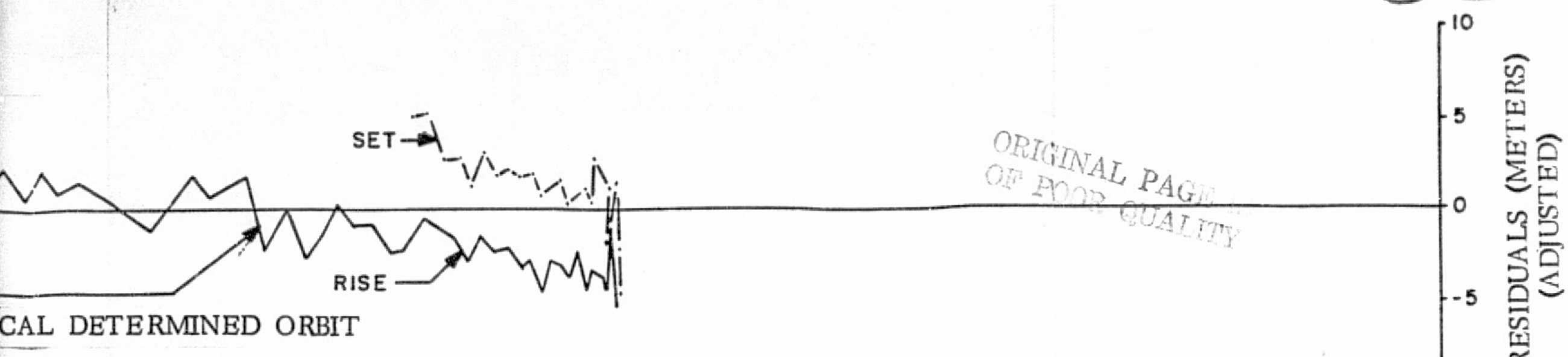

ORIGINAL PAGE
OF POOR QUALITY

SECOR ADJUSTMENTS

RANGE BIAS = −22.67 ± .51 METERS

TIME BIAS = −1.39 ± .20 MILLISEC

RMS RESIDUAL = METERS

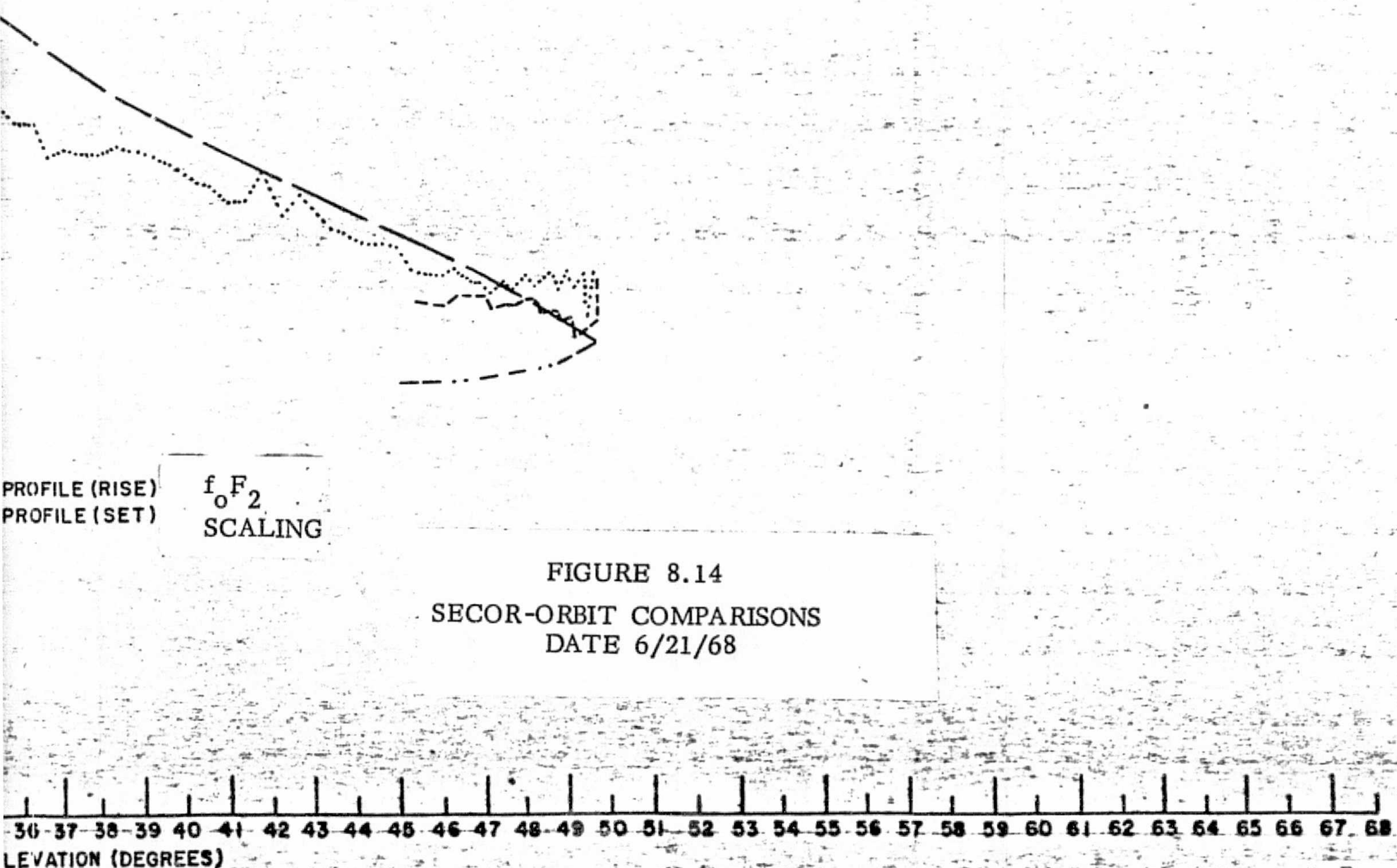

FIGURE 8.14

SECOR-ORBIT COMPARISONS

DATE 6/21/68

FOLDOUT FRAME

ORIGINAL PAGE IS
OF POOR QUALITY

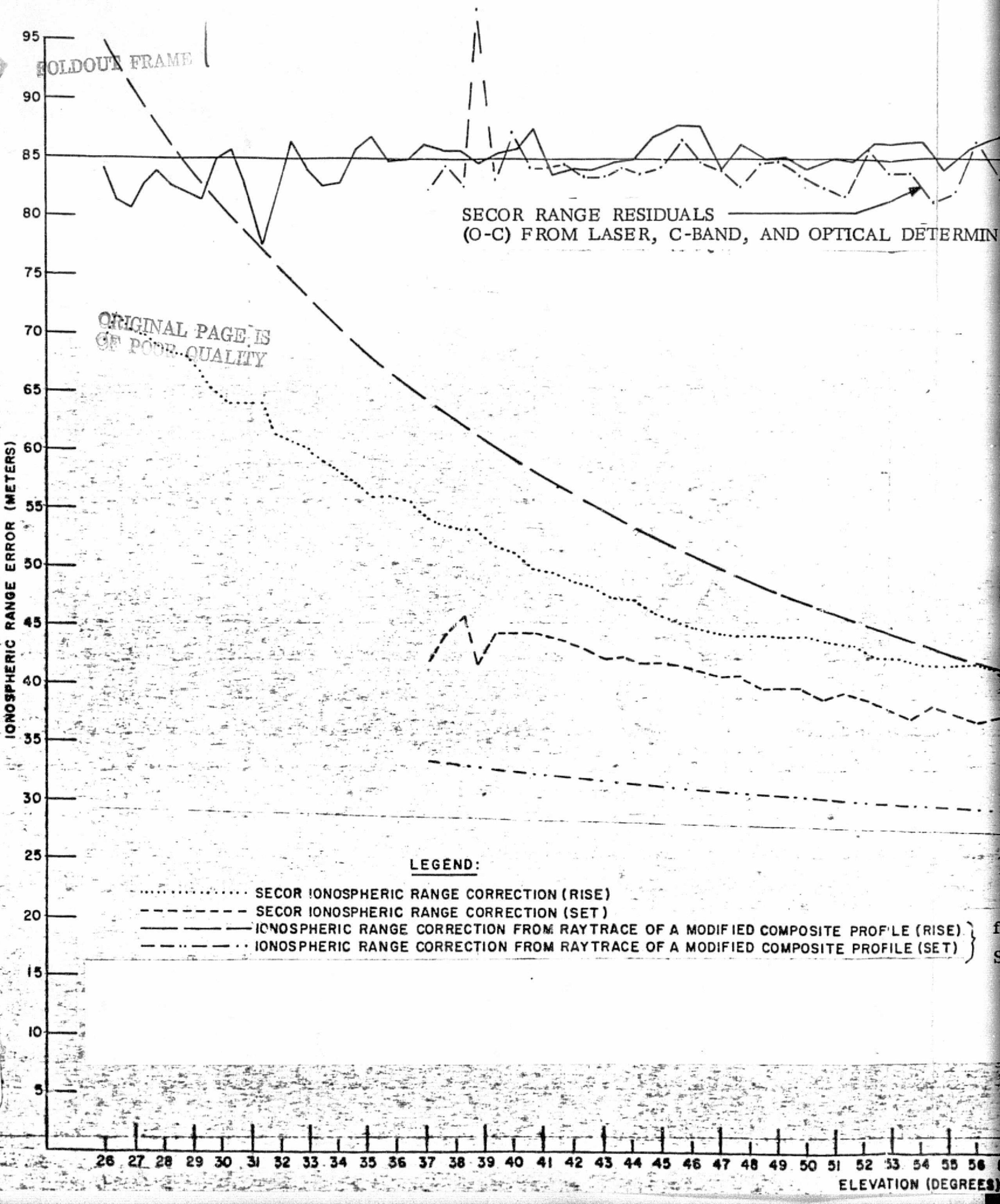

FOLDOUT FRAME 2

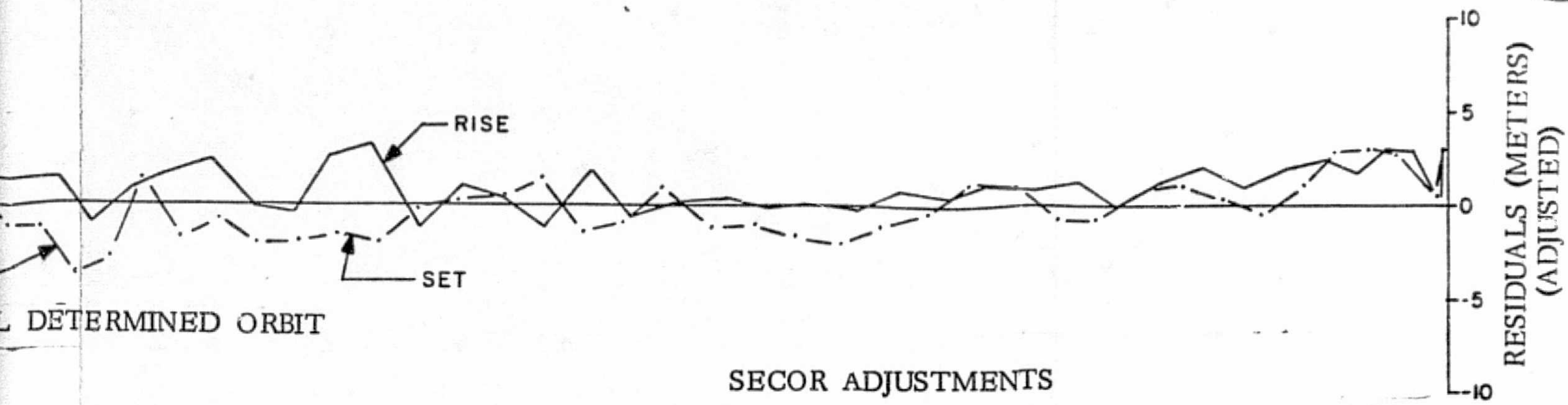

ORIGINAL PAGE IS OF POOR QUALITY

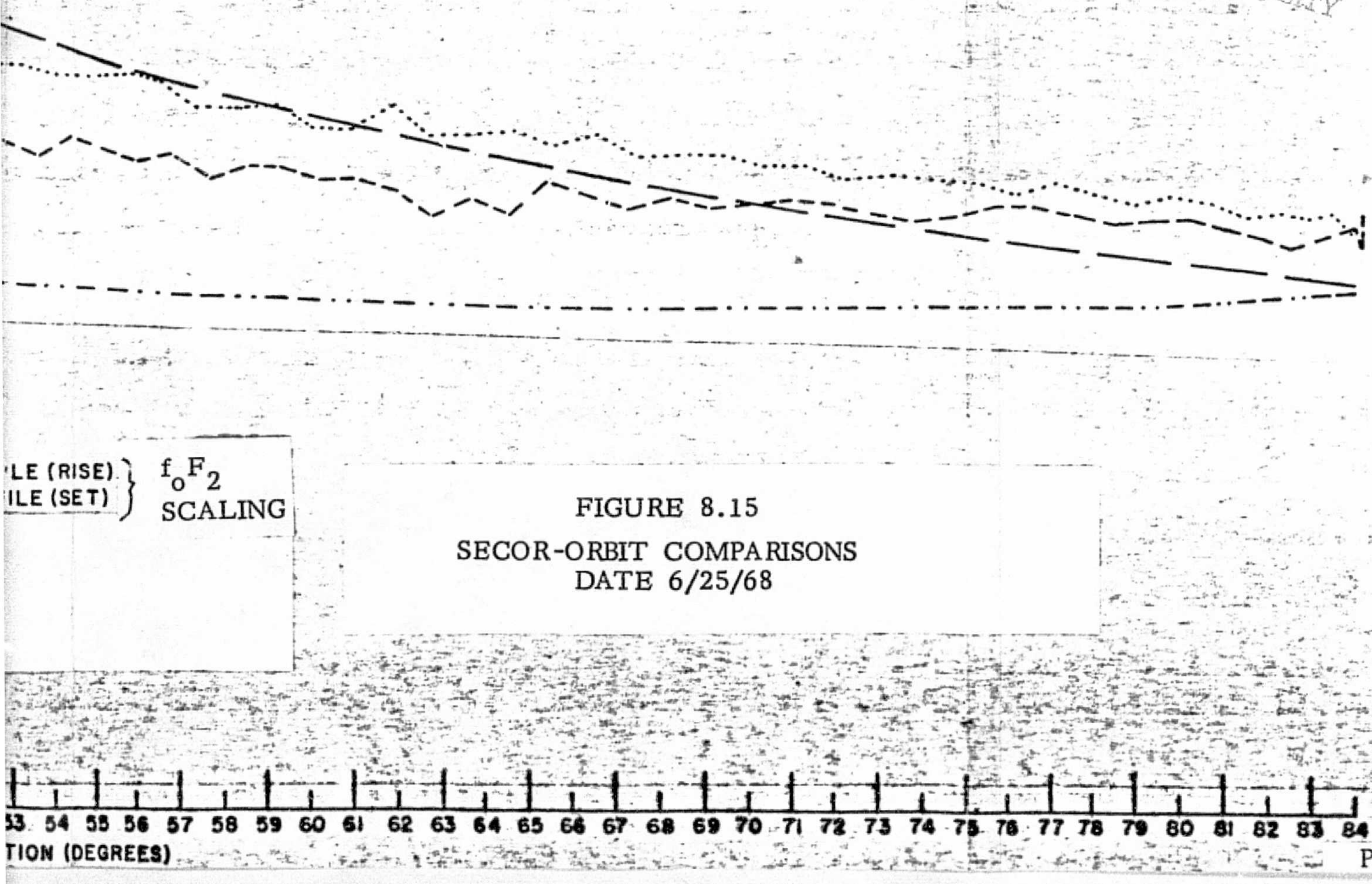

FIGURE 8.15
SECOR-ORBIT COMPARISONS
DATE 6/25/68

9. SUMMARY CONCLUSIONS

Ray Trace (Section 3)

3.1) After minor modification of the density extrapolation routine above the top of the ionosphere the REEK Program was found to be an extremely and consistently accurate basis for ray trace comparisons.

3.2) For certain purposes it is a reasonable approximation to ignore bending in the path integrals. For a simple slab model ionosphere the error in so doing is approximately

$$\frac{N^2 \tau}{2} \left(1 - \frac{\tau}{h}\right) \tan^2 \Phi \sec \Phi$$

where

N = (average) refractivity

τ = layer thickness

h = satellite height

Φ = zenith angle

The error is quadratic in N and vanishes at vertical incidence.

3.3) For the same slab model it is shown that the group range error is given exactly by the integral of group refractivity along the phase path.

3.4) Numerical comparisons of REEK and straight line raytrace on actual layers confirm the above general relationship.

3.5) For a representative ionospheric case of f_oF_2 = 5.6 MHz, f = 434 MHz (SECOR), $N_{max} \approx 84 \cdot 10^{-6}$, the maximum error in the straight line assumption is 0.11 meters out of 73 meters.

3.6) For the troposphere, the range error in ignoring bending becomes significant, i.e., equal to or greater than 2% for elevation angles less than about 10^o. This is a significant limitation of any troposphere correction method which ignores bending.

3.7) The neglect of f^{-3} (gyromagnetic) terms in the ionospheric refractivity can result in errors as great as 2% at frequencies of the order of 100 MHz. As this can be compared to the neglect of bending error, which varies as f^{-4}, and is typically 0.2% at 100 MHz. Thus above 100 MHz the neglect of bending error is generally less than 1/10 that due to neglect of f^{-3} terms in the refractivity.

3.8) It is proven analytically in Section 3.3 that the ionospheric group range error is given exactly by the integral of group refractivity along the phase path.

3.9) The error in the use of the superposition principal to determine ionospheric and tropospheric errors separately was studied numerically. With typical values at 100 to 400 MHz the error is less than 10^{-3} of the range error at low elevation angles.

Analytic Corrections (Section 4)

4.1) All of the tropospheric analytic forms considered are of essentially identical form above 10° elevation.

4.2) Below 10° elevation angle the NAP-1 and GDAP formulations are a good approximation to the correct variation down to the lowest angles. These corrections are of the general form

$$\Delta R(E) = \Delta R(90^{\circ}) \csc E \left[\frac{2}{1 + \sqrt{1 + .004 \csc^2 E}} \right]$$

$$\Delta E(E) = N_s \operatorname{ctn} E \left[\frac{2}{1 + \sqrt{1 + .004 \csc^2 E}} \right]$$

4.3) A special regression study was conducted, based on 85 days of actual radiosonde profile data taken during WICE and considering various possible models for the total range error in terms of measured values of pressure, temperature, and humidity at ground level. The best model was found to be the one which depended on N(P, T, H), i.e., the ground level refractivity alone. This is the same in form as the NBS regression model.

4.4) The predictive capability of this special regression for the 85 day data from which it was derived was compared to that of the two NBS regression models established on Cape Canaveral data and on a widespread US data base, and to the Hopfield bi-quartic prediction. The standard of comparison was REEK raytracing of the radiosonde measured profiles.

The special Wallops regression was of course best (.149 m rms) followed by Hopfield (.223 m rms) NBS "Cape Canaveral" regression (.258 m rms), and NBS "Standard Sample regression" (.281 m rms).

4.5) For the Ionosphere the minimum elevation angles are never less than about 18^{o} in the ionosphere even for horizontal takeoff at the ground. For this reason, most of the analytic forms studies, with the exception of the Freeman and GEOVAP formulations provide reasonably good models down to the lowest ground elevation angles.

Moment Expansions (Section 5)

5.1) A moment series expansion, useful for ionospheric and tropospheric range, elevation angle, and range rate errors is developed in the form

$$\Delta R(E) \sum_{m=0}^{M} G_m(E) M_m$$

where $M_m = m^{th}$ moment of the profile refractivity distribution

$$= \int_0^{\infty} N(h)\,(h - h_c)^m \, dh$$

$$G_m(E) = \text{geometrical coefficient}$$

$$\approx \frac{1}{m!} \frac{d^m}{dh^m} \sec(\Phi(h)) \Big|_{h=h_c}$$

The utility of the expansion derives from the fact that the layer characteristics are totally characterized by the moments M_m (independent of E) while the elevation angle dependence is totally characterized by the coefficients $G_m(E)$ (independent of the layer characteristics).

5.2) For most purposes the expansion need be carried only to the $M = 2$ term for full accuracy.

5.3) The series is always convergent for the ionosphere but is convergently beginning but ultimately diverges for the troposphere below about 2^o elevation angle.

5.4) For both the ionosphere and the troposphere the moment series expansion corrections for ΔR, ΔE, and $\Delta\dot{R}$ agreed better with the REEK ray-traces than did any of the other analytic corrections tested.

Profile Determinations (Section 6)

6.1) Four different methods of profile prediction were available for comparison, the Jackson composite bottomside-topside sounder reductions, the ESSA bottomside sounder extrapolations, the Freeman model based on 3-month predictions (no longer published) and based on long-time predictions (CCIR Report 340) of f_oF_2 and f 3000 MUF.

6.2) It was found that the discrepancies between the various profile estimates could be expressed efficiently in terms of the moment series particularly since only the zeroeth order moment differences are significant. The first and second order moment differences are responsible for less than 1/10 of the range error differences (in meters) of that due to the zeroeth order moment even for the worst case of lowest elevation angles (Figure 6.2).

6.3) The four predictions listed above were compared in terms of M_o with the SECOR measurements as a reference (Table 6.2). The rms differences relative to SECOR and therefore rough estimates of the absolute error of the various predictions were

Profile Measurements	$\overline{m}$	$\overline{\sigma}$	$\overline{\text{rms}}$ meters	%
Jackson Composite	−4.1	2.5	4.8	13
ESSA Bottomside Extrapolation (only 6 cases)	−1.5	3.4	3.7	10
Profile Predictions				
CCIR Report 340	−5.2	7.1	8.8	24
3 Mos. Advance Predictions	−9.1	6.9	11.4	32

6.4) The SECOR measurements demonstrated significant north-south gradient effects. Several methods were studied to estimate these geographical gradients in terms of both measured and predicted profiles. From measured profiles, gradients were inferred from the measured differences between Ottowa, Wallops and Grand Bahama. From the predicted profiles, gradients were inferred from the differences of predicted densities at each point along the ray, as a function of the actual geographical coordinates of the point on the ray.

None of the geographical scalings were particularly effective in predicting the actual (SECOR) north-south gradient effects. The most effective was that based on linear scaling in latitude based on bottomside f_oF_2 measurements from Ottowa, Wallops and Grand Bahama. For the 17 WICE ionosphere sample days the average south/north assymetry factor was 1.29 : 1. Application of the bottomside f_oF_2 scaling predicted the assymetry with an rms residual of .17 which represents a 60% unpredictable residual.

Multiple Frequency Comparisons (Section 7)

7.1) The SECOR and TRANET systems both made internal measurements of ionospheric error, the former in terms of range and the latter in terms of range-rate. In order to compare the two, either SECOR data had to be differentiated or TRANET had to be integrated, with the resulting constant of integration determined by other means. Regression methods were developed for the estimation of that constant of integration and applied to both SECOR and TRANET.

7.2) The first series of tests of the regression procedure were in an attempt to determine whether there was any systematic bias in the SECOR ionospheric measurements.

The ionosphere was modelled as of a given shape (Chapman or other) with fixed thickness parameter and undetermined maximum density at point of closest approach (N_m) and undetermined north-south (or time) gradient ($\dot{N}_m$).

The recovered biases (Table 7.1) ranged from about −4 to +9 meters (at 434 MHz). On any particular day the biases were reasonably insensitive to modelling assumptions (thickness and height of maximum) but from day to day there was no significant persistence of bias. It can probably be concluded that the recovered biases do not represent real SECOR errors but regression modelling errors due to the fact that the ionosphere departed significantly from a simple linear north-south gradient.

7.3) The TRANET data were integrated and a similar regression performed to fix the constant of integration. The results were compared to SECOR in terms of range error at point of closest approach (ε_4). The mean difference (Table 7.2) was 0.232 m with a standard deviation of 3.93 m or about 10% (at 434 MHz) which is closely comparable to the differences between SECOR and the best profile determination ray trace results. This provides a valid measure of accuracy with which absolute ionospheric measurements can be recovered from integrated TRANET by regression for the constant of integration. Point by point comparison of SECOR vs integrated TRANET yielded a standard deviation of 0.59 m which is a measure of the random instrumental disagreement of the two systems without regard to the constant of integration.

SECOR-ORBIT Comparisons (Section 8)

8.1) SECOR range data was compared to the best short arc orbital data as defined by LASER, Camera, and C-Band radar. Also in the same comparisons, the SECOR ionospheric data was compared to ray tracing ionospheric corrections based on the Jackson composite data and based on the geographically scaled Jackson composite data utilizing the scaling method previously found best, i.e., linear scaling in latitude based on bottomside f_oF_2 measurements at Ottowa, Wallops and Grand Bahama.

8.2) The ionospheric data comparisons reiterate the same conclusion found previously that the best geographic scaling is not very good at accounting for actual observed variations of ionosphere along the trajectory since the latter do not usually fit a constant gradient model very well.

8.3) The SECOR vs ORBIT range data comparisons yielded a statistically significant mean bias of -15.9 meters with a day-to-day standard deviation of 4.05 meters and a much larger than expected time bias of -1.11 milliseconds with $\sigma = .5$ milliseconds. These biases are probably largely a result of aliasing of non-linear variations of actual ionospheric content into the recovered time bias term.

REFERENCES

1. Davies, Kenneth, "Ionospheric Radio Propagation", NBS Monograph 80, U.S.Gov't. Printing Office, 1965.
2. Gabor, D., "Theory of Communication", JIEE, V.93, Pt.3, p.429, November 1946.
3. Trimble, G.D., "REEK-REEK 2, Spherically Stratified and Two-Dimensional Profile Refraction Corrections for Range and Elevation", RCA Math. Services, Tech.Memo 5350-70-4, April 1970.
4. Lefschetz, S.,"Lectures on Differential Equations", Princeton Press, 1948.
5. Parker, Zegulia, Berbert,"Wallops Island Collocation Experiment Support Plan", NASA Goddard, April 1968.
6. Mallinckrodt, A.J.,"Group and Phase Phenomena in an Inhomogeneous Ionosphere, CRL #567, October 21, 1970.
7. Mallinckrodt, Reich, Parker and Berbert,"Moment Expansion for Ionospheric Range Error", NASA GSFC, X-550-72-298, August 1972, CRL #577, 13 July,1971.
8. Mallinckrodt, A.J.,"Moment Series Extension for Angle, Range Rate, and More Rapid Convergence", CRL #595, 9 November,1972.
9. Mallinckrodt, A.J., "Profile Shape Parameters", Communications Research Laboratories, CRL Report No. 579, 3 September,1971.
10. Mallinckrodt, A.J.,"Tropospheric Correction", Communications Research Labs.,CRL Report #591, 31 July,1972.
11. Mallinckrodt, A.J.,"Refraction Formula Comparison", Communications Research Labs., CRL Report No. 594, 28 September,1972.
12. Mallinckrodt, A.J.,"Moment Series for Angle, Range Rate, and More Rapid Convergence", Communications Research Labs.,CRL Report No. 595, 9 November,1972.
13. Mallinckrodt, A.J.,"Refraction Errors of Short Horizontal Interferometers", Communications Research Labs., CRL Report No. 560, 22 April,1970.
14. Moss, S.J. and Wells, W.T.,"An Analysis of the GSFC Laser Ranging Data", submitted to Goddard Space Flight Center in fulfillment of Contract NAS5-9756-42, June 16, 1967.
15. Gross, J.W.,III,"Preprocessing Electronic Satellite Observations", NASA CR-1183, Contract No. NGR 36-008-093, Ohio State University, November 1968.
16. Berbert, J.H., Reich, R., Maresca, P.,Norris, P.,"Intercomparison of Collocated Laser Optical and GRARR Radio Ranging System Tracks on GEOS-A", GSFC Document X-514-67-447, September 1967.
17. Berbert, J.H. and Parker, H.C.,"Comparison of C-Band, SECOR, and TRANET with a Collocated Laser on 10 Tracks of GEOS 2", GSFC Report No. X-514-68-458, November 1968.
18. Berbert, J.H. and Parker, H.C.,"GEOS Satellite Tracking Corrections for Refraction in the Troposphere", GSFC X-514-70-55, February 1970.

REFERENCES, Cont'd.

19. Mallinckrodt, A.J., Parker, H.C. and Berbert, J.H.,"Refraction Corrections by Moment Expansions", 1974 URSI-IEEE Meeting, Boulder, Colo., 14-17 October,1974.

20. Berbert, J.H. and Parker, H.C.,"GEOS Satellite Tracking Corrections for Refraction in the Ionosphere", GSFC X-514-70-467, December 1970.

21. Mallinckrodt, A.J.,"REEK Modifications", CRL #570, 8 February,1971.

22. Bean, Cahoon, Samson, and Thayer,"A Worldwide Atlas of Atmospheric Radio Refractivity", ESSA Monograph #1, USGPS, 1966.

23. Bean, Cahoon, and Thayer,"Tables for the Statistical Prediction of Radio Ray Bending and Elevation Angle Error Using Surface Values of the Refractive Index", NBS Tech.Note No.44, U.S.Dept. of Commerce, National Bureau of Standards, March 16,1960.

24. Jackson, John E., "Comparisons Between Topside and Ground-Based Soundings", Proc.IEEE, V.57, No.6, p.976, June 1969.

25. GSFC Memoranda from John E. Jackson to John Berbert, October 9,15,21 and November 21,1969; July 24 and November 4,1970; May 20, February 3, 22,23,24,1971; all on the subject of composite bottomside-topside ionospheric profile estimates.
Also, Jackson, John E.,"The P'(f) to N(h) Inversion Problem in Ionospheric Soundings", GSFC X-625-71-186, May 1971.

26. Freeman, J.J.,"Final Report on Ionospheric Correction to Tracking Parameters", J.J. Freeman Associates, Cont. NAS 5-9782, 3 November, 1965.

27. "CCIR Atlas of Ionospheric Characteristics", Report 340, CCIR, Oslo,1966.

28. Parker, H.C.,"Comparison of the Jackson Profile Composites on Six Days to the ESSA Profiles", RCA Service Co., 3 February, 1971.

29. Tucker, A.J.,"Comparison of Ionospheric Corrections made by TRANET and SECOR Systems", University of Texas, Applied Research Laboratories, RSD-TL-74-6, 30 September,1974.

30. Reich, R.F. and Parker, H.C.,"A Method for Determination of the SECOR Ionospheric Range Correction (ICOR) Bias", RCA Service Corp., Lanham,Md., 23 September, 1970.

31. Hopfield, H.S.,"A Two-Quartic Refractivity Profile for the Troposphere, For Correcting Satellite Data", TG 1024, Johns Hopkins University, APL, September 1968.

32. Yionoulis, S.M.,"Algorithm to Compute Tropospheric Refraction Effects on Range Measurements", TG 1125, Johns Hopkins University, APL, July 1970.

33. Thayer, G.D. and Bean, B.R.,"An Analysis of Atmospheric Refraction Errors of Phase Measuring Radio Tracking Systems", Part 1, NBS Report 7254, NBS Boulder Labs., 5 June,1962.